Master's thesis

NTNU
Norwegian University of Science and Technology
Faculty of Information Technology and Electrical Engineering
Department of Engineering Cybernetics

Kenny Hoang Nguyen

Control of Unmanned Subsea Vehicles Operating at Exposed Fish Farms in Presence of Environmental Disturbances

Master's thesis in Cybernetics and Robotics
Supervisor: Jan Tommy Gravdahl
Co-supervisor: Walter Caharija and Sveinung Johan Ohrem
June 2021

NTNU
Norwegian University of
Science and Technology

Kenny Hoang Nguyen

Control of Unmanned Subsea Vehicles Operating at Exposed Fish Farms in Presence of Environmental Disturbances

Master's thesis in Cybernetics and Robotics
Supervisor: Jan Tommy Gravdahl
Co-supervisor: Walter Caharija and Sveinung Johan Ohrem
June 2021

Norwegian University of Science and Technology
Faculty of Information Technology and Electrical Engineering
Department of Engineering Cybernetics

NTNU
Norwegian University of
Science and Technology

Abstract

This thesis proposes two control laws for velocity and heading control of a remotely operated vehicle (ROV) for autonomously traversing of an aquaculture net pen. The primary control objective for both controllers is to achieve error-free tracking of time-varying references enabling path following. The ROV is subject to external disturbances, input saturation and parameter variations and uncertainties. Therefore, it is particularly important that the control laws are robust towards these limitations. With this development of a robust control law, the level of autonomy of an ROV is increased in the sense that it can perform operations at the aquaculture net-pen with less monitoring and management of the process by a human operator. This may result in lower intervention costs and improved operations.

The first control law was developed using a simplified dynamic position (DP) model as a control plant model. The resulting closed-loop system was proven to have uniformly globally asymptotically stable (UGAS) and uniformly locally exponentially stable (ULES) equilibrium point at the origin. When considering robustness, saturation and integrator windup turned out to be a significant problem. This required anti-windup schemes to be implemented in the calculation of the controller's integral terms to handle the effects of thruster saturation. The controller was implemented and validated using SINTEF's simulation software FhSim, on a process plant model of the Argus Mini ROV. The controller was also validated in a field trial at SINTEF ACE, a full-scale operational fish farm meant for research within aquaculture technology. The results from the field trial were very positive as the controller was able to achieve the control objective with low tracking error. The controller achieved root-mean-square error (RMSE) of less than 0.05m/s. The validation of these controllers considered trajectory tracking of velocity and heading references given by a path following algorithm.

The second controller was developed using a more complex control plant model that also considered Coriolis forces. This controller ensured that the origin of the error systems was UGAS. This controller was also implemented and validated with FhSim, using the same process plant model of the Argus Mini ROV. The simulations from FhSim show that the control objective is achieved being able to track the time-varying velocity and heading references.

To summarize, both control laws was shown with simulations achieved the control objective. The first control law was field tested achieving great results, which a draft paper of the results appended in this thesis to be published has been written.

Sammendrag

Denne masteroppgaven foreslår to reguleringslover for hastighets- og retningsregulering av en ROV for autonom traversering av en not for bruk i fiskeoppdrett. Hovedmålet til begge reguleringslovene er å avviksfri følging av tidsvarierende referanseverdier som muliggjør ruteføling ved hjelp av en baneføligingslov. ROVen er utsatt for eksterne miljøforstyrrelser, pådragsmetning, og parametervariasjoner og usikkerheter. Derfor er det særlig viktig at reguleringslovene er robuste mot disse begrensningene. Met utviklingen av en robust reguleringslov, øker autonomien til ROVen ved at den i større grad kan utføre operasjoner i fiskenoten med mindre overvåkning og prosesstyring fra en menneskelig operator. Dette fører til mer kostnadseffektive og forbedrede operasjoner på farmen.

Den første reguleringsloven ble utviklet for en forenklet DP-modell som kontrollmodell. Det resulterende lukket-sløyfe-systemet ble bevist å ha UGAS og ULES likevektspunkt i origo. For betraktning av robustheten, var pådragsmetning og integraloppnøstning et stort problem. Tiltak mot integraloppnøstningen ble implementert i utregningene for kontrollerens integral-ledd for å håndtere effektene fra pådragsmetningen. Dette forbedret resultatene betraktelig. Regulatoren ble implementert og validert i SINTEFs simuleringsprogram FhSim, på en prosessmodell av Argus Mini ROVen. Reguleringsloven ble også validert i et feltforsøk på SINTEF ACE, en fullskala operasjonell fiskemerd for forskning innenfor havbruksteknologi. Resultatene fra feltforsøket var veldig gode, siden regulatorene klarte å oppnå reguleringsmålet med lite avvik på referanseføligingen. Regulatoren oppnådde en RMSE på mindre enn 0.05m/s. Disse forsøkene og simuleringene ble utført med referanseføling av hastighet- og retningsreferanser gitt av en baneføligingsalgoritme.

Den andre regulatoren ble utviklet med en mer kompleks kontrollmodell, som også betraktet koriolis-krefter. Denne regulatoren sørget at origo til lukket-sløyfesystemet var UGAS. Regulatoren ble også implementert og validert med FhSim, og brukte samme prosessmodell av Argus Mini ROV. Simuleringene fra FhSim viste at reguleringsmålet ble oppnådd, og klarte å følge de tidsvarierende hastighets- og retningsreferansene.

For oppsummering, så ble begge regulatorene vist med simuleringer oppnåde reguleringsmålet. Den første regulatoren ble også felttestet med gode resultater. Derfor er det skrevet et utkast for en artikkel av resultatet lagt ved denne masteroppgaven, for publisering ved senere tidspunkt.

Preface and Acknowledgements

This master's thesis is submitted at Norwegian University of Science and Technology (NTNU) as the final requirement of a 5-year MSc program Cybernetics and Robotics. It has been written over the last six months under the supervision of Professor Jan Tommy Gravdahl, Dr. Walter Caharija and Dr. Sveinung Johan Ohrem. This thesis has been carried out as a collaboration with SINTEF Ocean, and continues the work of my specialization project delivered December 2020.

The adaptive controller has been developed and implemented by me in collaboration with Walter. In detecting limitations and ameliorating these, Sveinung helped massively in suggesting different anti-windup schemes that solved the main robustness problems detected for it. I worked further with this controller attempting to handle couplings in the models, and received massive help by Professor Antonio Loría with the stability proofs, and would like to thank him for that.

The past six months have been exciting, educational, frustrating, and last but not least also fun. It has been strongly affected by the ongoing COVID-19 pandemic, and I was not able to participate physically on the field trial in Hitra which I have been looking forward to. In my place, Herman Biørn Amundsen at SINTEF Ocean participated the field trial and tested the controllers for me.

I would therefore start by thanking my supervisor Professor Jan Tommy Gravdahl for giving me this exciting thesis and for valuable feedback and support throughout the past year. I would also thank my co-supervisors Dr. Walter Caharija and Dr. Sveinung Johan Ohrem for their uplifting spirits, as well as their knowledge and counseling throughout the past year. This thesis would not have been possible without them. I would also like to thank Herman Biørn Amundsen and SINTEF Ocean for helping me with the resources needed to go through and complete this thesis. I would also like to thank my family for their support throughout the study time, and to all my friends in Trondheim for making these past five years unforgettable.

Trondheim, 7th June 2021

Kenny Hoang Nguyen

Contents

List of Tables

List of Figures

List of Abbreviations

ROV	Remotely Operated Vehicle
DOF	Degrees of Freedom
NED	North-East-Down
CO	Center of Origin
CG	Center of Gravity
CB	Center of Buoyancy
UGS	Uniformly Globally Stable
UGAS	Uniformly Globally Asymptotically Stable
UGES	Uniformly Globally Exponentially Stable
ULES	Uniformly Locally Exponentially Stable
DP	Dynamic Position
RMSE	Root-mean-square Error
ODEs	Ordinary Differential Equations
MAE	Mean Absolute Error

Part I

Introduction

Chapter 1

Introduction

This master thesis derives, assesses and tests two control laws that can be used for speed and heading control in a step towards an autonomous remotely operated vehicle (ROV) for inspections of aquaculture net pens. The net pens are often at locations with different time-varying environmental loads such as wind, wave and most prominent ocean current. These environmental loads, especially the ocean current, can be problematic for the speed and heading controllers, as they often result in deviations from the desired set-point values complicating the control designs. The thesis will address this problem by designing two control laws aiming to reach the control objective and suppress the effects of the environmental disturbances, mainly ocean currents.

1.1 Motivation

Norway is a leading producer of farmed salmon worldwide and produced 1.36 million tonnes with a value of 68 BNOK in 2019 [1]. In order to increase production and deal with some of the issues related to today's production methods, e.g. sea lice infestations, many fish farmers believe moving their facilities to more exposed locations forestall these issues. However, many of today's aquaculture industry operations depend on manual labour and close human interaction. One such operation is the control of ROVs. The workload on ROV operators is often quite intense, as they are required to both navigate the ROV in a dynamically changing environment while at the same time monitor and avoid the structures. Therefore, increasing the level of autonomy of an ROV could be beneficial to the ROV operators, but also the fish farmers, as it could lower the costs and improve the effectiveness of the operations [2].

Autonomous ROVs operating in dynamic environments such as sea-based aquacul-

ture net pens, require robust control laws to achieve the desired objectives, e.g. maintain a specific heading angle or follow a path. At SINTEF Ocean, an Argus Mini ROV is currently used as a research vehicle for testing different control strategies and autonomous functions. This ROV is presently equipped with PI speed controllers in the surge and sway velocity degrees of freedom (DOF), and a PID controller in the heading DOF. The speed controllers have a major shortcomings, as the ROV is not able to reach the desired speed when subject to strong ocean currents and increasing the integral gains does not help since it leads to unstable behaviour. This worsens the performance of the vehicle, when executing tasks such as path following. As a step towards more robust autonomous operations for ROVs in general, it is, therefore, of interest to develop a more robust control algorithm for the surge, sway and heading DOFs.

The developed controller must ensure that the ROV is capable of following a time-varying speed and heading references while under the influence of ocean currents. The controller should also be robust towards variations and uncertainties in the system parameters, such as mass and damping coefficients, as these are not perfectly known. The goal of this thesis is, therefore, to primarily develop and implement a robust control law for surge, sway and heading DOFs. For these control laws, it will be attempted to prove that the closed-loop systems of their respective control plant models have desired stability properties.

1.2 Contributions

In this thesis, two model-based control laws for marine vehicles modelled in 3-DOF, i.e., surge, sway and yaw, are presented. The first controller is derived using a simplified 3-DOF control plant model, while the second controller considers a more complex 3-DOF control plant model. The first controller, referred to as C1 for the remainder of the thesis, is based upon [3] and first proposed in the preproject [4] that leads to this thesis, utilizes an adaption law to ensure that the origin of the full error system is uniformly globally asymptotically stable (UGAS) and uniformly locally exponentially stable (ULES). The second controller, referred to as C2 for the remainder of this thesis, is a modified version of C1. In C2, the adaptive law is expanded and overparameterized to consider some unknown quadratic ocean current terms. Furthermore, C2 utilizes a more complex control plant model, and as such, this controller is assumed to be more robust than C1. Due to the complexity of the control plant model, the origin for only some of the states of the closed-loop system with C2 was only proven to be UGAS through Lyapunov stability theory, with the origin of the remaining states being proven to be uniformly globally stable (UGS).

Both controllers were validated in simulations, and C1 was tested in a field experiment.

The contributions can be summarized as follows:

- Velocity control laws in surge and sway were designed based on a control plant model.
- The origin of the closed-loop system with the aforementioned control law was proven to be uniformly globally asymptotically stable.
- The aforementioned controller was shown to be robust against some modelling errors using perturbation theory.
- The aforementioned controller was modified to be robust against actuator saturation and prevents integrator windup.
- The aforementioned controller was software validated and field validated with excellent results showing vast improvement from the previous implemented PI control law.
- The control law was modified and extended to include the heading based on a slightly more complex control plant model.
- The new control law was proven that some of the states uniformly globally asymptotically converged to the origin, in addition to being bounded for the remaining states.
- The control law was software validated with a promising yaw response.

1.3 Problem Description

The overall problem in this thesis is to improve the level of autonomy and control robustness for underwater vehicles. The Argus Mini ROV is utilized as a test platform. The main task to achieve this is, therefore, to design and implement robust control laws capable of tracking time-varying references. The following subproblems to solve this task are therefore proposed for this thesis:

1. Develop a control plant model for ROVs, with the Argus Mini ROV in mind as a test case.
2. Develop a control law for the control plant model where the control objective is trajectory tracking with minimal tracking error.

3. Detect and ameliorate limitations of the controller to increase robustness.
4. Validate the control law through simulations in FhSim with a more complex process plant model than the process plant model used in [4].
5. Validate the control law at the SINTEF ACE full scale aquaculture laboratory.
6. Augment the control plant model for the ROV and modify and expand the control law accordingly.
7. Calculate and derive the properties of this modified control law.
8. Test the modified control law through simulations in FhSim.

1.4 Outline

This thesis consists of five parts and 14 chapters.

- Part II presents the necessary relevant background theory used to model, derive and analyze the control laws and closed-loop system in this thesis.
  - Chapter 2 presents the theory for marine craft dynamics used in this thesis to model the ROV.
  - Chapter 3 presents the basic principles for guidance, navigation and motion control of marine crafts.
  - Chapter 4 presents some stability definitions, theorems and lemmas that are used for the derivations of the control laws in this thesis.
  - Chapter 5 presents the literature that this thesis builds on, in addition to related works for the control of marine vehicles.
- Part III describes the method and derivations of control laws used in the thesis.
  - Chapter 6 presents the control objectives that the rest of the parts are attempting to achieve.
  - Chapter 7 models and simplifies the models for the Argus Mini ROV. The two control plant models and their assumptions are presented in this chapter.
  - Chapter 8 presents the first control law based on a simplified dynamic position control plant model. The stability proof for the closed-loop system, limitation and robustness analysis is also presented here,

  - Chapter 9 presents the second control law based on an expanded control plant model. Stability proofs for this nonlinear model are presented here.

- Part IV describes the simulations and experiment setup, in addition to presenting the results from simulations and field experiments.
  - Chapter 10 presents the simulation setup.
  - Chapter 11 presents the results of the first control law based on a dynamic position control plant model. Here the results from the simulations are presented, validating the derivations done. In addition, results from field experiments are presented, validating the control law in practice.
  - Chapter 12 presents the results of the second control law based on the coupled augmented control plant model. Only results from simulations are given as a software validation for this control law.
- Part V discusses the results from previous parts, in addition to comparing the different control laws based on these results.

The results achieved with the first control law was above expectations, and a paper for publishing of the results has been written and a draft is given in Appendix B.

Part II

Theory

Chapter 2

Marine Craft

When simulating a physical model, it is important to be aware that simulations do not model reality perfectly [4]. More often than not, simplifications are done because it is difficult to model perfectly or complex models even give numerical unstable simulations. There are, therefore, two important distinctions in modelling the designer has to be aware of when developing models of marine crafts. In this thesis, the design of the controllers is based on a **control plant model**, which models the main physical properties of reality. The designer can use it in the stability and robustness analysis of controllers. The other distinction is a model as close to reality as needed; this model is called the **process plant model** and is used in numerical performance and robustness analysis as well as control system testing. With a lack of process knowledge and thereby proper modelling, the control plant model is often used in place of the process plant model, resulting in bad controller designs [5].

Regardless, both plant models in this master's thesis are derived based on the same fundamental differential equations for marine crafts. The notations and equations are represented using Fossen's robot-like vectorial model in [6]. It is a compact representation that exploits the physical properties and couplings in the differential equations for a 6-DOF marine craft, inspired by the classic robotic model representation:

$$\mathbf{M}(\mathbf{q})\ddot{\mathbf{q}} + \mathbf{C}(\mathbf{q}, \dot{\mathbf{q}})\mathbf{q} = \boldsymbol{\tau} \tag{2.1}$$

2.1 Notation for Marine Craft

The notation of the different DOF follows the nomenclature from SNAME given in [7] and is regiven in Table 2.1.

Vector	Vector	State	Description	DOF
$\boldsymbol{\eta}_{nb}^{n}$	$\boldsymbol{p}_{nb}^{n}$	x	North position	1
		y	East position	2
		z	Down position	3
	$\boldsymbol{\Theta}_{nb}$	ϕ	Attitude about x-axis	4
		θ	Attitude about y-axis	5
		ψ	Attitude about z-axis	6
$\boldsymbol{\nu}_{nb}^{b}$	$\boldsymbol{v}_{nb}^{b}$	u	Surge velocity	1
		v	Sway velocity	2
		w	Heave velocity	3
	$\boldsymbol{\omega}_{nb}^{b}$	p	Roll rate	4
		q	Pitch rate	5
		r	Yaw rate	6

Table 2.1: SNAME notation conventions

In this thesis, vectors and matrices are expressed in **bold**. A vector with subscripts and superscripts are in this thesis used as $\boldsymbol{v}_{nb}^{b}$ and this is read as *the linear velocity of the center of origin in BODY frame with respect to the origin of the NED frame, expressed in the coordinates of the BODY frame*. It will often also be implicit in this thesis what the vectors describes, such that the subscripts and superscripts are omitted.
Angular representations are done with Euler angles symbolized with the three-dimensional $\boldsymbol{\Theta}_{nb}$ and is read as the *Euler angles of the BODY frame relative to the NED frame*. The position and orientation, and velocity of any marine vessels are defined in NED and BODY frame, respectively. Therefore, they are defined in two vectors where they contain the states of the marine craft in their appropriate reference frames. The vectors are summarized in Table 2.1.

2.2 Reference Frames

It is convenient to express motion relatively to reference frames to analyze the motion of marine crafts. For instance, for operations over large distances, ship operations going from one part of the world to another, it is common to use an Earth-centered Earth-fixed reference frame to describe the ship's position and attitude. However, for operations confined to smaller areas, which the ROV in this thesis are limited to, the reference frames as explained in [6] that are used are:

NED: The *North-East-Down (NED)* coordinate system which is denoted $\{n\} = (x_n, y_n, z_n)$ with the origin o_n. In this frame, x_n is the axis pointing towards the

Earth's true North, y_n towards the east, and z_n points downwards, normal to the tangential plane on the Earth surface. This frame can be seen as a tangent plane on the Earth's surface as illustrated in Figure 2.1, which is an assumption that holds for small areas on Earth. This frame is considered inertial in this thesis.

BODY: The *BODY* frame, denoted as $\{b\} = (x_b, y_b, z_b)$, is a moving coordinate system that has its origin o_b fixed to the object of interest. In this thesis, x_b is defined as the axis going from aft to fore, the y_b axis pointing starboard and z_b going from top to bottom of the vessel, with the origin o_b at a point on the craft. An illustration of how the frame can be defined on an Argus Mini ROV is shown in Figure 2.2.

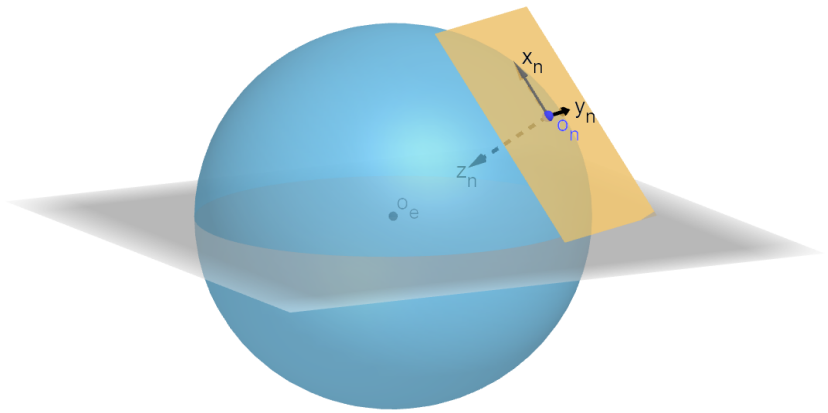

Figure 2.1: An arbitrary NED frame on Earth's surface. Figure inspired by [8]

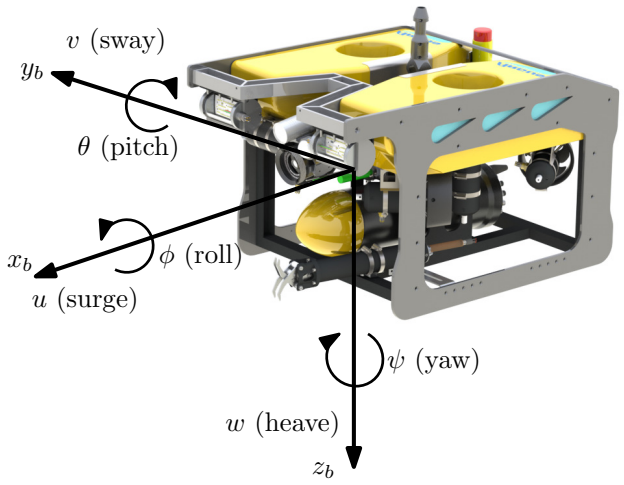

Figure 2.2: BODY frame illustrated on the Argus Mini ROV. Figure inspired by [9]

2.3 Transformations Between Frames

To relate the BODY frame, fixed on the moving vessel, and NED frame, which is assumed inertial, a transformation matrix $\mathbf{J}_{\boldsymbol{\Theta}}(\boldsymbol{\eta})$ is defined. The transformation matrix consists of a linear velocity rotation matrix $\mathbf{R}(\boldsymbol{\Theta}_{nb}) \in \mathbb{R}^{3\times3}$ and angular velocity transformation matrix $\mathbf{T}(\boldsymbol{\Theta}_{\boldsymbol{nb}}) \in \mathbb{R}^{3\times3}$.

$$\mathbf{J}_{\boldsymbol{\Theta}}(\boldsymbol{\eta}) = \begin{bmatrix} \mathbf{R}(\boldsymbol{\Theta}_{nb}) & \mathbf{0}_{3\times3} \\ \mathbf{0}_{3\times3} & \mathbf{T}(\boldsymbol{\Theta}_{\boldsymbol{nb}}) \end{bmatrix} \tag{2.2}$$

The linear velocity rotation matrix is defined as the Euler angles rotation:

$$\mathbf{R}(\boldsymbol{\Theta}_{nb}) = \begin{bmatrix} c\psi c\theta & -s\psi c\phi + c\psi s\theta s\phi & s\psi s\phi + c\psi c\phi s\theta \\ s\psi c\theta & c\psi c\phi + s\phi s\theta s\psi & -c\psi s\phi + s\theta s\psi c\phi \\ -s\theta & c\theta s\phi & c\theta c\phi \end{bmatrix} \tag{2.3}$$

where $s(\,\cdot\,) = \sin(\,\cdot\,)$ and $c(\,\cdot\,) = \cos(\,\cdot\,)$. This matrix belongs to the special orthogonal group which can be read more about in [6, p. 20], where the most important properties are $\mathbf{R}\mathbf{R}^{\mathbf{T}} = \mathbf{R}^{\mathbf{T}}\mathbf{R} = \mathbf{I_3}$ and $\det\mathbf{R} = 1$. The angular velocity transformation matrix are defined using:

$$\dot{\boldsymbol{\Theta}}_{nb} = \mathbf{T}_{\Theta}(\boldsymbol{\Theta}_{nb})\boldsymbol{\omega}^{b}_{nb} \tag{2.4}$$

This, according to [6, p. 25], results in

$$\mathbf{T}_{\Theta}^{-1}(\boldsymbol{\Theta}_{nb}) = \begin{bmatrix} 1 & 0 & -s\theta \\ 0 & c\phi & c\theta s\phi \\ 0 & -s\phi & c\theta c\phi \end{bmatrix} \implies \mathbf{T}_{\Theta}(\boldsymbol{\Theta}_{nb}) = \begin{bmatrix} 1 & s\phi t\theta & c\phi t\theta \\ 0 & c\phi & -s\phi \\ 0 & s\phi/c\theta & c\phi/c\theta \end{bmatrix} \tag{2.5}$$

Here it is used that $t(\,\cdot\,) = \tan(\,\cdot\,)$.

Remark 2.1. Note that Eq.(2.5) has a singularity at $\theta = \pm 90^{\circ}$ which is a well known problem with Euler angles. To overcome this problem, writing the kinematics using quaternions is an alternative. Quaternions are a non-minimal attitude representation. See, for instance, [6, 10] for how quaternions can be used to replace Euler angles.

2.4 Kinematic Equations

With the transformation matrices the 6-DOF kinematic differential equation can be written as:

$$\begin{gathered} \dot{\boldsymbol{\eta}}_{nb}^{n} = \mathbf{J}_{\Theta}(\boldsymbol{\eta})\boldsymbol{\nu}_{nb}^{b} \\ \Updownarrow \\ \begin{bmatrix} \dot{\boldsymbol{p}}_{nb}^{n} \\ \dot{\boldsymbol{\Theta}}_{nb} \end{bmatrix} = \begin{bmatrix} \mathbf{R}(\boldsymbol{\Theta}_{nb}) & \mathbf{0}_{3\times 3} \\ \mathbf{0}_{3\times 3} & \mathbf{T}(\boldsymbol{\Theta}_{\boldsymbol{nb}}) \end{bmatrix} \begin{bmatrix} \boldsymbol{v}_{nb}^{b} \\ \boldsymbol{\omega}_{nb}^{b} \end{bmatrix} \end{gathered} \tag{2.6}$$

This results from the relation that the time derivative of position is the velocity. However, since it is desired for it to be written relative to the NED frame, a transformation from the BODY frame has to be done.

2.5 Kinetic Equations

A general 6-DOF kinetic equation of motion for marine vehicle can, according to [6], be expressed as

$$\mathbf{M}\dot{\boldsymbol{\nu}} + \mathbf{C}(\boldsymbol{\nu})\boldsymbol{\nu} + \mathbf{D}(\boldsymbol{\nu})\boldsymbol{\nu} + \boldsymbol{g}(\boldsymbol{\eta}) + \boldsymbol{g}_0 = \boldsymbol{\tau}_c + \boldsymbol{\tau}_{wind} + \boldsymbol{\tau}_{wave} \tag{2.7}$$

where

- $\mathbf{M} = \mathbf{M}_{RB} + \mathbf{M}_A$ is the mass matrix including the rigid body and added mass terms
- $\mathbf{C}(\boldsymbol{\nu}) = \mathbf{C}_{RB}(\boldsymbol{\nu}) + \mathbf{C}_A(\boldsymbol{\nu})$ is the Coriolis-centripetal matrix for rigid body and added mass terms

- $\mathbf{D}(\boldsymbol{\nu})$ is the damping matrix, it is convenient to write the total hydrodynamic damping as the sum of a linear part due to potential damping and possible skin friction and nonlinear part due to quadratic damping and higher-order terms.
- $\boldsymbol{g}(\boldsymbol{\eta})$ is a vector of gravitational and buoyancy forces and moments
- $\boldsymbol{g}_0$ is a vector used for pretrimming or ballast control
- $\boldsymbol{\tau}_c$ is a vector of control inputs
- $\boldsymbol{\tau}_{wind}$ and $\boldsymbol{\tau}_{wave}$ is the forces acting on the vessel caused by wind and wave motions

The rigid-body system inertia matrix or mass matrix is unique and satisfies $\mathbf{M}_{RB} = \mathbf{M}_{RB}^T > 0$ according to [6, p. 53], and it can therefore be written as:

$$\mathbf{M}_{RB} = \begin{bmatrix} \mathbf{M}_{11}^{RB} & \mathbf{M}_{12}^{RB} \\ \mathbf{M}_{21}^{RB} & \mathbf{M}_{22}^{RB} \end{bmatrix} \tag{2.8}$$

with $\mathbf{M}_{12}^{RB} = (\mathbf{M}_{21}^{RB})^T$.

For the coriolis-centripetal matrix an important property is that it is defined to be skew-symmetric [6], and by choosing the parameterization:

$$\mathbf{C}_{RB}(\boldsymbol{\nu}) = \begin{bmatrix} \mathbf{0}_{3\times 3} & -\boldsymbol{S}(\mathbf{M}_{11}^{RB}\boldsymbol{\nu}_1 + \mathbf{M}_{12}^{RB}\boldsymbol{\nu}_2) \\ -\boldsymbol{S}(\mathbf{M}_{11}^{RB}\boldsymbol{\nu}_1 + \mathbf{M}_{12}^{RB}\boldsymbol{\nu}_2) & -\boldsymbol{S}(\mathbf{M}_{21}^{RB}\boldsymbol{\nu}_1 + \mathbf{M}_{22}^{RB}\boldsymbol{\nu}_2) \end{bmatrix} \tag{2.9}$$

where $\boldsymbol{\nu}_1$ and $\boldsymbol{\nu}_2$ are the first three and last three elements of $\boldsymbol{\nu}$, respectively, this property is satisfied.

2.5.1 Hydrodynamics

Added mass forces:
When a rigid body moves in a fluid, the additional inertia of the fluid surrounding the body has to be considered. The fluid is accelerated by the body itself, and a force is necessary to achieve this acceleration. The fluid exerts a reaction force which is equal in magnitude in opposite direction. This reaction force is the added mass contribution [10]. For $\mathbf{M}_A$ there are in general no specific properties. However, for a body completely submerged in fluid the matrix can be considered positive definite. Furthermore, for a submerged body with low velocity and three-plane symmetry, as Assumption 2.3 states, the added mass can be approximated as:

$$\mathbf{M}_A = -\text{diag}\{X_{\dot{u}}(0), Y_{\dot{v}}(0), Z_{\dot{w}}(0), K_{\dot{p}}(\omega_{roll}), M_{\dot{q}}(\omega_{pitch}), N_{\dot{r}}(0)\} \tag{2.10}$$

where ω_{roll} and ω_{pitch} are the natural frequency in roll and pitch respectively, as stated in [9]. $X_{\dot{u}}(0)$ are the inertial force along the x-axis due to an acceleration $\dot{u}$ in x direction. This also yields for the other two axes as well. [6]

Likewise, the Coriolis-centripetal matrix for rigid-body, the Coriolis-centripetal matrix for the added mass can be derived using the parameterization from Eq.(2.9). However, in this case, the added mass matrix is used instead of the rigid-body mass matrix, and the velocity vector $\boldsymbol{\nu}$ is replaced with the *relative velocity* vector $\boldsymbol{\nu}_r$. The relative velocity vector will be explained more in-depth in the section for ocean current.

Damping forces:
The damping matrix for marine vessels is normally computed with a hydrodynamic potential theory program, where viscous effects are neglected. Consequently, it is, therefore, necessary to add viscous forces to the model manually. Without going far into details for how damping can be modelled, it is safe to say that it is hard to precisely model, and can for control design purposes, complicate the design more than it benefits [6].

Hydrodynamic damping for the marine craft is mainly caused by potential damping, skin friction, wave drift damping, and damping from vortex shedding. For vehicles operating fully submerged, especially at water depths where waves have little effects, potential damping and other wave-related damping effects can be neglected. The damping forces can, conveniently, in many cases, be simplified to be the sum of its linear component and nonlinear effects:

$$\mathbf{D}(\boldsymbol{\nu}_r) = \mathbf{D} + \mathbf{D}_n(\boldsymbol{\nu}_r) > 0 \tag{2.11}$$

This damping matrix is strictly positive since it is well known that energy is dissipated through damping [11]. Due to the neglection of wave-related damping effects, the linear damping term stems from skin friction and the nonlinear term from vortex shedding, which is quadratic. In low-speed manoeuvring, the linear terms will dominate the nonlinear terms and vice versa in high speed. This theory from [6] typically assumes slender body types and will therefore not necessarily be accurate for ROVs [9]. One can consequently approximate the ROV to be a box and calculate the damping from this; however, due to the cavities, exposed cables, and other appendages such as cameras, the box approximation will lead to underestimations [11].
Diagonal damping matrices are used in modelling of ROVs, as done in [9, 11], since it is difficult to find values for non-diagonal damping terms with calculations or experiments. The diagonal terms will also be dominating terms, so the removal

of off-diagonal terms are neglible. Therefore the linear and nonlinear damping matrices can be given as:

$$\begin{aligned} \mathbf{D} &= -\text{diag}\{X_u, Y_v, Z_w, K_p, M_q, N_r\} \\ \mathbf{D_n}(\boldsymbol{\nu}_r) &= -\text{diag}\{X_{|u|u}|u_r|, Y_{|v|v}|v_r|, Z_{|w|w}|w_r|, K_{|p|p}|p_r|, M_{|q|q}|q_r|, N_{|r|r}|r_r|\} \end{aligned} \tag{2.12}$$

where these coefficients and how to find them can be approximated and found from experiments as written about in [11].

2.6 Subsystems

2.6.1 Kinematic subsystem

For many applications, motion in certain DOFs can be neglected, and therefore define subsystems of the differential equation Eq.(2.6). The Argus Mini ROV's specifications are given in [12], and for this ROV, the following assumption can be made:

Assumption 2.1. *Due to the nature of passive stabilization properties from gravity for this ROV. The roll, ϕ, and pitch, θ, can be approximated to be zero. It means that $\phi \approx 0$ and $\theta \approx 0$.*

The first assumption means the vessel will not reach the singularity under normal conditions, avoiding the numerical instability.

Remark 2.2. The assumption is made for most ROVs, which can be seen in other literature such as [8, 9, 10, 13]. ROVs are usually designed to be naturally stable in roll and pitch.

The assumption made for roll and pitch can be used to neglect the motion in those states. This reduces the states to $\boldsymbol{\eta} = \begin{bmatrix} x^n & y^n & z^n & \psi^n \end{bmatrix}^T$, $\boldsymbol{\nu} = \begin{bmatrix} u^b & v^b & w^b & r^b \end{bmatrix}^T$.

In addition, the following assumption from [13] can also be made for the Argus Mini ROV in heave:

Assumption 2.2. *The vehicle is neutrally buoyant, and the motion in heave can therefore be neglected. In addition, the vehicle center of gravity (CG) and the center of buoyancy (CB) are located along the same vertical axis in $\{b\}$.*

Remark 2.3. Most ROVs are designed to be slightly positively buoyant. Therefore, in the case of a system shut down, the ROV will slowly rise to the surface. However, the ROV has heave thrusters that are used to independently control the depth of the ROV with a depth controller. The ROV can, therefore, for all practical

purposes be assumed neutrally buoyant. One can also assume that the heave DOF is independent from the rest and that no couplings exists between i.e. surge and heave, sway and heave, and heading and heave.

This assumption can therefore be used to simplify the kinematic equations even more, reducing it to a 3-DOF differential equation where $\boldsymbol{\eta} = \begin{bmatrix} x & y & \psi \end{bmatrix}^T$, $\boldsymbol{\nu} = \begin{bmatrix} u & v & r \end{bmatrix}^T$ and the rotation matrix

$$\mathbf{R}(\psi) \triangleq \begin{bmatrix} \cos(\psi) & -\sin(\psi) & 0 \\ \sin(\psi) & \cos(\psi) & 0 \\ 0 & 0 & 1 \end{bmatrix} \tag{2.13}$$

Which can be seen is a principal rotation matrix about z-axis. Decoupling the heave velocity from the horizontal velocity is an assumption that can be made to simplify design of the horizontal controllers in this thesis.

2.6.2 Simplification for Kinetic Equations

Considering the Argus Mini ROV in this thesis, the following assumptions are made

Assumption 2.3. *The ROV is symmetric in port-starboard, fore-aft and bottom-top*

Assumption 2.4. *The body-fixed frame $\{b\}$ center of origin (CO) is located in the CG.*

Remark 2.4. All the Assumption 2.1-2.4 made are common assumptions in modelling of ROVs, see for instance [6, 10, 13].

To summarize this section about kinetics, from the assumptions, matrices for the ROV have the following properties:

- $\mathbf{M}_{RB} = \mathbf{M}_{RB}^T = \text{diag}\{m_{11}^{RB}, m_{22}^{RB}, ..., m_{66}^{RB}\} > 0$
- $\dot{\mathbf{M}}_{RB} = \mathbf{0}$
- $\mathbf{M}_A = \mathbf{M}_A^T = \text{diag}\{m_{11}^A, m_{22}^A, ..., m_{66}^A\}$
- $\dot{\mathbf{M}}_A = \mathbf{0}$
- $\mathbf{D}(\boldsymbol{\nu}_r) = \mathbf{D} + \mathbf{D}_n(\boldsymbol{\nu}_r) > 0$
- $\mathbf{D} = \text{diag}\{d_{11}, d_{22}, ..., d_{66}\}$, $d_{ii} > 0 \forall i = \{1, 2, ...6\}$
- $\mathbf{D}_n(\boldsymbol{\nu}_r) = \text{diag}\{d_{n11}|u_r|, d_{n22}|v_r|, ..., d_{n66}|r_r|\}$, $d_{nii} > 0 \forall i = \{1, 2, ...6\}$

- $\mathbf{C}(\boldsymbol{\nu}) = -\mathbf{C}(\boldsymbol{\nu})^T$

In addition with Assumption 2.1 and Assumption 2.2, it is possible to look at the horizontal motion isolated for the kinetic equations. This means that for the horizontal DOF, $\boldsymbol{g}(\boldsymbol{\eta}) = \boldsymbol{g}_0 = \mathbf{0}$.

2.7 Environmental Forces

When modelling marine vessels it is common to include three environmental forces in the modelling. That is models for the wind, waves and ocean currents. In the general kinetic equation Eq.(2.7), the wave and wind forces are assumed with the principle of superposition and enters the equation as external generalized forces in $\boldsymbol{\tau}_{wind}$ and $\boldsymbol{\tau}_{wave}$.

Assumption 2.5. *The ROV is completely submerged in deep water at all times when the controller this thesis considers is active. Therefore, wind and wave forces can be neglected, and the only environmental disturbance that needs to be taken into account is the ocean current.*

Remark 2.5. The velocity measurements which is needed for the velocity controllers are only available when the camera of the ROV is directed towards the net. In this case, it is only possible when it is submerged.

2.7.1 Ocean Current

In [6, p. 221], ocean currents are described as:

> Ocean currents are horizontal and vertical circulation systems of ocean waters produced by gravity, wind friction, water density variation in different parts of the ocean. Besides wind-generated currents, the heat exchange at the sea surface, together with salinity changes develop an additional sea current component (...).

For our purposes, to simplify the controller designs, the following assumption about ocean currents can therefore be made:

Assumption 2.6. *The ocean current is constant, irrotational and bounded with a velocity vector* $\mathbf{V}_c = [V_x, V_y, V_z, 0, 0, 0]^T$ *in* $\{n\}$. *Being bounded means that there exists a constant* $V_{max} > 0$ *such that* $||\mathbf{V}_c|| < V_{max}$. *Furthermore, due to the current being constant,* $\dot{\mathbf{V}}_c = \mathbf{0}$.

Remark 2.6. Due to the assumption that pitch and roll are neglected for the ROV, a z-component in the ocean current would affect the heave of ROV isolated, which is completely decoupled and controlled separately. Therefore, it will not affect the motion in the horizontal plane for the ROVs $\{b\}$. This is an assumption that also has been done in [13]. The current vector can therefore reduce its vector to only be in DOF $1, 2$ and 6, meaning it is written as: $\mathbf{V}_c = [V_x, V_y, 0]^T$ in $\{n\}$.

Remark 2.7. Another remark here is that the assumption on the ocean current is made in the NED frame, and in many earlier works on control, the current is assumed to be constant in the BODY frame. This assumption is easily violated during turning as it has been stated in [14]. It is, therefore, necessary to transform the current force effects to the BODY frame.

To simulate and model the ocean currents effect on the motion of the ROV, the relative velocity vector is defined to be:

$$\boldsymbol{\nu}_r^b = \boldsymbol{\nu}^b - \boldsymbol{\nu}_c^b \tag{2.14}$$

where it is used that $\boldsymbol{\nu}_c^b = \mathbf{J}_\psi^T(\psi)\mathbf{V}_c$, where $\mathbf{J}_\psi(\psi)$ is the rotation matrix in 3-DOF from $\{b\}$ to $\{n\}$ in horizontal plane, and the transpose therefore is the opposite rotation.
Note that the current is not constant in the BODY frame and the time derivative of the relative velocity vector is therefore

$$\dot{\boldsymbol{\nu}}_r^b = \dot{\boldsymbol{\nu}}^b - \dot{\boldsymbol{\nu}}_c^b \tag{2.15}$$

and $\dot{\boldsymbol{\nu}}_c^b = \dot{\mathbf{J}}_\psi^T(\psi)\mathbf{V}_c$ where

$$\dot{\mathbf{J}}_\psi(\psi) = \begin{bmatrix} -r\sin(\psi) & -r\cos(\psi) & 0 \\ r\cos(\psi) & -r\sin(\psi) & 0 \\ 0 & 0 & 0 \end{bmatrix} \tag{2.16}$$

2.8 Actuation

Most of this section was written about in [4], and regiven here in this section. A brief theory of the actuation of the ROV is presented here. Mainly with a focus on the control allocation matrix $\mathbf{B}$ and the limitations of the thrusters.
The body fixed frame has its x and y axis going in surge and sway respectively. The angles of the thrusters are relative to the parallell frames of body fixed frame but centered at the position where the forces of the thrusters are exerted at. For the ROV in this thesis, which has four thrusters on the horizontal plane, the thruster allocation matrix $\mathbf{B}$ for 3-DOF is given by

$$\mathbf{B} = \begin{bmatrix} b_{11} & b_{12} & b_{13} & b_{14} \\ b_{21} & b_{22} & b_{23} & b_{24} \\ b_{31} & b_{32} & b_{33} & b_{34} \end{bmatrix} \tag{2.17}$$

where

$$b_{1i} = \cos(\alpha_i) \tag{2.18}$$
$$b_{2i} = \sin(\alpha_i) \tag{2.19}$$
$$b_{3i} = x_{l_i}\sin(\alpha_i) - y_{l_i}\cos(\alpha_i) \tag{2.20}$$

and $i = \{1, ..., 4\}$. Here x_{l_i} and y_{l_i} is the x, y-coordinates of the i'th thrusters center relative to the BODY frame.

Furthermore, it is important to take into account the limitations of the thrusters. One well-known limitation of any thrusters is that generating force cannot happen instantaneously. There are limitations of how fast the thrusters can go from 0 to max thrust, and in simulations, a simple way to model this is using a rate slew limiter.

An upper bound of how much force a thruster can exert is another limitation that needs to be considered. When the thrusters try to give a higher actuation than it is physically possible capable of, it goes into saturation, an effect that might be destabilizing for closed-loop systems in practice if the designer does not handle this nonlinear effect properly.

The matrix $\mathbf{B} \in \mathbb{R}^{3\times n}$ maps the control input vector $\mathbf{f} \in \mathbb{R}^n$, where n is number of thrusters on the ROV actuating the control forces $\tau \in \mathbb{R}^3$. The control forces are described by the vector $\begin{bmatrix}\tau_u & \tau_v & \tau_r\end{bmatrix}^T = \mathbf{Bf}$. The thruster allocation matrix $\mathbf{B}$ has full rank for $n \geq$DOF, and is therefore, in this thesis, fully actuated in surge, sway and yaw. The maximum control forces, $\tau_{u_{max}}$, $\tau_{v_{max}}$ and $\tau_{r_{max}}$, when the thrusters each can only exert a bounded force can be calculated so that it can be taken into account for control design. The location and the positive direction of the thrusters can look like Figure 2.3. To calculate $\tau_{u_{max}}$ and $\tau_{v_{max}}$, the vectors from the forces in each thruster need to be summed up and decomposed in surge and sway. These calculations are done to find the total force that the ROV can exert in surge and sway and the total moment in yaw independent of each other. This results in

$$\begin{aligned}\tau_{u_{max}} &= \sum_{i=1}^{n}\left(|F_{max}|\cos(\alpha_i)\right) \\ \tau_{v_{max}} &= \sum_{\text{odd i}}\left(|F_{max}|\sin(\alpha_i)\right) + \sum_{\text{even i}}\left(-|F_{min}|\sin(\alpha_i)\right)\end{aligned} \tag{2.21}$$

Here F_{max} and F_{min} are the forces each thruster has available in a positive and negative direction, respectively. To find the maximum force in the opposite direction, F_{max} and F_{min} need to switch place in the calculations done above. To

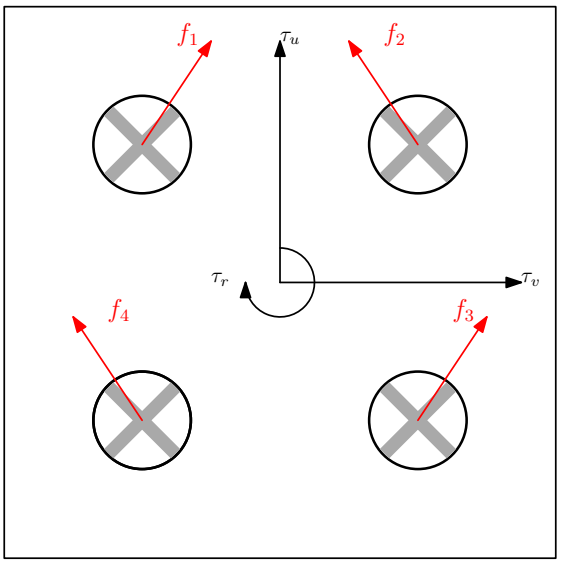

Figure 2.3: Generic horizontal thruster locations on an ROV with positive force vectors

calculate the maximum torque or moment that these thrusters can exert we need to find the vector of the arm from centre of origin to the point where the thrusters exert a force on the ROV. The maximum torque from the thrusters is given as the sum of the torque of each thruster individually that contributes to that rotational movement. The torque is calculated with

$$\tau_{r_{max}} = \sum_{i=1}^{n} |\mathbf{r_i} \times \mathbf{f_i}| \tag{2.22}$$

where the the vectors $\mathbf{r_i} = \begin{bmatrix} x_{l_i} & y_{l_i} & 0 \end{bmatrix}^T$ for $i = \{1, ..., n\}$ and the force vectors for each thrusters in Figure 2.3 are given as

$$\begin{aligned} \mathbf{f_i} &= \begin{bmatrix} |F_{max}|\cos(\alpha_i) & |F_{max}|\sin(\alpha_i) & 0 \end{bmatrix}^T, \quad i = \{1, 4\} \\ \mathbf{f_i} &= \begin{bmatrix} |F_{min}|\cos(\alpha_i) & |F_{min}|\sin(\alpha_i) & 0 \end{bmatrix}^T, \quad i = \{2, 3\} \end{aligned} \tag{2.23}$$

More general terms, sum up the maximum force from each thruster contributing to a positive rotational moment. The last element in all vectors is set to 0 because the forces of these thrusters are assumed to only be effective in the horizontal plane.

In order to make the simulations as realistic as possible, the saturations have to be set at each thruster force which can be found by using the Moore-Penrose pseudo-inverse of the thruster allocation matrix defined from [6, p. 405] as:

$$\mathbf{B}^{\dagger} = \mathbf{B}^T(\mathbf{B}\mathbf{B}^T)^{-1} \tag{2.24}$$

2.9 Summary

Gathering the most important result from this chapter, the kinematic and kinetic equations for ROVs in horizontal degrees of freedoms to be used in control designs, given in [6, p. 188], can be written as:

$$\begin{aligned} \dot{\boldsymbol{\eta}} &= \mathbf{J}_{\psi}(\psi)\boldsymbol{\nu} \\ \mathbf{M}_{RB}\dot{\boldsymbol{\nu}}^{b} + \mathbf{C}_{RB}(\boldsymbol{\nu}^{b})\boldsymbol{\nu}^{b} + \mathbf{M}_{A}\dot{\boldsymbol{\nu}}_{r}^{b} + \mathbf{C}_{A}(\boldsymbol{\nu}_{r}^{b})\boldsymbol{\nu}_{r}^{b} + \mathbf{D}(\boldsymbol{\nu}_{r}^{b})\boldsymbol{\nu}_{r}^{b} &= \mathbf{B}\mathbf{f} \end{aligned} \tag{2.25}$$

where $\mathbf{J}_{\psi}$ is the rotation from $\{b\}$ to $\{n\}$ using the principal rotation matrix about the z-axis.

Chapter 3

ROV Guidance, Navigation and Control

The basics of marine motion control systems will be presented in this chapter. A motion control system consists usually of three independent blocks; guidance, navigation and control (GNC) systems. The interconnections between these systems are illustrated in Figure 3.1.

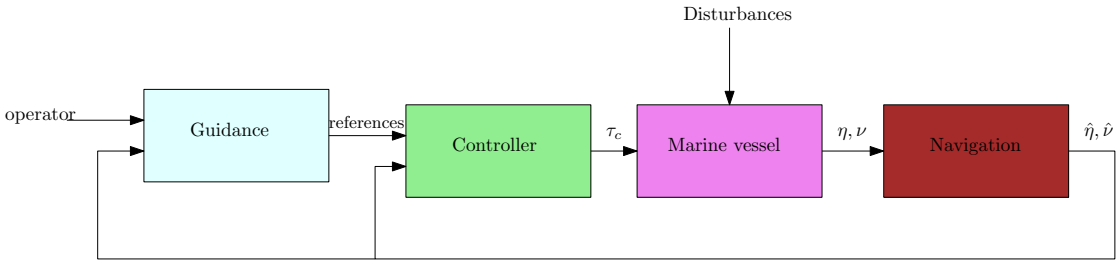

Figure 3.1: Typical GNC system interconnection. Figure inspired by [9]

The focus in this thesis will mainly stay on the controller block of the system.

3.1 Control Systems

A control system computes the necessary actuation forces to achieve some control objective [9]. One typical control objective is, for instance, set-point regulation. For a control system, the inputs are typically the desired reference value, also called the set-point for a state, and state estimations to say where the vessel is at the given moment. The control system's output values for actuation forces to "tell" the vessel what the actuators should do to make a move towards the desired set-point.

This section presents a brief introduction to marine motion control, and for further reading, the reader is referred to [6, 10].

3.1.1 PID Controllers

A widely used controller in the industry is the PID controller and its different combinations of P, PI, and PD controllers. It offers the simplest yet most efficient solution to many real-world control problems [15]. It utilizes the control error $e = x - x_d$ to calculate the actuator input τ. Where x_d is the desired set-point, and x is the state measurement or estimation. The control designer chooses the gains K_p, K_i and K_d to scale the input to an appropriate value. With this, the different controllers can be written as given in Table 3.1.

P	$\tau = -K_p e$
PI	$\tau = -K_p e - K_i \int_0^t e dt$
PD	$\tau = -K_p e - K_d \dot{e}$
PID	$\tau = -K_p e - K_d \dot{e} - K_i \int_0^t e dt$

Table 3.1: The control laws for different PID controllers

With a naïve approach, the control gains are tuned by looking at the system response; however, this approach is prone to human errors, and there might exist a set of better parameters yielding a better response. The gain K_p can be seen as a proportional gain and affects the immediate error of the desired state and current state. The K_d term can be interpreted as a damping gain and affects the error's derivative or rate of change. The K_i affects the summed error over time and is used to reduce constant disturbance acting on the system.

A more analytical approach to tuning the different gains might be using pole placement by analyzing the transfer function of the closed-loop system and analyzing its stability margins [16]. This method, however, requires good system knowledge, and often for nonlinear models, becomes impossible. One technique for pole placement with nonlinear models is to view the nonlinear terms as a constant disturbance term and place the poles based on the linear terms. The integrator part of the controller can then handle the disturbance term.

3.1.2 Control Design Methods

Especially when dealing with nonlinear systems, different nonlinear controller designs are used to achieve desired closed-loop responses.

Feedback linearization controllers:
This controller design method is based on transforming nonlinear systems into equivalent closed-loop linear systems. Then, a traditional controller like the PID controller mentioned earlier can be used [6]. This method, however, requires that the vessel model is known, and the system is input-output linearizable [17]. Having modelling errors can potentially be destabilizing when using feedback linearizing. Due to the complexity of deriving kinetic models for a marine vessel, the controller's performance using feedback linearizing can be unsatisfying in practice.

Consider the nonlinear marine craft dynamics on the form

$$\mathbf{M}\dot{\boldsymbol{\nu}} + \boldsymbol{n}(\boldsymbol{\nu}, \boldsymbol{\eta}) = \boldsymbol{\tau} \tag{3.1}$$

where the states $\boldsymbol{\nu}$ and $\boldsymbol{\eta}$ are assumed available, for instance through measurements and approximations, the coefficients in $\boldsymbol{n}$ are known. The nonlinearities can be cancelled out by choosing the control law as:

$$\boldsymbol{\tau} = \mathbf{M}\bar{\boldsymbol{\tau}} + \boldsymbol{n}(\boldsymbol{\nu}, \boldsymbol{\eta}) \tag{3.2}$$

where $\bar{\boldsymbol{\tau}}$ is a commanded control vector that for instance can be chosen as a PID-controller for each state [6, p. 451].

Backstepping controllers:
Backstepping controllers are another design method utilizing recursive construction of control Lyapunov functions to decide the feedback control law. Like the feedback linearization controllers, it cancels nonlinearities, but it also gives the designer the choice of keeping good stabilizing nonlinear terms, like, for instance, nonlinear damping terms. This method provides the system with additional robustness, especially when it is well known that cancellation of nonlinearities requires precise models, which is hard to achieve in practice [6, p. 457].

The idea of backstepping is most easily described with a demonstration. Consider a simple nonlinear scalar system:

$$\begin{aligned} \dot{x}_1 &= f(x_1) + x_2 \\ \dot{x}_2 &= u \\ y &= x_1 \end{aligned} \tag{3.3}$$

where u is the controller input to the system, and it is desired to control y to zero. The design starts with the system x_1 and continues with x_2.
A change of coordinates is introduced:

$$\boldsymbol{z} = \boldsymbol{\phi}(\boldsymbol{x}) \tag{3.4}$$

where $\boldsymbol{z}$ is a new state vector and $\boldsymbol{\phi}(\boldsymbol{x})$ is a global diffeomorphism transformation, which in short terms means it is a mapping with smooth functions $\boldsymbol{\phi}(\boldsymbol{x})$ and $\boldsymbol{\phi^{-1}}(\boldsymbol{z})$. Hence the inverse transformation

$$\boldsymbol{x} = \boldsymbol{\phi^{-1}}(\boldsymbol{z}) \tag{3.5}$$

is guaranteed.

For the first step of the controller design for this system, choose the first backstepping variable as $z_1 = x_1$. The state x_2 is chosen as the *virtual* control input and is defined to be the sum of a stabilizing function α_1 and the new state variable z_2.

$$x_2 = \alpha_1 + z_2 \tag{3.6}$$

A control Lyapunov function (CLF) can be chosen as:

$$\begin{aligned} V_1 &= \frac{1}{2} z_1^2 \\ \dot{V}_1 &= z_1(f(z_1) + \alpha_1 + z_2) \\ &= z_1(f(z_1) + \alpha_1) + z_1 z_2 \end{aligned} \tag{3.7}$$

The attention can then be turned to design the stabilizing function, and therefore choose

$$\alpha_1 = -f(z_1) - k_1 z_1 \tag{3.8}$$

where $k_1 > 0$ is the feedback gain. Now the first equation is:

$$\dot{z}_1 = -k_1 z_1 + z_2 \tag{3.9}$$

it is therefore easy to see that when $z_2 = 0$, the system for z_1 is stabilized.
The second step for the design is to compute the z_2 dynamics from time differentiation of Eq.(3.6).

$$\begin{aligned} z_2 &= x_2 - \alpha_1 \\ \dot{z}_2 &= \dot{x}_2 - \dot{\alpha}_1 \\ &= u - \dot{\alpha}_1 \end{aligned} \tag{3.10}$$

A CLF for this system is therefore

$$\begin{aligned} V_2 &= V_1 + \frac{1}{2}z_2^2 \\ \dot{V}_2 &= \dot{V}_1 + \dot{z}_2 z_2 \\ &= (-k_1 z_1^2 + z_1 z_2) + z_2(u - \dot{\alpha}_1) \\ &= -k_1 z_1^2 + z_2(u - \dot{\alpha}_1 + z_1) \end{aligned} \tag{3.11}$$

meaning the control law can be chosen as

$$u = \dot{\alpha}_1 - z_1 - k_2 z_2 \tag{3.12}$$

with $k_2 > 0$ and

$$\dot{\alpha}_1 = \frac{\partial f(x_1)}{\partial x_1}\dot{x}_1 - k_1 \dot{x}_1 \tag{3.13}$$

this yields:

$$\dot{V}_2 = -k_1 z_1^2 - k_2 z_2^2 < 0, \forall z_1, z_2 \neq 0 \tag{3.14}$$

meaning that $z_1, z_2 \to 0 \implies x_1 \to 0$.
To summarize the process, this design method utilizes Lyapunov functions to choose the control input and stabilize the output.

3.1.3 Control Allocation

Control allocation is about distributing generalized control forces $\boldsymbol{\tau} \in \mathbb{R}^n$ to actuators in terms of control inputs $\boldsymbol{u} \in \mathbb{R}^r$. If $r > n$, this means the problem is overactuated, and $r < n$ means it is underactuated. This computation mapping the control inputs to the generalized control forces is a model-based optimization problem that considers physical limitations such as maximum input amplitude and rate saturation. [6, p. 398]

3.2 Guidance Systems

Guidance can be defined as "The process for guiding the path of an object towards a given point, which in general may be moving" [18]. Another way of formulating this is that a guidance system computes a reference position, velocity, or acceleration vectors used as inputs for the control system of the GNC interconnections [9]. The inputs to the guidance systems are usually set-points or instructions given by a human operator. For guidance, three scenarios are usually considered [6, p. 235]:

- Set-point regulation: It is the most basic guidance system where an operator provides a constant input or set point. Examples of set-point regulation are constant depth, speed control, or regulation to zero value.

- Trajectory tracking: For instance, the position and velocity of a marine craft track a desired time-varying position and velocity reference signals. Tracking control can be used for course-changing manoeuvres, speed-changing, and attitude control. If, for instance, a constant set-point is used as an input to a low-pass filter, also called a reference model, in an open-loop guidance system, the outputs of the filter will be smooth time-varying reference trajectories for the position, velocity, and acceleration (PVA).

- Path following: This is to follow a pre-defined path indepentent of time. This is typical for ships in transit between continents or underwater vehicles used to map the seabed.

3.3 Navigation Systems

The navigation part of the system involves determining and processing the states of the vessel. It involves using sensors to collect raw data. These raw measurements in turn have to be processed to be useful. In the first step they are handled by a signal processing unit, or program for quality check and wild-point removal. In the second step, these raw measurements are transmitted to the computer which have a state estimator that is capable of noise filtering, prediction and reconstruction of unmeasured states, wherein the most famous algorithm for state estimation is the Kalman filter.

In this thesis, the most relevant part of the navigation system is the Doppler Velocity Log (DVL), which is used in the ROV to measure velocities used in feedback to the controllers. This sensor is widespread in maritime applications. They are usually mounted to measure the vehicle's velocity with respect to the seabed, but in this case, it will measure the velocity of the vehicle with respect to the net pen. It sends multiple hydro-acoustic signals towards the seabed or net pen, and the velocity is then calculated by measuring the Doppler shift in the reflected acoustic signals.[13]

Chapter 4

Mathematical Review

In this chapter, some essential mathematical identities, theorems, and lemmas used in the thesis are presented here.

4.1 Norms and $\mathcal{L}_p$-spaces

To understand the mathematics, the definitions of vector norms and $\mathcal{L}_p$-spaces are presented here and details about them can be read more about in [17]:

Definition 4.1. Norm: p-norms on $\mathbb{R}^n$ are defined as

$$\left.\begin{array}{ll} \|x\|_p & = \left(\sum_{i=1}^{n} |x_i|^p\right)^{\frac{1}{p}}, p \in [1,\infty) \\ \|x\|_\infty & = \max_i |x_i| \end{array}\right\} p-\text{norms} \tag{4.1}$$

Definition 4.2. $\mathcal{L}_p$-space: A piecewise continuous function, $u : [0,\infty) \to \mathbb{R}^m$, is in the $\mathcal{L}_p^m$-space for $1 \leq p < \infty$ if and only if

$$\|u\|_{\mathcal{L}_p} = \left(\int_0^\infty \|u(t)\|^p dt\right)^{1/p} < \infty \tag{4.2}$$

with the special case of the $\mathcal{L}_\infty$ being defined to be that

$$\|u\|_{\mathcal{L}_\infty} = \sup_{t\geq 0} \|u(t)\| < \infty \tag{4.3}$$

Definition 4.3. κ and κ_∞ functions: A continuous function $\alpha : [0,a) \to [0,\infty)$ is said to belong to class κ if

- it is strictly increasing.

- it is such that $\alpha(0) = 0$.

furthermore the same functions belongs to κ_∞ if

- belongs to class κ
- it is such that $a = \infty$
- it is such that $\lim_{r\to\infty} \alpha(r) = \infty$

where this definition is taken from [17].

4.2 Stability

To understand the proofs, a fundamental understanding of stability is necessary.

Definition 4.4. According to [17], the equilibrium point $\boldsymbol{x} = 0$ of $\dot{\boldsymbol{x}} = \boldsymbol{f}(t, \boldsymbol{x})$ is

- stable, if for each $\epsilon > 0$ there exists $\delta = \delta(\epsilon) > 0$ such that

$$\|\boldsymbol{x}(t_0)\| < \delta \implies \|\boldsymbol{x}(t)\| < \epsilon, \forall t \geq t_0 \geq 0$$

- uniformly stable, if for each $\epsilon > 0$, there is $\delta = \delta(\epsilon) > 0$, independent of t_0, such that the equation above is satisfied.
- unstable, if it is not stable.
- asymptotically stable if it is stable and δ can be chosen such that:

$$\|\boldsymbol{x}(t_0)\| < \delta \implies \lim_{t\to\infty} \boldsymbol{x}(t) = 0 \tag{4.4}$$

- uniformly asymptotically stable if it is uniformly stable and there is a positive constant c, independent of t_0, such that for all $\|\boldsymbol{x}(t_0)\| < c$, $\lim_{t\to\infty} \boldsymbol{x}(t) \to 0$, uniformly in t_0.
- globally uniformly asymptotically stable if it is uniformly stable, $\delta(\epsilon)$ can be chosen to satisfy $\lim_{\epsilon\to\infty} \delta(\epsilon) = \infty$ and for each pair of positive numbers η and c there is $T = T(\eta, c) > 0$ such that

$$\|\boldsymbol{x}(t)\| < \eta, \forall t \geq t_0 + T(\eta, c), \forall \|\boldsymbol{x}(t_0)\| < c \tag{4.5}$$

Usually the mathematics of Definition 4.4 is not used directly, but is the fundamentals for all stability proofs given. A more direct way of proving stability is using Lyapunov's stability theorem:

Theorem 4.1. ***Lyapunov's stability theorem:*** *Let* $\boldsymbol{x} = 0$ *be an equilibrium point for* $\dot{\boldsymbol{x}} = \boldsymbol{f}(\boldsymbol{x})$ *and* $\mathbf{D} \subset \mathbb{R}^n$ *be a domain containing* $\boldsymbol{x} = 0$*. Let* $V : \mathbf{D} \to \mathbb{R}$ *be a continuously differentiable function such that*

$$V(\mathbf{0}) = 0 \text{ and } V(\boldsymbol{x}) > 0, \forall \boldsymbol{x} \in D \backslash \{\mathbf{0}\}$$
$$\dot{V}(\boldsymbol{x}) \leq 0, \forall \boldsymbol{x} \in D$$

Then, $\boldsymbol{x} = \mathbf{0}$ *is* ***stable****. Moreover, if*

$$\dot{V}(\boldsymbol{x}) < 0, \forall \boldsymbol{x} \in \mathbf{D} \backslash \{\mathbf{0}\}$$

then $\boldsymbol{x} = \mathbf{0}$ *is asymptotically stable. Furthemore, if in addition* $\|\boldsymbol{x}\| \to \infty \implies V(\boldsymbol{x}) \to \infty$*, then the origin is globally asymptotically stable. [17, Theorem 4.1]*

Expanding this to exponentially stability, which is a stronger stability property:

Theorem 4.2. *Let* $\boldsymbol{x} = \mathbf{0}$ *be an equilibrium point for* $\dot{\boldsymbol{x}} = \boldsymbol{f}(t, \boldsymbol{x})$ *and* $\mathbf{D} \subset \mathbb{R}^n$ *be a domain containing* $\boldsymbol{x} = \mathbf{0}$*. Let* $V : [0, \infty) \times \mathbf{D} \to \mathbb{R}$ *be a continously differentiable function such that*

$$k_1 \|\boldsymbol{x}\|^a \leq V(t, \boldsymbol{x}) \leq k_2 \|\boldsymbol{x}\|^a$$
$$\frac{\partial V}{\partial t} + \frac{\partial V}{\partial \boldsymbol{x}} \boldsymbol{f}(t, \boldsymbol{x}) \leq -k_3 \|\boldsymbol{x}\|^a$$

$\forall t \geq 0$ *and* $\forall \boldsymbol{x} \in \mathbf{D}$*, where* k_1, k_2, k_3 *and* a *are positive constants. Then* $\boldsymbol{x} = \mathbf{0}$ *is exponentially stable. If the assumptions hold globally then the origin is globally exponentially stable.*
[17, Theorem 4.10]

For an autonomous system that can be written on the linear form $\dot{\boldsymbol{x}} = \mathbf{A}\boldsymbol{x}$, the following, easier applicable, theorem can also be used to show asymptotically stability.

Theorem 4.3. ***Lyapunov's indirect stability method:*** *The equilibrium point of* $\dot{\boldsymbol{x}} = \mathbf{A}\boldsymbol{x}$ *is* ***stable*** *if and only if all eigenvalues of* $\mathbf{A}$ *satisfy* $Re\lambda_i \leq 0$ *and for every eigenvalue with* $Re\lambda_i = 0$ *and algebraic multiplicity* $q_i \geq 2$*,* $rank(\mathbf{A} - \lambda_i \mathbf{I}) = n - q_i$ *where* n *is the dimension of* $\boldsymbol{x}$*. The equilibrium point* $\boldsymbol{x} = 0$ *is (globally)* ***asymptotically stable*** *if and only if all eigenvalues of* $\mathbf{A}$ *satisfy* $Re\lambda_i < 0$ *[17, Theorem 4.5].*

It can also be shown that all linear systems that are (globally) asymptotically stable are also (globally) exponentially stable. Proofs for these theorems can all be found and read more about in [17].

In some cases, there is often hard to prove that there exists a Lyapunov function that fulfills Theorem 4.1 or even eigenvalues to fulfill Theorem 4.3 to show convergense of the states. Barbalat's Lemma can in the case of autonomous systems therefore often be utilized to show convergence of some of the states.

Lemma 4.1. ***Barbalat's Lemma:*** *if $f, \dot{f} \in \mathcal{L}_\infty$ and $f \in \mathcal{L}_p$ for some $p \in [1, \infty)$, then $f(t) \to 0$ as $t \to \infty$ [19, Lemma 3.2.5].*

For readers interested in the proof for this Lemma and examples using this Lemma, they are then referred to [19].

Another Lemma that can be used in the same way as Barbalat's Lemma but be extended to also yield for time-varying systems is the integration lemma which can be used to show that the origin is uniformly globally asymptotically stability solution of the ordinary differential equations (ODEs).

Lemma 4.2. ***Integration Lemma:*** *Consider the system*

$$\dot{\boldsymbol{x}} = \boldsymbol{f}(t, \boldsymbol{x}) \tag{4.6}$$

The origin of Eq.(4.6) *is UGAS if it is UGS and there exists a continuous positive definite function $\gamma : \mathbb{R}^n \to \mathbb{R}_{\geq 0}$ and for each $\boldsymbol{r}, \nu > 0$ there exists $\beta_{\boldsymbol{r}\nu} > 0$, such that for all $t_0 \geq 0, |\boldsymbol{x}_0| \leq \boldsymbol{r}$ and all $t \geq t_0$, the solution $\boldsymbol{x}(\,\cdot\,, t_0, \boldsymbol{x}_0)$ satisfies*

$$\int_{t_0}^{\infty} \left[\gamma(\boldsymbol{x}, (\boldsymbol{\tau}, t_0, \boldsymbol{x}_0)) - \nu\right] d\tau \leq \beta_{\boldsymbol{r}\nu} \tag{4.7}$$

The proof for this Lemma and details can be read more about in [20, Lemma 2].

4.3 Robustness

Up until now the mathematical lemmas and theorems have focused on stability, and what stability properties is it possible to prove for a general system. What if a system is on the form of $\dot{\boldsymbol{x}} = \boldsymbol{f}(t, \boldsymbol{x}) + \boldsymbol{g}(t, \boldsymbol{x})$ and it can be shown that the nominal system $\dot{\boldsymbol{x}} = \boldsymbol{f}(t, \boldsymbol{x})$ is exponentially stable, is it possible to say something how robust the system is for some unmodelled perturbations $\boldsymbol{g}(t, \boldsymbol{x})$?

Lemma 4.3. ***Vanishing perturbation:*** *Let $\boldsymbol{x} = \boldsymbol{0}$ be an exponentially stable equilibrium point of a nominal system*

$$\dot{\boldsymbol{x}} = \boldsymbol{f}(t, \boldsymbol{x})$$

Let $V(t, \boldsymbol{x})$ be a Lyapunov function that satisfies Theorem 4.2 with $a = 2$, and in addition satisfies

$$\left\| \frac{\partial V}{\partial \boldsymbol{x}} \right\| \leq k_4 \|\boldsymbol{x}\| \tag{4.8}$$

in $[0, \infty) \times \mathbf{D}$. Then suppose the perturbation term $\boldsymbol{g}(t, \boldsymbol{x})$ satisfies

$$\begin{aligned} \|\boldsymbol{g}(t, \boldsymbol{x})\| &\leq \gamma \|\boldsymbol{x}\|, \forall t \geq 0, \forall \boldsymbol{x} \in \mathbf{D} \\ \gamma &< \frac{k_3}{k_4} \end{aligned} \tag{4.9}$$

Then the origin is an exponentially stable equilibrium point of the perturbed system

$$\dot{\boldsymbol{x}} = \boldsymbol{f}(t, \boldsymbol{x}) + \boldsymbol{g}(t, \boldsymbol{x})$$

Moreover, if all assumptions hold globally, then the origin is globally exponentially stable.

Chapter 5

Literature review

5.1 Theorem for UGAS Systems

Recall from the example for backstepping controllers regiven in Chapter 3, it was possible to design a control to write the system on a specific form and control $x_1 \to 0$. In [3] this idea is extended to be even more general and for (non-)autonomous systems that it is possible to prove it is UGAS and ULES given the system matrices fulfills certain conditions. This system is given on the form:

$$\begin{aligned} \dot{\boldsymbol{x}}_1 &= \boldsymbol{h}(\boldsymbol{x}_1, t) + \mathbf{G}(\boldsymbol{x}, t)\boldsymbol{x}_2 \\ \dot{\boldsymbol{x}}_2 &= -\mathbf{P}\mathbf{G}(\boldsymbol{x}, t)^T \left(\frac{\partial W(\boldsymbol{x}_1, t)}{\partial \boldsymbol{x}_1} \right), \mathbf{P} = \mathbf{P}^T > 0 \end{aligned} \tag{5.1}$$

Note that it looks similar to the scalar system Eq.(3.3), only expanded to multivariable form. Following theorem then holds for this system, when assumptions A1 and A2, which is regiven here, is true.

Theorem 5.1. *The origin of Eq.*(5.1) *is UGAS and ULES*

A short summary of the assumptions is that it bounds the matrices for the general case where the system is nonautonomous. The assumptions that need to be checked are:

Assumption 5.1. *Define* $\mathbf{G}_0(\boldsymbol{x}_2, t) := \mathbf{G}(\boldsymbol{x}, t)|_{\boldsymbol{x}_1 \equiv \mathbf{0}}$. *Assume there exists a continuous nondecreasing functions* $\boldsymbol{\rho}_j : \mathbb{R}_{\geq 0} \to \mathbb{R}_{\geq 0}$ *for (j=1,2) such that for all* $t \geq 0, x \in \mathbb{R}^{n_1+n_2}$*:*

$$\max \left\{ \|\boldsymbol{h}(\boldsymbol{x}_1, t)\|, \left\| \frac{\partial W(\boldsymbol{x}_1, t)}{\partial \boldsymbol{x}_1} \right\| \right\} \leq \boldsymbol{\rho}_1(\|\boldsymbol{x}_1\|)\|\boldsymbol{x}_1\| \tag{5.2}$$

$$\max \{\|\mathbf{G}(\boldsymbol{x}, t)\|, \|\mathbf{G}_0(\boldsymbol{x}_2, t)\|\} \leq \boldsymbol{\rho}_2(\|\boldsymbol{x}\|) \tag{5.3}$$

and, for each compact set $\mathbf{K} \subset \mathbb{R}^{n_2}$ *there exists a constant* $b_m > 0$ *such that*

$$\mathbf{G}_0(\boldsymbol{x}_2, t)^T \mathbf{G}_0(\boldsymbol{x}_2, t) \geq b_m \mathbf{I} \tag{5.4}$$

$\forall (\boldsymbol{x}_2, t) \in \mathbf{K} \times \mathbb{R}_{\geq 0}$

The second assumption for this theorem is simply that:

Assumption 5.2. *There exist class-*κ_∞ *functions* α_1 *and* α_2 *and a strictly positive real number* $c > 0$ *such that*

$$\alpha_1(\|\boldsymbol{x}_1\|) \leq W(\boldsymbol{x}_1, t) \leq \alpha_2(\|\boldsymbol{x}_1\|) \tag{5.5}$$

$$\frac{\partial W(\boldsymbol{x}_1, t)}{\partial t} + \frac{\partial W(\boldsymbol{x}_1, t)}{\partial \boldsymbol{x}_1} \boldsymbol{h}(\boldsymbol{x}_1, t) \leq -c\|\boldsymbol{x}_1\|^2 \tag{5.6}$$

Moreover, if $\alpha_2(s) \propto s^2$ *for sufficiently small* s*, then the origin is ULES.*

where this second assumption says there exists a Lyapunov function, $W(\boldsymbol{x}_1, t)$, for subsystem $\dot{\boldsymbol{x}}_1 = \boldsymbol{h}(\boldsymbol{x}_1, t)$, such that the origin of that system is exponentially stable per Theorem 4.2.

The proof for this theorem can be summarized in short terms that if it can be shown that the origin of system Eq.(5.1) is uniformly globally stable, in addition to showing that the origin has global uniform attractivity, then the origin is UGAS. The assumptions are to give properties to the different matrices for the proof. This method of thinking is a way of dividing the task to show asymptotically stability for the different states.

5.2 Control Systems

This thesis is in many ways an extension of [9], which briefly presented some strategies for motion control. However, this thesis will be going more in-depth on the control systems so that the work done in [9] can perform optimally. In [4] some controllers were proposed to be tested to find the most promising with respect to robustness. Especially controllers based on adaptive feedback linearization PID controllers were popular amongst them, which were used in [13, 14, 21, 22]. In addition, [9] proposed a first-order sliding mode controller and a super-twisting algorithm controller from [23] for the ROV, where they were simulated in the project [4] for fall 2020. In the project, a process plant model was proposed, which all the controllers were tested on. In addition to this, a simplified dynamic positioning control plant model was used to propose an adaptive controller studied in this thesis.

The adaptive feedback linearizing controller that was proposed in [13] looked promising during the preliminary simulations done in [4]. The error for the velocity tracking from this controller was little and more or less the same as the other promising controller, as was concluded in the project [4]. The simulations in [13], likewise [4], also showed that the controller more or less tracked the desired velocities perfectly. However, field tests from the same article [13] showed that it had significantly deteriorating results than the simulations. Basin wall following using DVL showed great results where the controller managed to a large extent track the velocity references, with some deviations. When the ROV reached a corner, it struggled to follow the reference from what seems like a too fast and large change so that it was not physically possible for it to reach the reference. However, the biggest problem for this controller was that during the net-pen following trial, where the velocity reference was constant, the closed-loop system got a constant deviation and, at the same time, became more oscillatory. This behaviour might be from thrusters going into saturation; however, it is hard to say for sure if the oscillations come from saturation or other factors without information of what happened to the ROV under the test. However, based on the data from these two field tests in [13] it seems as the controller used was somewhat satisfactory but still has potential for improvement since the controller had some deviations with velocity tracking.

The first-order sliding mode controller proposed in [9] simulated in [4] was also on par with the other nonlinear controllers in [4]. The simulations showed that the controller had more or less perfect velocity tracking during simulations. Unlike the feedback adaptive linearizing controller, the sliding mode controller has not been tested in the field, and it is therefore hard to say if it would perform as well in practice as it does in theory. However, a major difference between the sliding mode controller and the other nonlinear controllers was that the control input was more active or had chattering, which increases wear and tear on the actuators of the ROV. An attempt of dealing with this problem was to introduce a higher-order sliding mode controller, for instance, the super-twisting adaptive algorithm from [23].

The results from [13] also suggests that the control plant model used is not good. It was proven with the control plant model, which essentially is the process plant model without nonlinear damping in [4], that the feedback linearization controller resulted in an error-free trajectory tracking. In practice, this did not happen to a large extent. This result shows how important modelling is, especially when utilizing feedback linearizing, and the control plant models suggested in this thesis

also has to consider how well it models reality.

The super-twisting adaptive algorithm (STA) from [23] was also proposed in [9], and attempted to be simulated in [4]. For some reason, the simulation done in MATLAB was unsuccessful; the step-length in the simulation was variable and became too small such that the amount of data generated became larger than the memory that was available from the computer. Using fixed-step length showed that it was oscillatory, and it was not easy to understand why it did not work. An error in the setup of the controller is also a possibility. With this many variables that might have caused a malfunctioning controller and simulations made it hard to justify using this controller for velocity control, but simulations using FhSim gave results that exceeded the results from the first-order sliding mode controller. Nonetheless, like the first-order sliding mode controller, this has not been tested in the field, and it is hard to say that this will give better results than the other controllers that have been studied in [4]. Since the STA controller, according to [9] had some problems with large changes in the reference, which can ultimately lead to high-gain instability, the controller was not further researched and tested with field trials.

The adaptive controller, which was called the "DP controller" in [4] was the controller that seemed most promising for robustness. Even though the velocity tracking had great results, it wielded some other nice properties that increased the robustness, especially that the origin of the whole closed-loop system with the ocean current estimations were globally asymptotically stable. However, the assumptions made for the control plant model did not hold when simulating with the process plant model, which again resulted in ocean current estimations that no longer was error-free. It is, however, essential to remember the control objective, which is to follow the time-varying references with as little error as possible and not estimate perfectly. Even when the ocean current estimations were no longer error-free, it was still stable in the sense that it did not oscillate or grow unbounded, and the velocity controller still managed to reach the control objective. The robustness of this controller needs to be discussed further, especially when there are modelling errors and other factors present, which might affect the controller to an extent where it no longer reaches its control objective.

Part III

Method

Chapter 6

Overview and Objective

In this part of the thesis, two control laws will be derived with two different control plant models. The control laws are derived based on the same idea, with inspiration from the backstepping method, and utilizes [3] to achieve properties for the closed-loop system. The work here is a continuation of the work done in [4] and the literature review from Chapter 5. First, the two control plant models will be presented with their necessary assumptions and matrices. The first control plant model is a simplified DP model, which is a simplification of the general kinetic equation Eq.(2.25), valid for low-speed vessels. The second control plant model is an expansion of the first control plant model, modelling the Coriolis-centripetal forces as well. Then, control laws are derived based on the two control plant models and are then analyzed to ensure closed-loop stability of the origin and robustness for the given models.

The main focus will be on the control part of a typical GNC system, and therefore, emphasis will be laid on the physical limitations that may affect the performance of the controllers. It is mainly the actuation limitations and modelling errors that are considered for the robustness of the controller. The controller derived for the dynamic position model, C1, is analyzed with perturbation theory to prove that the control objective will be attained despite modelling errors. In addition, some improvement for C1 will be made to handle actuation saturation, which might destabilise the closed-loop system in practice if untreated. C1 are then tested with a more complex process plant model in FhSim for software validation before it is tested experimentally at SINTEF ACE live fishing farm for field validation.

Then, the second controller, C2, will be designed for the second more complex control plant model. It will be shown that the controller will give a closed-loop system that globally converges asymptotically to the origin for the error states. The controller is then implemented in FhSim for software validation. With prom-

ising results, the controller can then possibly, at a later time, be field validated for future work. For this thesis, this controller was not ready in time for field testing.

The overall objective for both controllers is error-free tracking of time-varying references. The net following algorithm that was written about in [9] provides the desired time-varying values ψ_d, u_d and v_d that the controllers calculate an actuation $\boldsymbol{\tau}_c$ that makes sure the marine vessel follows with as little error as possible. That is $\psi \to \psi_d$, $u \to u_d$ and $v \to v_d$ in finite time. The control objective for the controllers is therefore more formalized defined to be:

$$\lim_{t\to\infty}(\psi - \psi_d(t)) = 0 \tag{6.1a}$$

$$\lim_{t\to\infty}(u - u_d(t)) = 0 \tag{6.1b}$$

$$\lim_{t\to\infty}(v - v_d(t)) = 0 \tag{6.1c}$$

6.1 Outline

This part of the thesis is organized as follows:

- In Chapter 7 the process plant model and the control plant models with the assumptions needed for them to be valid are proposed. Furthermore, the maximum actuation, or more specific, the total force from the thrusters in each DOF in the horizontal plane are calculated. This is used in the software for the controller design.
- Chapter 8 proposes and derives the first controller based on the simplified control plant model. In addition, robustness analysis and improvement of the control law is proposed to handle limitations of the controller as well.
- Chapter 9 proposes and derives the second controller based on an augmented model that is closer to the process plant model, but still neglects nonlinear damping.

Chapter 7

Modelling of the Argus Mini ROV

7.1 Modelling the Kinetic Equations

In this section, the different plant models are presented. The section starts with presenting the 3-DOF process plant model that was implemented in [4] in Simulink. This model was used to test different controllers before implementing them in a more complex simulation software: FhSim. Then the first control plant model, which is a simplification of the process plant model, based on a simplified DP model, is presented with the necessary assumptions to be valid. The last control plant model is an intermediate model of the first control plant model and the process plant model. This second control plant model will, in addition, take into account the Coriolis-centripetal forces in the equations.

7.1.1 Process Plant Model

Like the kinematic equations, the kinetic equation can also reduce its degrees of freedom. Assumption 2.1-2.4 suggests that the horizontal motion of the ROV is completely decoupled from the vertical motion of the ROV. It is, therefore, possible to only look at the horizontal motion, and model the ROV in 3-DOF; surge, sway and yaw. The heave motion can, as it has been stated earlier, be controlled with a separate heave controller with separate thrusters and is out of scope for this thesis. Reducing the DOF for a marine vessel is common in many previous works, see [13, 14, 21, 22], and is done in this thesis to limit the controller design to the horizontal plane. The different matrices and vectors in the 3-DOF model can, therefore, be

defined as:

$$\boldsymbol{\eta} = [x, y, \psi]^T, \quad \boldsymbol{\nu} = [u, v, r]^T$$
$$\mathbf{M}_i = \begin{bmatrix} m_{11}^i & 0 & 0 \\ 0 & m_{22}^i & 0 \\ 0 & 0 & m_{66}^i \end{bmatrix}, \quad \mathbf{C}_i(\boldsymbol{\nu}) = \begin{bmatrix} 0 & 0 & -m_{22}^i v \\ 0 & 0 & m_{11}^i u \\ m_{22}^i v & -m_{11}^i u & 0 \end{bmatrix} \tag{7.1}$$

where $i \in \{RB, A\}$

$$\mathbf{D} = \begin{bmatrix} d_{11} & 0 & 0 \\ 0 & d_{22} & 0 \\ 0 & 0 & d_{66} \end{bmatrix}, \mathbf{D}_n(\boldsymbol{\nu}_r) = \begin{bmatrix} d_{n11}|u_r| & 0 & 0 \\ 0 & d_{n22}|v_r| & 0 \\ 0 & 0 & d_{n66}|r| \end{bmatrix} \tag{7.2}$$

where it is defined that: $d_{njj}, d_{jj} > 0, j = \{1, 2, 6\}$, to obtain positive definite damping matrices.
The relative velocity vector, defined as in Section 2.7, results in:

$$\mathbf{V}_c^n = \begin{bmatrix} V_x \\ V_y \\ 0 \end{bmatrix}, \quad \boldsymbol{\nu}_c^b = \mathbf{J}^T(\psi)\mathbf{V}_c^n = \begin{bmatrix} V_x \cos(\psi) + V_y \sin(\psi) \\ -V_x \sin(\psi) + V_y \cos(\psi) \\ 0 \end{bmatrix} \tag{7.3a}$$

$$\dot{\mathbf{V}}_c^n = \begin{bmatrix} 0 \\ 0 \\ 0 \end{bmatrix}, \quad \dot{\boldsymbol{\nu}}_c^b = \left(\dot{\overbrace{\mathbf{J}(\psi)}}\right)^T \mathbf{V}_c^n = \begin{bmatrix} -rV_x \sin(\psi) + rV_y \cos(\psi) \\ -rV_x \cos(\psi) - rV_y \sin(\psi) \\ 0 \end{bmatrix} \tag{7.3b}$$

$$\boldsymbol{\nu}_r^b = \boldsymbol{\nu}^b - \boldsymbol{\nu}_c^b = \begin{bmatrix} u_r \\ v_r \\ r \end{bmatrix} = \begin{bmatrix} u - V_x \cos(\psi) - V_y \sin(\psi) \\ v + V_x \sin(\psi) - V_y \cos(\psi) \\ r \end{bmatrix} \tag{7.3c}$$

$$\dot{\boldsymbol{\nu}}_r^b = \dot{\boldsymbol{\nu}}^b - \dot{\boldsymbol{\nu}}_c^b = \begin{bmatrix} \dot{u} + rV_x \sin(\psi) - rV_y \cos(\psi) \\ \dot{v} + rV_x \cos(\psi) + rV_y \sin(\psi) \\ \dot{r} \end{bmatrix} \tag{7.3d}$$

The equation using these vectors and matrices is given in Eq.(2.25), and this 3-DOF model was used as the process plant model in the preliminary simulations. This is a more complex model than the control plant model, and a robust controller designed should ideally reach the control objective with this process model before doing physical field tests. In SINTEF's simulation tool, FhSim, a slightly more complex 6-DOF process plant model is used. The details of this process plant model are not considered in this thesis. However, some of the parameters such as damping and mass in 6-DOF are needed to set up the process plant model in FhSim.

7.1.2 Simplified Dynamic Positioning Model

For further simplification of the model, the low-frequency model of [5] is proposed as the first control plant model. The main assumption for this model is that the ROV is low-speed and is valid for low-speed manoeuvring up to approximately 2m/s according to [6, p. 152]. With only ocean current present in the system as a disturbance term, the bias term of [5] is replaced with a relative velocity vector $\boldsymbol{\nu}_r$ to model the effect of this disturbance on the system. In addition, the following assumption for damping is made:

Assumption 7.1. *The damping is linear to reduce the complexity of the controllers*

Remark 7.1. In general, the motion of an underwater vehicle moving at high speed will be highly nonlinear and coupled. However, in low-speed vehicles like an ROV, the nonlinearity can be neglected due of the effects of the coupled states are negligible. The assumption is a mild assumption for controller design since any nonlinear damping should enhance the directional stability of the vessel due to the nature of hydrodynamic damping forces. [13, 22].

The general kinetic equation Eq.(2.25) is therefore reduced to be on the form:

$$\mathbf{M}_{RB}\dot{\boldsymbol{\nu}}^b + \mathbf{M}_A\dot{\boldsymbol{\nu}}_r^b = \boldsymbol{\tau}^b - \mathbf{D}\boldsymbol{\nu}_r^b \tag{7.4}$$

Compared to the process plant, the main differences are that damping is assumed linear, and the Coriolis-centripetal forces are neglected. The values for the different matrices in this equation are identical to the matrices for the 3-DOF process plant model: Eq.(7.1)-(7.3). According to [6], the Coriolis-centripetal forces can be neglected when designing the DP control systems if the ocean currents are properly compensated, which the work for the controller in this thesis will.

7.1.3 Augmented Control Plant Model

Here the control plant model also take into account the Coriolis-centripetal forces, which it was believed from the preliminary simulations in [4] had a greater effect on heading of the ROV than anticipated. Assumption 7.1 is still assumed for this model. It is, more or less, an expansion of Eq.(7.4) by adding the Coriolis-centripetal forces to the model:

$$\mathbf{M}_{RB}\dot{\boldsymbol{\nu}}^b + \mathbf{M}_A\dot{\boldsymbol{\nu}}_r^b + \mathbf{C}_{RB}(\boldsymbol{\nu}^b)\boldsymbol{\nu}^b + \mathbf{C}_A(\boldsymbol{\nu}_r^b)\boldsymbol{\nu}_r^b = \boldsymbol{\tau}^b - \mathbf{D}\boldsymbol{\nu}_r^b \tag{7.5}$$

Compared to the process plant model, the main difference is that damping is assumed linear. The matrices are still defined as Eq.(7.1)-(7.3).

7.2 Actuation of Argus Mini ROV

The ROV is equipped with six azimuth thrusters that each can exert a force of approximately 120N in positive direction and 80N in opposite direction of the thrusters, according to thruster data obtained from testing of the ROV. Four of them are in the horizontal plane affecting surge, sway and yaw, and the remaining two thrusters affect heave. Relative to the CO at the body-fixed coordinate system, the four horizontal thrusters are located at the ROV according to Table 7.1. The thruster positions are taken from [13] which is data from the same ROV that

	x_{l_i}	y_{l_i}	α_i
Thruster 1	0.202m	-0.216m	35°
Thruster 2	0.202m	0.216m	-35°
Thruster 3	-0.265m	0.195m	35°
Thruster 4	-0.265m	-0.195m	-35°

Table 7.1: Thruster allocations values

has been used in this thesis. The position of the locations of the horizontal working thrusters are visualized in Figure 7.1. The two heave thrusters are positioned

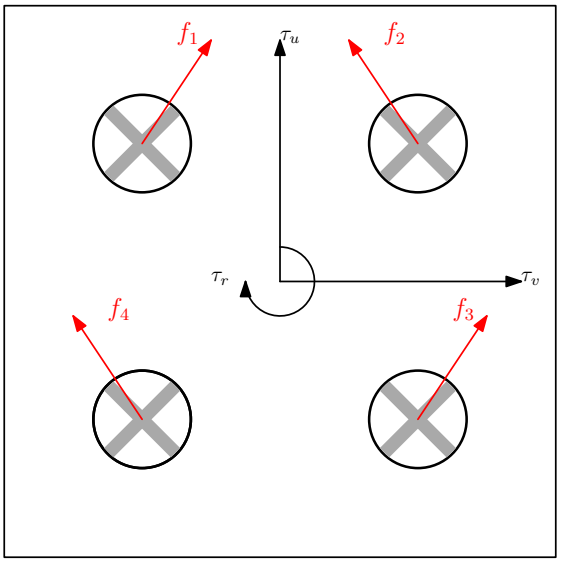

Figure 7.1: Horizontal thruster locations showing positive force direction

between the thrusters in fore and aft of the ROV and only works in vertical direction, they are not shown in Figure 7.1.

Using the control allocation matrix found in Section 2.8, the control inputs $\boldsymbol{\tau}$ can be transformed to the needed forces to be exerted from each thruster, which is each saturated, then transformed back to the control inputs to the plant model in a simulation.

Using the formulas from Section 2.8 for calculation of maximum thrust the ROV can give in each horizontal DOF, they resulted in the values given in Table 7.2.

	Upper limit	Lower limit
τ_u	393.19N	-262.13N
τ_v	229.43N	-229.43N
τ_r	120.9Nm	-120.9Nm

Table 7.2: The limits of actuation for Argus Mini ROV

Chapter 8

Introducing the First Controller

Based on the simplified DP model given by Eq.(7.4), which by all earmarks seems to be valid since the ROV is not able to reach velocities greater than 2m/s from the thrusters alone. It can be written on component form with the matrices and vectors from Eq.(7.1)-(7.3) as:

$$\begin{cases} m_{11}\dot{u} + m_{11}^{A} r(V_x \sin(\psi) - V_y \cos(\psi)) + d_{11}(u - V_x \cos(\psi) - V_y \sin(\psi)) = \tau_u \\ m_{22}\dot{v} + m_{22}^{A} r(V_x \cos(\psi) + V_y \sin(\psi)) + d_{22}(v + V_x \sin(\psi) - V_y \cos(\psi)) = \tau_v \\ m_{66}\dot{r} + d_{66} r = \tau_r \\ \dot{\psi} = r \end{cases}$$

Here it is used that $m_{ij} = m_{ij}^{RB} + m_{ij}^{A}$.

8.1 Proposal of the Controllers

8.1.1 Yaw Controller

Yaw is decoupled from velocities, so a PD-controller for heading from Section 3.1 with feed-forward can be implemented:

$$\tau_r = -k_{p_\psi}\widetilde{\psi} - k_{d_\psi}\widetilde{r} + m_{66}\dot{r}_d + d_{66} r_d \tag{8.1}$$

where the error terms are defined as:

$$\begin{aligned} \widetilde{\psi} &= \psi - \psi_d \\ \widetilde{r} &= r - r_d \end{aligned}$$

Insert for yaw and yaw rate, resulting in:

$$\begin{cases} m_{66}\dot{\widetilde{r}} + d_{66}\widetilde{r} + k_{p_\psi}\widetilde{\psi} + k_{d_\psi}\widetilde{r} = 0 \\ \dot{\widetilde{\psi}} = \widetilde{r} \end{cases}$$

$$\begin{bmatrix} \dot{\widetilde{r}} \\ \dot{\widetilde{\psi}} \end{bmatrix} = \begin{bmatrix} -\frac{d_{66}+k_{d_\psi}}{m_{66}} & -\frac{k_{p_\psi}}{m_{66}} \\ 1 & 0 \end{bmatrix} \begin{bmatrix} \widetilde{r} \\ \widetilde{\psi} \end{bmatrix} \tag{8.2}$$

Corollary 1. *Choose $k_{d_\psi} > 0 > -d_{66}$ and $k_{p_\psi} > 0$, then the equilibrium point at the origin of the closed-loop system Eq.(8.2) is uniformly globally exponentially stable (UGES).*

Proof. Calculating the eigenvalues λ as the zeros in the characteristic equation:

$$\lambda^2 + \frac{d_{66} + k_{d_\psi}}{m_{66}}\lambda + \frac{k_{p_\psi}}{m_{66}} = 0$$

with $k_{d_\psi} > 0 > -d_{66}$ and $k_{p_\psi} > 0$, the eigenvalues become strictly negative. Then, by Theorem 4.3 the origin of the closed-loop system for heading is UGES. Q.E.D.

Having a reference model for tracking of the desired heading ψ_d, results also in $r_d \to 0$ and $\dot{r}_d \to 0$ as $\psi \to \psi_d$. Note that due to how yaw and yaw angular rate is coupled then, $\psi \equiv \psi_d \implies r_d \equiv 0$.

8.1.2 Velocity Controllers

Assumption 8.1. ***UGES heading:*** *Heading of the ROV is such that $\psi = \psi_d \implies r = r_d = 0$*

Remark 8.1. The heading dynamics can be seen as an independent system in cascade with the velocities dynamics. When the origin of the heading dynamics is UGAS, with the proof of [24, 25], the interconnection of the cascade system is bounded, and the velocity dynamics are bounded, then the origin of the whole cascaded system is UGAS. This is utilized to prove that even with the heading dynamics, the origin of the cascade system is UGAS. The cascade system is illustrated in Figure 8.1.

With Assumption 8.1, the velocity equations can therefore be written as:

$$\begin{cases} m_{11}\dot{u} + d_{11}u - d_{11}(V_x\cos(\psi_d) + V_y\sin(\psi_d)) = \tau_u \\ m_{22}\dot{v} + d_{22}v + d_{22}(V_x\sin(\psi_d) - V_y\cos(\psi_d)) = \tau_v \end{cases}$$

Which can be rewritten to:

$$\begin{bmatrix} \dot{u} \\ \dot{v} \end{bmatrix} = \begin{bmatrix} \frac{\tau_u}{m_{11}} \\ \frac{\tau_v}{m_{22}} \end{bmatrix} - \begin{bmatrix} \frac{d_{11}}{m_{11}} & 0 \\ 0 & \frac{d_{22}}{m_{22}} \end{bmatrix} \begin{bmatrix} u \\ v \end{bmatrix} + \begin{bmatrix} \frac{d_{11}}{m_{11}}\cos(\psi_d) & \frac{d_{11}}{m_{11}}\sin(\psi_d) \\ -\frac{d_{22}}{m_{22}}\sin(\psi_d) & \frac{d_{22}}{m_{22}}\cos(\psi_d) \end{bmatrix} \begin{bmatrix} V_x \\ V_y \end{bmatrix} \tag{8.3}$$

The control law for the velocities can then be chosen as:

$$\boldsymbol{\tau}_2^b = \mathbf{D}_2\boldsymbol{v}_d + \mathbf{M}_2\dot{\boldsymbol{v}}_d - \mathbf{M}_2\mathbf{K}_{p_2}\widetilde{\boldsymbol{v}} - \mathbf{M}_2\mathbf{G}(t)\hat{\boldsymbol{V}}_c \tag{8.4}$$

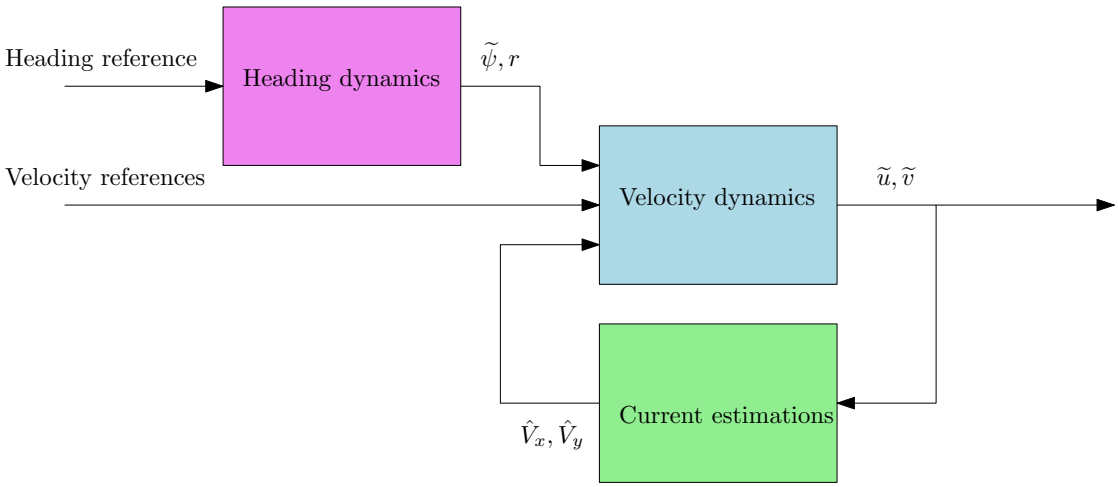

Figure 8.1: Closed-loop dynamics of horizontal system

where the vectors are defined as: $\boldsymbol{\tau}_2^b = [\tau_u, \tau_v]^T$, $\hat{\boldsymbol{V}}_c = [\hat{V}_x, \hat{V}_y]^T$, $\boldsymbol{v}_d = [u_d, v_d]^T$, $\dot{\boldsymbol{v}}_d = [\dot{u}_d, \dot{v}_d]^T$ and $\widetilde{\boldsymbol{v}} = [\widetilde{u}, \widetilde{v}]^T$. The matrices are defined as

$$\begin{aligned} \mathbf{D}_2 &= \begin{bmatrix} d_{11} & 0 \\ 0 & d_{22} \end{bmatrix}, \mathbf{M}_2 = \begin{bmatrix} m_{11} & 0 \\ 0 & m_{22} \end{bmatrix} \\ \mathbf{K}_{p_2} &= \begin{bmatrix} k_{p_u} & 0 \\ 0 & k_{p_v} \end{bmatrix}, \mathbf{G}(t) = \begin{bmatrix} \frac{d_{11}}{m_{11}} \cos(\psi_d) & \frac{d_{11}}{m_{11}} \sin(\psi_d) \\ -\frac{d_{22}}{m_{22}} \sin(\psi_d) & \frac{d_{22}}{m_{22}} \cos(\psi_d) \end{bmatrix} \end{aligned} \tag{8.5}$$

This control law summarized is a sum of feedforward terms, a P-controller and a term for handling the unknown ocean current.

With the error terms defined as:

$$\begin{aligned} \widetilde{u} &= u - u_d \\ \widetilde{v} &= v - v_d \\ \widetilde{V}_x &= V_x - \hat{V}_x \\ \widetilde{V}_y &= V_y - \hat{V}_y \end{aligned} \tag{8.6}$$

This results in the system for the velocities:

$$\dot{\widetilde{\boldsymbol{v}}} = -\boldsymbol{A}\widetilde{\boldsymbol{v}} + \mathbf{G}(t)\widetilde{\boldsymbol{V}}_c \tag{8.7}$$

where the vectors are defined as $\dot{\widetilde{\boldsymbol{v}}} = [\dot{\widetilde{u}}, \dot{\widetilde{v}}]^T$, $\widetilde{\boldsymbol{V}}_c = [\widetilde{V}_x, \widetilde{V}_y]^T$ and the matrix:

$$\boldsymbol{A} = \begin{bmatrix} \frac{d_{11}}{m_{11}} + k_{p_u} & 0 \\ 0 & \frac{d_{22}}{m_{22}} + k_{p_v} \end{bmatrix} \tag{8.8}$$

where it now becomes apparent that using the UGAS theorem [3] recited in Section 5.1, that the first term in the closed-loop system is $\boldsymbol{h}(\boldsymbol{x}_1, t) = -\boldsymbol{A}\widetilde{\boldsymbol{v}}$ and the second term is $\mathbf{G}(\boldsymbol{x}, t)\boldsymbol{x}_2$ in Eq.(5.1), by choosing: $\boldsymbol{x}_1 = \widetilde{\boldsymbol{v}}$, $\boldsymbol{x}_2 = \widetilde{\boldsymbol{V}}_c$, $\mathbf{G}(\boldsymbol{x}, t) = \mathbf{G}(t)$ and:

$$\begin{aligned} W(\boldsymbol{x}_1, t) &= \frac{1}{2}\widetilde{u}^2 + \frac{1}{2}\widetilde{v}^2 = \frac{1}{2}\boldsymbol{x}_1^T\boldsymbol{x}_1 \\ \left(\frac{\partial W(\boldsymbol{x}_1, t)}{\partial \boldsymbol{x}_1}\right)^T &= \begin{bmatrix}\widetilde{u} \\ \widetilde{v}\end{bmatrix} \end{aligned} \tag{8.9}$$

Which fulfills Assumption 5.2 of the theorem. It is therefore straightforward to see that the second equation of Eq.(5.1) becomes:

$$\dot{\widetilde{\boldsymbol{V}}}_c = -\boldsymbol{\Gamma}\mathbf{G}^T(t)\widetilde{\boldsymbol{v}}, \quad \boldsymbol{\Gamma} = \boldsymbol{\Gamma}^T > 0 \tag{8.10}$$

where $\boldsymbol{\Gamma}$ is a tuneable diagonal matrix. Recall that ocean current is assumed constant and irrotational so $\dot{\widetilde{V}}_x = -\dot{\hat{V}}_x$, $\dot{\widetilde{V}}_y = -\dot{\hat{V}}_y$.

Corollary 2. *Let $k_{p_u} > 0$ and $k_{p_v} > 0$, then the solutions $(\widetilde{u}, \widetilde{v}, \widetilde{V}_x, \widetilde{V}_y) \to 0$ uniformly globally asymptotically, and sufficiently close to the origin it converges locally uniformly and exponentially to the origin, according to [3].*

Proof. For the corollary to be true the two assumptions in Section 5.1 needs to be proven to hold. It can be easily seen that

$$\max\left\{\|\boldsymbol{h}(\boldsymbol{x}_1, t)\|, \left\|\frac{\partial W(\boldsymbol{x}_1, t)}{\partial \boldsymbol{x}_1}\right\|\right\} \leq \boldsymbol{\rho}_1(\|\boldsymbol{x}_1\|)\|\boldsymbol{x}_1\| \tag{8.11}$$

by for instance choosing $\boldsymbol{\rho}_1(\|\boldsymbol{x}_1\|) = k_1\|\boldsymbol{x}_1\|$ where it exists a $k_1 > 0$ to fulfill Eq.(8.11). Furthermore, the same can also be shown to also yields for $\max\{\|\mathbf{G}(\boldsymbol{x}, t)\|, \|\mathbf{G}_0(\boldsymbol{x}_2, t)\|\} \leq \boldsymbol{\rho}_2(\|\boldsymbol{x}\|)$ because it can be shown that they are upper bounded by a constant by looking at each elements independently. Here it is defined that $\mathbf{G}_0(\boldsymbol{x}_2, t) = \mathbf{G}(\boldsymbol{x}, t)|_{\boldsymbol{x}_1 = \mathbf{0}}$, where in this case is the same matrix.

At last, it can be shown that:

$$
\begin{aligned}
&\mathbf{G}_0(\boldsymbol{x}_2,t)^T\mathbf{G}_0(\boldsymbol{x}_2,t) = ... \\
&= \begin{bmatrix} \left(\frac{d_{11}}{m_{11}}\right)^2\cos^2(\psi_d) + \left(\frac{d_{22}}{m_{22}}\right)^2\sin^2(\psi_d) & \left(\left(\frac{d_{11}}{m_{11}}\right)^2 - \left(\frac{d_{22}}{m_{22}}\right)^2\right)\cos(\psi_d)\sin(\psi_d) \\ \left(\left(\frac{d_{11}}{m_{11}}\right)^2 - \left(\frac{d_{22}}{m_{22}}\right)^2\right)\cos(\psi_d)\sin(\psi_d) & \left(\frac{d_{11}}{m_{11}}\right)^2\sin^2(\psi_d) + \left(\frac{d_{22}}{m_{22}}\right)^2\cos^2(\psi_d) \end{bmatrix} \\
&= \begin{bmatrix} \left(\frac{d_{11}}{m_{11}}\right)^2\cos^2(\psi_d) + \left(\frac{d_{22}}{m_{22}}\right)^2\sin^2(\psi_d) & \frac{1}{2}\left(\left(\frac{d_{11}}{m_{11}}\right)^2 - \left(\frac{d_{22}}{m_{22}}\right)^2\right)\sin(2\psi_d) \\ \frac{1}{2}\left(\left(\frac{d_{11}}{m_{11}}\right)^2 - \left(\frac{d_{22}}{m_{22}}\right)^2\right)\sin(2\psi_d) & \left(\frac{d_{11}}{m_{11}}\right)^2\sin^2(\psi_d) + \left(\frac{d_{22}}{m_{22}}\right)^2\cos^2(\psi_d) \end{bmatrix} \\
&\geq b_m\mathbf{I}
\end{aligned}
$$

The inequality is interpreted as "$\mathbf{G}_0(\boldsymbol{x}_2,t)^T\mathbf{G}_0(\boldsymbol{x}_2,t)$ needs to be sufficiently positive definite". That means that by using Sylvester's criterion, inspection of principle minors can be calculated to check if it is positive definite. First principle minor is positive, being lower bounded by $\min\{(d_{11}/m_{11})^2, (d_{22}/m_{22})^2\}$. The second principle minor is calculated to be:

$$
\begin{aligned}
&|\mathbf{G}_0(\boldsymbol{x}_2,t)^T\mathbf{G}_0(\boldsymbol{x}_2,t)| = ... \\
&= \left(\left(\frac{d_{11}}{m_{11}}\right)^2\cos^2(\psi_d) + \left(\frac{d_{22}}{m_{22}}\right)^2\sin^2(\psi_d)\right)\left(\left(\frac{d_{11}}{m_{11}}\right)^2\sin^2(\psi_d) + \left(\frac{d_{22}}{m_{22}}\right)^2\cos^2(\psi_d)\right) \\
&\quad - \left(\left(\frac{d_{11}}{m_{11}}\right)^2 - \left(\frac{d_{22}}{m_{22}}\right)^2\right)^2\sin^2(\psi_d)\cos^2(\psi_d) \\
&= \left(\frac{d_{11}}{m_{11}}\right)^2\left(\frac{d_{22}}{m_{22}}\right)^2(\sin^4(\psi_d) + 2\cos^2(\psi_d)\sin^2(\psi_d) + \cos^4(\psi_d)) \\
&= \left(\frac{d_{11}}{m_{11}}\right)^2\left(\frac{d_{22}}{m_{22}}\right)^2(\sin^2(\psi_d) + \cos^2(\psi_d))^2 \\
&= \left(\frac{d_{11}}{m_{11}}\right)^2\left(\frac{d_{22}}{m_{22}}\right)^2 > 0
\end{aligned}
$$

This means that Assumption 5.1 holds.

Furthermore, it can be seen that:

$$
\begin{aligned}
W(\boldsymbol{x}_1,t) &= \frac{1}{2}\boldsymbol{x}_1^T\boldsymbol{x}_1 \\
&= \frac{1}{2}\|\boldsymbol{x}_1\|^2
\end{aligned}
\tag{8.12}
$$

which can be upper and lower bounded by class-κ_∞ functions on the form of for instance $\alpha(\|\boldsymbol{x}_1\|) = k\|\boldsymbol{x}_1\|^2$ for a $k > 0$. In addition it can also be shown that there exists a constant $c > 0$ such that:

$$\frac{\partial W(\boldsymbol{x}_1, t)}{\partial \boldsymbol{x}_1}\boldsymbol{h}(\boldsymbol{x}_1, t) = -\boldsymbol{x}_1^T \boldsymbol{A}\boldsymbol{x}_1 \leq -c\|\boldsymbol{x}_1\|^2 \tag{8.13}$$

This means that Assumption 5.2 also holds. Thus, since both assumptions for the Theorem 5.1 holds, then the corollary has been proven true. Q.E.D.

The controller was also derived in [4], and is repeated here for more thorough robustness analysis.

8.1.3 Summary of the Controller

To summarize the two control laws, the velocity controller can be written as:

$$\boldsymbol{\tau}_2^b = \mathbf{D}_2\boldsymbol{v}_d + \mathbf{M}_2\dot{\boldsymbol{v}}_d - \mathbf{M}_2\mathbf{K}_{p_2}\widetilde{\boldsymbol{v}} - \mathbf{M}_2\mathbf{G}(t)\hat{\boldsymbol{V}}_c \tag{8.14}$$

where the vectors are defined as: $\boldsymbol{\tau}_2^b = [\tau_u, \tau_v]^T$, $\hat{\boldsymbol{V}}_c = [\hat{V}_x, \hat{V}_y]^T$, $\boldsymbol{v}_d = [u_d, v_d]^T$, $\dot{\boldsymbol{v}}_d = [\dot{u}_d, \dot{v}_d]^T$ and $\widetilde{\boldsymbol{v}} = [\widetilde{u}, \widetilde{v}]^T$. The matrices are defined as:

$$\begin{aligned}
\mathbf{D}_2 &= \begin{bmatrix} d_{11} & 0 \\ 0 & d_{22} \end{bmatrix}, \mathbf{M}_2 = \begin{bmatrix} m_{11} & 0 \\ 0 & m_{22} \end{bmatrix} \\
\mathbf{K}_{p_2} &= \begin{bmatrix} k_{p_u} & 0 \\ 0 & k_{p_v} \end{bmatrix}, \mathbf{G}(t) = \begin{bmatrix} \frac{d_{11}}{m_{11}}\cos(\psi_d) & \frac{d_{11}}{m_{11}}\sin(\psi_d) \\ -\frac{d_{22}}{m_{22}}\sin(\psi_d) & \frac{d_{22}}{m_{22}}\cos(\psi_d) \end{bmatrix}
\end{aligned} \tag{8.15}$$

The heading controller can be written as:

$$\tau_r = -k_{p_\psi}\widetilde{\psi} - k_{d_\psi}\widetilde{r} + m_{66}\dot{r}_d + d_{66}r_d \tag{8.16}$$

The total control law inserted into the DP model Eq.(7.4) is then:

$$\boldsymbol{\tau}^b = \begin{bmatrix} \boldsymbol{\tau}_2^b \\ \tau_r \end{bmatrix} \tag{8.17}$$

This controller will from now on be called for C1.

8.2 Analysis of Controller Robustness

This section considers two factors for the robustness of the controller: the cascade system and the effects of modelling errors on the stability and robustness of the controller. For the cascade system, more specific the interconnection is analyzed to

make sure that the theorems from [24, 25] holds. Modelling errors are well known from, for instance, [5], are always to some degree present.

The velocity and heading dynamics in cascade can be written on the closed-loop system form:

$$\Sigma_1 : \begin{cases} m_{11}\dot{\widetilde{u}} + (d_{11} + k_{p_u} m_{11})\widetilde{u} - d_{11}\widetilde{V}_x \cos(\psi_d) - d_{11}\widetilde{V}_y \sin(\psi_d) + \boldsymbol{V}_c^T \boldsymbol{\phi}_u \boldsymbol{\theta} = 0 \\ m_{22}\dot{\widetilde{v}} + (d_{22} + k_{p_v} m_{22})\widetilde{v} + d_{22}\widetilde{V}_x \sin(\psi_d) - d_{22}\widetilde{V}_y \cos(\psi_d) + \boldsymbol{V}_c^T \boldsymbol{\phi}_v \boldsymbol{\theta} = 0 \\ \dot{\widetilde{\boldsymbol{V}}}_c = -\boldsymbol{\Gamma}\mathbf{G}(t)^T \widetilde{\boldsymbol{v}} \end{cases}$$

$$\Sigma_2 : \begin{cases} \dot{\widetilde{r}} = -\frac{d_{66}+k_{d_\psi}}{m_{66}}\widetilde{r} - \frac{k_{p_\psi}}{m_{66}}\widetilde{\psi} \\ \dot{\widetilde{\psi}} = \widetilde{r} \end{cases}$$

where $\boldsymbol{\theta} = [r, \widetilde{\psi}]^T$, $\boldsymbol{V}_c = [V_x, V_y]^T$, $\widetilde{\boldsymbol{V}}_c = [\widetilde{V}_x, \widetilde{V}_y]^T$ and:

$$\boldsymbol{\phi}_u = \begin{bmatrix} m_{A11}\sin(\widetilde{\psi} + \psi_d) & -d_{11}\left(\cos(\psi_d)\frac{\cos(\widetilde{\psi})-1}{\widetilde{\psi}} - \sin(\psi_d)\frac{\sin(\widetilde{\psi})}{\widetilde{\psi}}\right) \\ m_{A11}\cos(\widetilde{\psi} + \psi_d) & -d_{11}\left(\sin(\psi_d)\frac{\cos(\widetilde{\psi})-1}{\widetilde{\psi}} + \cos(\psi_d)\frac{\sin(\widetilde{\psi})}{\widetilde{\psi}}\right) \end{bmatrix} \tag{8.18}$$

$$\boldsymbol{\phi}_v = \begin{bmatrix} -m_{A22}\cos(\widetilde{\psi} + \psi_d) & d_{22}\left(\sin(\psi_d)\frac{\cos(\widetilde{\psi})-1}{\widetilde{\psi}} + \cos(\psi_d)\frac{\sin(\widetilde{\psi})}{\widetilde{\psi}}\right) \\ m_{A22}\sin(\widetilde{\psi} + \psi_d) & -d_{22}\left(\cos(\psi_d)\frac{\cos(\widetilde{\psi})-1}{\widetilde{\psi}} - \sin(\psi_d)\frac{\sin(\widetilde{\psi})}{\widetilde{\psi}}\right) \end{bmatrix} \tag{8.19}$$

The identities used to obtain the terms connected to r in the matrices for $\boldsymbol{\phi}_i$, where $i = \{u, v\}$, are given in Appendix A. An illustration of the cascade system is shown in Figure 8.2.

The possible singularity for $\widetilde{\psi} \to 0$ in $\boldsymbol{\phi}_u, \boldsymbol{\phi}_v$ can be calculated, using L'Hôpital's rule, going to a value bounded in the interval $[-1, 1]$. For more details and proof about L'Hôpital's rule, the reader is referred to [26]. It has already been shown that the origin of the nominal system, in other words setting $r = \widetilde{\psi} = 0$, is UGAS. The second system, Σ_2, which is the input to Σ_1, has been shown to have an origin that is UGES, including UGAS. The last assumption that needs to hold for the theorem in [25] is that the interconnection is bounded. Then by inspecting each element in both $\boldsymbol{\phi}$ separately it is apparent that the matrices are bounded by the constants $m_{11}^A, m_{22}^A, d_{11}, d_{22}$ since the varying variables are bounded by $\cos(\cdot)$ and $\sin(\cdot)$ in the interval of -1 and 1. Therefore the last assumption on the interconnection is fulfilled, and the origin of the cascade system can therefore be concluded to be UGAS.

For robustness despite perturbation, looking at the closed-loop velocity dynam-

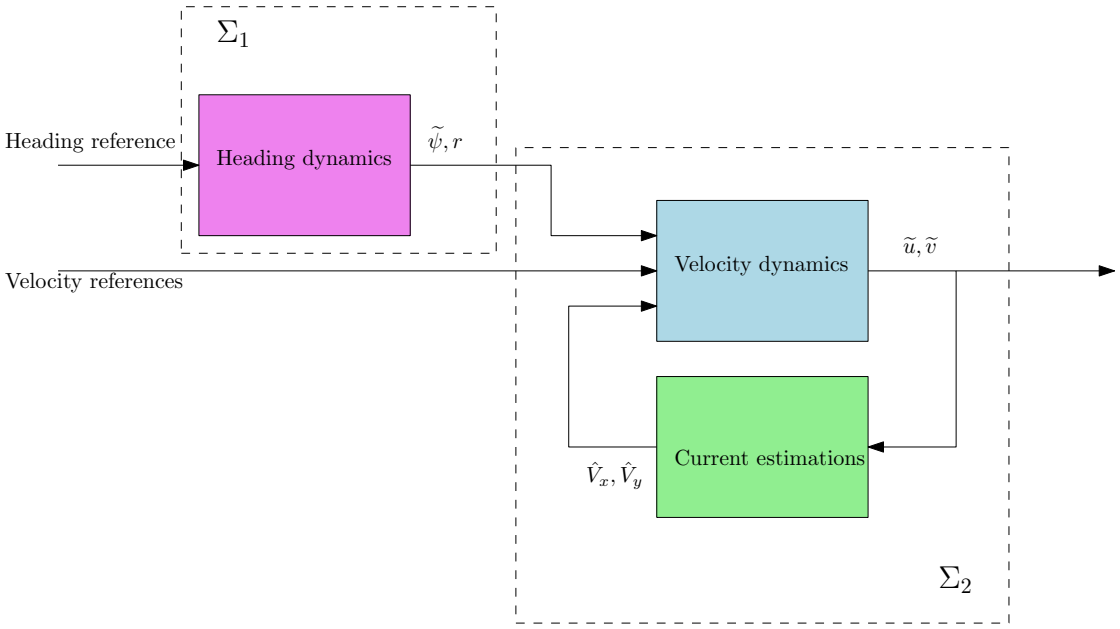

Figure 8.2: Cascaded system of heading and velocities

ics with the assumption that the error in yaw is 0:

$$\begin{aligned} \dot{\widetilde{\boldsymbol{v}}} &= -\boldsymbol{A}\widetilde{\boldsymbol{v}} + \mathbf{G}(t)\widetilde{\boldsymbol{V}}_c \\ \dot{\widetilde{\boldsymbol{V}}}_c &= -\boldsymbol{\Gamma}\mathbf{G}^T(t)\widetilde{\boldsymbol{v}} \end{aligned} \tag{8.20}$$

Then, if the control plant model has modelling error in the form of for instance that the mass or damping in system is too high or low then these modelling errors can be seen as perturbations on the system. With these modelling errors the system can always be written as a sum of the correct system and a term of modelling errors. Let the closed-loop system system Eq.(8.20) be the nominal system $\boldsymbol{f}(\boldsymbol{x})$, and the perturbation term added to this be $\boldsymbol{g}(\boldsymbol{x})$. Earlier it has been proven using [3] that the origin of the closed-loop system Eq.(8.20) is UGAS and ULES. Thus it can be shown that it exists a strict Lyapunov function $V(\mathbf{x})$ that fulfills

$$\begin{aligned} k_1\|\boldsymbol{x}\|^2 \leq V(\boldsymbol{x}) \leq k_2\|\boldsymbol{x}\|^2 \\ \frac{\partial V}{\boldsymbol{x}}\boldsymbol{f}(\boldsymbol{x}) \leq -k_3\|\boldsymbol{x}\|^2 \\ \left\|\frac{\partial V}{\partial \boldsymbol{x}}\right\| \leq k_4\|\boldsymbol{x}\| \end{aligned}$$

in a domain $\mathbf{D} \subseteq \mathbb{R}^n$ with $k_1, k_2, k_3, k_4 > 0$ for $\boldsymbol{x} = \begin{bmatrix} \widetilde{u} & \widetilde{v} & \widetilde{r} & \widetilde{\psi} \end{bmatrix}^T$. Then if the perturbation term is bounded such that

$$\|\boldsymbol{g}(\boldsymbol{x})\| \leq \gamma \|\boldsymbol{x}\| \forall \boldsymbol{x} \in \mathbf{D}$$
$$\gamma < \frac{k_3}{k_4}$$

then the origin of the perturbed system is still exponentially stable in $\mathbf{D}$ as stated in Lemma 4.3 given in Chapter 4.

8.3 Other Limitations

One major limitation of this controller is integrator windup. Studying the control law for the velocities, a parallel to a PI-controller can be drawn. Table 3.1 shows that the PI-controller can be written on the form

$$\tau = -K_p e - K_i \int_0^t e dt \tag{8.21}$$

or another way to write the same equation is:

$$\begin{aligned} \tau &= -K_p e - K_i z \\ \dot{z} &= e \end{aligned} \tag{8.22}$$

Comparing this Eq.(8.22) to the control law for C1, Eq.(8.4) for velocities, the first and second terms can be seen as the feed-forward terms, the third term as the proportional part or "$K_p e$", and the last term is the integration part or "$K_i z$". As mentioned in Section 2.8, the physical ROV has limitations on the actuation, and thrusters becoming saturated might become a problem for the integration term of the controllers. This is a well-known problem called integrator windup and occurs when actuators become saturated, and if not taken into account, the integration term in the controller might cause oscillatory solutions and yield problematic behaviour [27]. There is, therefore, necessary to implement anti-windup schemes to avoid integrator windup.

Two well-known anti-windup schemes are clamping and back calculations. The main difference is that clamping stops the integrator when it is detected that the actuation is in saturation, and back calculations subtract the overshooting saturation value from the actual controller output in the integrator. For more details and an example of how back calculations can be implemented, the reader is referred to [28]. In this thesis, clamping for the anti-windup scheme is utilized. By using

Table 7.2, an approximation of the saturation limits for the thrusters can be used to detect whether or not the integration term should be clamped or not.

Another tool that is utilized in this thesis alongside clamping to avoid integrator-windup is projection. Because the integrator in this case can also be seen as an estimation of the ocean current velocities, utilizing they are variables that are bounded and will physically not become larger than some given value, projection can be used to bound the integration term. In this thesis the following equation are used to bound $\hat{V}_x$ and $\hat{V}_y$ separately:

$$\begin{aligned} \dot{\hat{V}}_i &= \mathbf{\Gamma}_i \text{Proj}\left(\hat{V}_i, \mathbf{G}(\mathbf{x}, t)^T \widetilde{\boldsymbol{v}}\right) \\ \text{Proj}(\hat{V}_i, y) &\triangleq \begin{cases} y & \text{if} \quad g(\hat{V}_i) < 0 \vee g(\hat{V}_i) \geq 0 \wedge \nabla g^T y \leq 0 \\ y - \frac{\nabla g \nabla g^T y g(\hat{V}_i)}{\|\nabla g\|^2} & \text{if} \quad g(\hat{V}_i) \geq 0 \wedge \nabla g^T y > 0 \end{cases} \\ g(\hat{V}_i) &= \frac{(\epsilon_{V_i} + 1)\hat{V}_i^T \hat{V}_i - \hat{V}_{\max}^2}{\epsilon_{V_i} \hat{V}_{\max}^2} \end{aligned} \tag{8.23}$$

where $g(\hat{\theta})$ is a smooth function, and ϵ_θ and $\hat{V}_{\max}$ are tuning parameters, where $\hat{V}_{\max}$ is the boundary value. This equation is taken from [29], and implemented for bounding the integrator such that windup is prevented. The projection operator is separately implemented for the estimations $\hat{V}_i$ in each direction $i = \{x, y\}$.

Another limitation of the controller is that the physical ROV has limited bandwidth. It is, therefore, often desirable to smooth out the reference values so that the references do not act like a step-response causing oscillatory behaviour of the system states. Smoothing is done by using a reference model, which in this thesis will be a first-order reference model for the velocities and a third-order reference model for the heading. They are made with the dynamics of the differential equation

$$T\dot{u}_d + u_d = u_r \tag{8.24}$$

where u_r is the step response to be smoothed out, and $\dot{u}_d$ and u_d are the dynamics, u_d is u_r smoothed out with a time constant of $T > 0$. This model is also used for the sway reference. For the heading, a mass-spring-damper system is used for the reference model:

$$\ddot{\psi}_d + 2\omega_n \zeta \dot{\psi}_d + \omega_n^2 \psi_d = \psi_r \tag{8.25}$$

The reason for the choices of these reference models is to smooth out the reference signal and get feed-forward variables that can be used to achieve trajectory tracking. The controllers should also work even without these reference models, but then the feed-forward terms will all have to be turned off or set to 0. The reader

is referred to [6] to read more about reference models. Note that in this whole section about the reference model, abuse of notation occurs since u_r, v_r, ψ_r, are used for the reference values to be smoothed out. In this thesis, especially u_r and v_r are used as relative velocities, but in this section only, they are used to separate the desired reference values into the reference model and the desired values from the reference models inputs.

Chapter 9

Expanding the Controller

The linear dynamic positioning model used in the previous chapter is a simplified model that holds under the assumptions that have been given for neglecting different terms. However, is it possible to design a controller that has stability properties for a model closer to the process plant model? Especially when the Coriolis-centripetal force is modelled, which causes a constant deviation in the heading. In this chapter, the theorem and ideas used to derive the velocity controllers in Chapter 8 are expanded to consider this effect, especially in heading, and attempt to suppress the deviation.

9.1 Control Plant Model

To develop this controller, the control plant model used in previous chapter given in Eq.(7.4) is expanded to the model in Eq.(7.5) from Section 7.1.3, which in component form is given as:

$$\begin{cases} m_{11}\dot{u} + m_{11}^A r(V_x \sin(\psi) - V_y \cos(\psi)) \\ \qquad + d_{11}(u - V_x \cos(\psi) - V_y \sin(\psi)) - m_{22} vr - m_{22}^A r(V_x \sin(\psi) - V_y \cos(\psi)) = \tau_u \\ m_{22}\dot{v} + m_{22}^A r(V_x \cos(\psi) + V_y \sin(\psi)) \\ \qquad + d_{22}(v + V_x \sin(\psi) - V_y \cos(\psi)) + m_{11} ur - m_{11}^A r(V_x \cos(\psi) + V_y \sin(\psi)) = \tau_v \\ m_{66}\dot{r} + d_{66} r + (m_{22} - m_{11}) uv + (m_{22}^A - m_{11}^A)(\boldsymbol{v}^T \boldsymbol{\phi}(\psi) \boldsymbol{V}_c - \frac{1}{2} \boldsymbol{V}_c^T \boldsymbol{\phi}(2\psi) \boldsymbol{V}_c) = \tau_r \\ \dot{\psi} = r \end{cases}$$

where it is defined that: $\boldsymbol{V}_c = \begin{bmatrix} V_x & V_y \end{bmatrix}^T$, $\boldsymbol{v} = \begin{bmatrix} u & v \end{bmatrix}^T$ and

$$\boldsymbol{\phi}(x) = \begin{bmatrix} \sin(x) & -\cos(x) \\ -\cos(x) & -\sin(x) \end{bmatrix} \tag{9.1}$$

Rewrite the equations using the error terms

$$\widetilde{u} = u - u_d \Leftrightarrow u = \widetilde{u} + u_d, \quad \dot{\widetilde{u}} = \dot{u} - \dot{u}_d \Leftrightarrow \dot{u} = \dot{\widetilde{u}} + \dot{u}_d \tag{9.2}$$

$$\widetilde{v} = v - v_d \Leftrightarrow v = \widetilde{v} + v_d, \quad \dot{\widetilde{v}} = \dot{v} - \dot{v}_d \Leftrightarrow \dot{v} = \dot{\widetilde{v}} + \dot{v}_d \tag{9.3}$$

$$\widetilde{\psi} = \psi - \psi_d \Leftrightarrow \psi = \widetilde{\psi} + \psi_d, \quad \dot{\widetilde{\psi}} = \dot{\psi} - \dot{\psi}_d \Leftrightarrow \dot{\psi} = \dot{\widetilde{\psi}} + \dot{\psi}_d \tag{9.4}$$

$$\dot{\widetilde{r}} = \dot{r} - \dot{r}_d \Leftrightarrow \dot{r} = \dot{\widetilde{r}} + \dot{r}_d \tag{9.5}$$

Then each degree of freedom is looked at separately to derive the control law.

9.1.1 Deriving Controller for DOF 1 Surge

For surge, rewritten with error terms, the equation is now:

$$\begin{aligned} &m_{11}\dot{\widetilde{u}} + m_{11}^A r(V_x \sin(\psi) - V_y \cos(\psi)) + d_{11}(\widetilde{u} - V_x \cos(\psi) - V_y \sin(\psi)) - m_{22}\widetilde{v}\widetilde{r} \\ &-m_{22}^A r(V_x \sin(\psi) - V_y \cos(\psi)) + m_{11}\dot{u}_d + d_{11}u_d - m_{22}(\widetilde{v}r_d + \widetilde{r}v_d + v_d r_d) = \tau_u \end{aligned}$$

Set $\begin{bmatrix} V_x & V_y \end{bmatrix}^T = \mathbf{0}$ and choose control based on feedback linearization to achieve UGES response.

$$\tau_u = m_{11}\dot{u}_d + d_{11}u_d - m_{22}vr - m_{11}k_{p_u}\widetilde{u}$$

The system is now

$$m_{11}\dot{\widetilde{u}} + d_{11}\widetilde{u} + m_{11}k_{p_u}\widetilde{u} = 0$$

which is UGES for $k_{p_u} > 0$. However since $\begin{bmatrix} V_x & V_y \end{bmatrix}^T \neq \mathbf{0}$, then the control law can be augmented to:

$$\begin{aligned} \tau_u = {} & m_{11}\dot{u}_d + d_{11}u_d - m_{22}vr - m_{11}k_{p_u}\widetilde{u} + m_{11}^A r(\hat{V}_x \sin(\psi) - \hat{V}_y \cos(\psi)) \\ & - m_{22}^A r(\hat{V}_x \sin(\psi) - \hat{V}_y \cos(\psi)) - d_{11}(\hat{V}_x \cos(\psi) + \hat{V}_y \sin(\psi)) \end{aligned} \tag{9.6}$$

which results in:

$$\begin{aligned} &m_{11}\dot{\widetilde{u}} + (m_{11}^A - m_{22}^A)r(\widetilde{V}_x \sin(\psi) - \widetilde{V}_y \cos(\psi)) + d_{11}\widetilde{u} \\ &\qquad - d_{11}(\widetilde{V}_x \cos(\psi) + \widetilde{V}_y \sin(\psi)) + m_{11}k_{p_u}\widetilde{u} = 0 \\ &\dot{\widetilde{u}} = -\left(\frac{d_{11}}{m_{11}} + k_{p_u}\right)\widetilde{u} + \frac{(m_{22}^A - m_{11}^A)}{m_{11}} r\left(\widetilde{V}_x \sin(\psi) - \widetilde{V}_y \cos(\psi)\right) \\ &\qquad + \frac{d_{11}}{m_{11}}\left(\widetilde{V}_x \cos(\psi) + \widetilde{V}_y \sin(\psi)\right) \end{aligned}$$

9.1.2 Deriving Controller for DOF 2 Sway

Then deriving the control law for sway, start with rewriting the equation using error terms:

$$\begin{aligned} &m_{22}\dot{\widetilde{v}} + m_{22}^A r(V_x\cos(\psi) + V_y\sin(\psi)) + d_{22}(\widetilde{v} + V_x\sin(\psi) - V_y\cos(\psi)) + m_{11}\widetilde{u}\widetilde{r} \\ &-m_{11}^A r(V_x\cos(\psi) + V_y\sin(\psi)) + m_{22}\dot{v}_d + d_{22}v_d + m_{11}(\widetilde{u}r_d + \widetilde{r}u_d + u_d r_d) = \tau_v \end{aligned}$$

Set $\begin{bmatrix} V_x & V_y \end{bmatrix}^T = \mathbf{0}$ and choose control based on feedback linearization to achieve UGES response.

$$\tau_v = m_{22}\dot{v}_d + d_{22}v_d + m_{11}ur - m_{22}k_{p_v}\widetilde{v}$$

The system is now

$$m_{22}\dot{\widetilde{v}} + d_{22}\widetilde{v} + m_{22}k_{p_v}\widetilde{v} = 0$$

which is UGES for $k_{p_v} > 0$. However, since $\begin{bmatrix} V_x & V_y \end{bmatrix}^T \neq \mathbf{0}$ then the control law can be augmented to

$$\begin{aligned} \tau_v = {} & m_{22}\dot{v}_d + d_{22}v_d + m_{11}ur - m_{22}k_{p_v}\widetilde{v} + m_{22}^A r(\hat{V}_x\cos(\psi) + \hat{V}_y\sin(\psi)) \\ & - m_{11}^A r(\hat{V}_x\cos(\psi) + \hat{V}_y\sin(\psi)) + d_{22}(\hat{V}_x\sin(\psi) - \hat{V}_y\cos(\psi)) \end{aligned} \tag{9.7}$$

which results in

$$\begin{aligned} m_{22}\dot{\widetilde{v}} + (m_{22}^A - m_{11}^A)r(\widetilde{V}_x\cos(\psi) + \widetilde{V}_y\sin(\psi)) + d_{22}\widetilde{v} & \\ + d_{22}(\widetilde{V}_x\sin(\psi) - \widetilde{V}_y\cos(\psi)) + m_{22}k_{p_v}\widetilde{v} = 0 & \\ \dot{\widetilde{v}} = -\left(\frac{d_{22}}{m_{22}} + k_{p_v}\right)\widetilde{v} - \frac{(m_{22}^A - m_{11}^A)}{m_{22}}r\left(\widetilde{V}_x\cos(\psi) + \widetilde{V}_y\sin(\psi)\right) & \\ - \frac{d_{22}}{m_{22}}\left(\widetilde{V}_x\sin(\psi) - \widetilde{V}_y\cos(\psi)\right) & \end{aligned}$$

9.1.3 Deriving Controller for DOF 6 Yaw

Likewise for yaw, start with rewriting the angular velocity and heading angle dynamics with error terms:

$$\begin{aligned} m_{66}\dot{\widetilde{r}} + d_{66}\widetilde{r} + (m_{22} - m_{11})uv + (m_{22}^A - m_{11}^A)(\boldsymbol{v}^T\boldsymbol{\phi}(\psi)\boldsymbol{V}_c - \frac{1}{2}\boldsymbol{V}_c^T\boldsymbol{\phi}(2\psi)\boldsymbol{V}_c) & \\ + m_{66}\dot{r}_d + d_{66}r_d = \tau_r & \end{aligned}$$

$$\dot{\widetilde{\psi}} = \widetilde{r}$$

Set $\begin{bmatrix} V_x & V_y \end{bmatrix}^T = \mathbf{0}$ and choose control based on feedback linearization to achieve UGES response.

$$\tau_r = m_{66}\dot{r}_d + d_{66}r_d + (m_{22} - m_{11})uv - m_{66}k_{p_\psi}\widetilde{\psi} - m_{66}k_{d_\psi}\widetilde{r}$$

The system is now

$$\begin{aligned} m_{66}\dot{\widetilde{r}} + d_{66}\widetilde{r} + m_{66}k_{p_\psi}\widetilde{\psi} + m_{66}k_{d_\psi}\widetilde{r} = 0 \\ \dot{\widetilde{\psi}} = \widetilde{r} \end{aligned}$$

Which is UGES for $k_{p_\psi} > 0$ and $k_{d_\psi} > 0 > -d_{66}$. However, since $\begin{bmatrix} V_x & V_y \end{bmatrix}^T \neq 0$ then the control law can be augmented to

$$\begin{aligned} \tau_r = m_{66}\dot{r}_d + d_{66}r_d + (m_{22} - m_{11})uv - m_{66}k_{p_\psi}\widetilde{\psi} - m_{66}k_{d_\psi}\widetilde{r} \\ +(m_{22}^A - m_{11}^A)\boldsymbol{v}^T\boldsymbol{\phi}(\psi)\hat{\boldsymbol{V}}_c - \frac{1}{2}(m_{22}^A - m_{11}^A)\hat{\boldsymbol{V}}_c^T\boldsymbol{\phi}(2\psi)\hat{\boldsymbol{V}}_c \end{aligned} \tag{9.8}$$

Use the control law found for yaw rate and define

$$\widetilde{\mathbf{e}} = \begin{bmatrix} \widetilde{e}_1 \\ \widetilde{e}_2 \\ \widetilde{e}_3 \end{bmatrix} = \begin{bmatrix} V_x^2 - \hat{V}_x^2 \\ V_xV_y - \hat{V}_x\hat{V}_y \\ V_y^2 - \hat{V}_y^2 \end{bmatrix} \tag{9.9}$$

then with the control law inserted, the closed-loop system becomes:

$$\begin{aligned} m_{66}\dot{\widetilde{r}} + d_{66}\widetilde{r} + m_{66}k_{d_\psi}\widetilde{r} + m_{66}k_{p_\psi}\widetilde{\psi} + (m_{22}^A - m_{11}^A)\left(\boldsymbol{v}^T\boldsymbol{\phi}(\psi)\widetilde{\boldsymbol{V}}_c + \widetilde{\mathbf{e}}^T\boldsymbol{\alpha}_e\right) = 0 \\ \dot{\widetilde{r}} = -\left(\frac{d_{66}}{m_{66}} + k_{d_\psi}\right)\widetilde{r} - k_{p_\psi}\widetilde{\psi} - \frac{(m_{22}^A - m_{11}^A)}{m_{66}}\boldsymbol{v}^T\boldsymbol{\phi}(\psi)\widetilde{\boldsymbol{V}}_c - \frac{m_{22}^A - m_{11}^A}{m_{66}}\widetilde{\mathbf{e}}^T\boldsymbol{\alpha}_e \end{aligned}$$

and

$$\dot{\widetilde{\psi}} = \widetilde{r}$$

where it is also defined that

$$\boldsymbol{\alpha}_e = \begin{bmatrix} -\frac{1}{2}\sin(2\psi) \\ \cos(2\psi) \\ \frac{1}{2}\sin(2\psi) \end{bmatrix} \tag{9.10}$$

To collect the control laws derived for the ROV, Eq.(9.6)-(9.8), on the horizontal plane, it can be written as:

$$\boldsymbol{\tau}^b = \mathbf{M}\dot{\boldsymbol{\nu}}_d + \mathbf{D}\boldsymbol{\nu}_d + \boldsymbol{s} + \hat{\boldsymbol{a}} - \mathbf{M}\mathbf{K}\widetilde{\boldsymbol{\nu}}_{\text{aug}} - \mathbf{M}_{\text{aug}}\mathbf{G}(\mathbf{x}, t)\hat{\boldsymbol{V}}_c \tag{9.11}$$

Where the vectors are defined as: $\dot{\boldsymbol{\nu}}_d = [\dot{u}_d, \dot{v}_d, \dot{r}_d]^T$, $\boldsymbol{\nu}_d = [u_d, v_d, r_d]^T$, $\widetilde{\boldsymbol{\nu}}_{\text{aug}} = [\widetilde{u}, \widetilde{v}, \widetilde{r}, \widetilde{\psi}]^T$. The feedback linearization vector is defined as:

$$\boldsymbol{s} = \begin{bmatrix} -m_{22}vr \\ m_{11}ur \\ (m_{22} - m_{11})uv \end{bmatrix} \tag{9.12}$$

and the last vector for handling the quadratic unknown terms are defined as:

$$\hat{\boldsymbol{a}} = \begin{bmatrix} 0 \\ 0 \\ \frac{1}{2}(m_{22}^A - m_{11}^A)(-\widehat{V_x^2}\sin(2\psi) + 2\widehat{V_x V_y}\cos(2\psi) + \widehat{V_y^2}\sin(2\psi)) \end{bmatrix} \tag{9.13}$$

the matrices are defined as:

$$\begin{aligned} \mathbf{M} = \begin{bmatrix} m_{11} & 0 & 0 \\ 0 & m_{22} & 0 \\ 0 & 0 & m_{66} \end{bmatrix}, \mathbf{M}_{\text{aug}} = \begin{bmatrix} m_{11} & 0 & 0 & 0 \\ 0 & m_{22} & 0 & 0 \\ 0 & 0 & m_{66} & 0 \end{bmatrix} \\ \mathbf{D} = \begin{bmatrix} d_{11} & 0 & 0 \\ 0 & d_{22} & 0 \\ 0 & 0 & d_{66} \end{bmatrix}, \mathbf{K} = \begin{bmatrix} k_{p_u} & 0 & 0 & 0 \\ 0 & k_{p_v} & 0 & 0 \\ 0 & 0 & k_{d_\psi} & k_{p_\psi} \end{bmatrix} \end{aligned} \tag{9.14}$$

and at last the $\mathbf{G}(\mathbf{x}, t)$ is defined here:

$$\begin{aligned} &\mathbf{G}(\mathbf{x}, t) = ... \\ &= \begin{bmatrix} \frac{(m_{22}^A - m_{11}^A)}{m_{11}} r\sin(\psi) + \frac{d_{11}}{m_{11}}\cos(\psi) & -\frac{(m_{22}^A - m_{11}^A)}{m_{11}} r\cos(\psi) + \frac{d_{11}}{m_{11}}\sin(\psi) \\ -\frac{(m_{22}^A - m_{11}^A)}{m_{22}} r\cos(\psi) - \frac{d_{22}}{m_{22}}\sin(\psi) & -\frac{(m_{22}^A - m_{11}^A)}{m_{22}} r\sin(\psi) + \frac{d_{22}}{m_{22}}\cos(\psi) \\ -\frac{(m_{22}^A - m_{11}^A)}{m_{66}}(u\sin(\psi) - v\cos(\psi)) & \frac{(m_{22}^A - m_{11}^A)}{m_{66}}(u\cos(\psi) + v\sin(\psi)) \\ 0 & 0 \end{bmatrix} \end{aligned} \tag{9.15}$$

This controller, Eq.(9.11) is from now on called C2. The adaptive laws that are utilized to obtain the estimations to be used in the control law are defined as:

$$\dot{\hat{\boldsymbol{V}}}_c = \boldsymbol{\Gamma}_1 \mathbf{G}^T(\mathbf{x}, t) \left(\frac{\partial W(\mathbf{x}_1, t)}{\partial \mathbf{x}_1} \right)^T \tag{9.16}$$

and for the quadratic error terms

$$\begin{bmatrix} \dot{\widehat{V_x^2}} \\ \dot{\widehat{V_x V_y}} \\ \dot{\widehat{V_y^2}} \end{bmatrix} = -\frac{m_{22}^A - m_{11}^A}{m_{66}} \boldsymbol{\Gamma}_2 \boldsymbol{\alpha}_e (m_{66}\widetilde{r} + \epsilon\widetilde{\psi}) \tag{9.17}$$

9.2 Stability Analysis

The closed-loop system can be written in full as:

$$
\begin{bmatrix} \dot{\widetilde{u}} \\ \dot{\widetilde{v}} \\ \dot{\widetilde{r}} \\ \dot{\widetilde{\psi}} \end{bmatrix} = \begin{bmatrix} -\left(\frac{d_{11}}{m_{11}} + k_{p_u}\right)\widetilde{u} + \frac{(m_{22}^A - m_{11}^A)}{m_{11}} r \left(\widetilde{V}_x \sin(\psi) - \widetilde{V}_y \cos(\psi)\right) \\ \qquad\qquad + \frac{d_{11}}{m_{11}} \left(\widetilde{V}_x \cos(\psi) + \widetilde{V}_y \sin(\psi)\right) \\ -\left(\frac{d_{22}}{m_{22}} + k_{p_v}\right)\widetilde{v} - \frac{(m_{22}^A - m_{11}^A)}{m_{22}} r \left(\widetilde{V}_x \cos(\psi) + \widetilde{V}_y \sin(\psi)\right) \\ \qquad\qquad - \frac{d_{22}}{m_{22}} \left(\widetilde{V}_x \sin(\psi) - \widetilde{V}_y \cos(\psi)\right) \\ -\left(\frac{d_{66}}{m_{66}} - k_{p_\psi}\widetilde{\psi} + k_{d_\psi}\right)\widetilde{r} - \frac{(m_{22}^A - m_{11}^A)}{m_{66}} \boldsymbol{v}^T \boldsymbol{\phi}(\psi) \widetilde{\boldsymbol{V}}_c - \frac{m_{22}^A - m_{11}^A}{m_{66}} \widetilde{\mathbf{e}}^T \boldsymbol{\alpha}_e \\ \qquad\qquad \widetilde{r} \end{bmatrix}
$$

$$
= \begin{bmatrix} -\left(\frac{d_{11}}{m_{11}} + k_{p_u}\right)\widetilde{u} \\ -\left(\frac{d_{22}}{m_{22}} + k_{p_v}\right)\widetilde{v} \\ -\left(\frac{d_{66}}{m_{66}} + k_{d_\psi}\right)\widetilde{r} - k_{p_\psi}\widetilde{\psi} \\ \widetilde{r} \end{bmatrix}
$$

$$
+ \begin{bmatrix} 0 \\ 0 \\ -\frac{m_{22}^A - m_{11}^A}{2m_{66}} \left(-e_1 \sin(2\psi) + 2e_2 \cos(2\psi) + e_3 \sin(2\psi)\right) \\ 0 \end{bmatrix}
$$

$$
+ \begin{bmatrix} \frac{(m_{22}^A - m_{11}^A)}{m_{11}} r \sin(\psi) + \frac{d_{11}}{m_{11}} \cos(\psi) & -\frac{(m_{22}^A - m_{11}^A)}{m_{11}} r \cos(\psi) + \frac{d_{11}}{m_{11}} \sin(\psi) \\ -\frac{(m_{22}^A - m_{11}^A)}{m_{22}} r \cos(\psi) - \frac{d_{22}}{m_{22}} \sin(\psi) & -\frac{(m_{22}^A - m_{11}^A)}{m_{22}} r \sin(\psi) + \frac{d_{22}}{m_{22}} \cos(\psi) \\ -\frac{(m_{22}^A - m_{11}^A)}{m_{66}} \left(u \sin(\psi) - v \cos(\psi)\right) & \frac{(m_{22}^A - m_{11}^A)}{m_{66}} \left(u \cos(\psi) + v \sin(\psi)\right) \\ 0 & 0 \end{bmatrix} \begin{bmatrix} \widetilde{V}_x \\ \widetilde{V}_y \end{bmatrix}
$$

$$
\begin{bmatrix} \dot{\widetilde{V}}_x \\ \dot{\widetilde{V}}_y \end{bmatrix} = -\boldsymbol{\Gamma}_1 \mathbf{G}(\mathbf{x}, t)^T \left(\frac{\partial W(\mathbf{x}_1, t)}{\partial \mathbf{x}_1}\right)^T, \quad \boldsymbol{\Gamma}_1 = \boldsymbol{\Gamma}_1^T > 0
$$

Where $\mathbf{G}(\mathbf{x},t)$ is defined as in previous section, and the following vectors are defined:

$$\mathbf{x}_1 = \begin{bmatrix} \widetilde{u} \\ \widetilde{v} \\ \widetilde{r} \\ \widetilde{\psi} \end{bmatrix}, \quad \mathbf{x}_2 = \begin{bmatrix} \widetilde{V}_x \\ \widetilde{V}_y \end{bmatrix},$$
$$\mathbf{h}(\mathbf{x}_1,t) = \begin{bmatrix} -\left(\frac{d_{11}}{m_{11}} + k_{p_u}\right)\widetilde{u} \\ -\left(\frac{d_{22}}{m_{22}} + k_{p_v}\right)\widetilde{v} \\ -\left(\frac{d_{66}}{m_{66}} + k_{d_\psi}\right)\widetilde{r} - k_{p_\psi}\widetilde{\psi} \\ \widetilde{r} \end{bmatrix}, \quad \boldsymbol{\sigma}(\mathbf{x}_1,\widetilde{\mathbf{e}}) = \begin{bmatrix} 0 \\ 0 \\ -\frac{m_{22}^A - m_{11}^A}{m_{66}}\widetilde{\mathbf{e}}^T\boldsymbol{\alpha}_e \\ 0 \end{bmatrix} \tag{9.18}$$

and in addition, define:

$$\begin{aligned} W(\mathbf{x}_1,t) &= \frac{1}{2}m_{11}\tilde{u}^2 + \frac{1}{2}m_{22}\tilde{v}^2 + \frac{1}{2}m_{66}\tilde{r}^2 + \frac{1}{2}m_{66}k_{p_\psi}\tilde{\psi}^2 + \epsilon\tilde{\psi}\tilde{r} \\ &= \frac{1}{2}\begin{bmatrix}\mathbf{x}_{11}^T & \mathbf{x}_{12}^T\end{bmatrix}\begin{bmatrix}\mathbf{P}_1 & \mathbf{0}_{2\times2} \\ \mathbf{0}_{2\times2} & \mathbf{P}_2\end{bmatrix}\begin{bmatrix}\mathbf{x}_{11} \\ \mathbf{x}_{12}\end{bmatrix} \\ \frac{\partial W(\mathbf{x}_1,t)}{\partial \mathbf{x}_1} &= \begin{bmatrix} m_{11}\widetilde{u} \\ m_{22}\widetilde{v} \\ m_{66}\widetilde{r} + \epsilon\widetilde{\psi} \\ m_{66}k_{p_\psi}\widetilde{\psi} + \epsilon\widetilde{r} \end{bmatrix} \end{aligned} \tag{9.19}$$

where $\mathbf{x}_{11} = [\tilde{u},\tilde{v}]^T$, $\mathbf{x}_{12} = [\tilde{r},\tilde{\psi}]^T$, $\mathbf{P}_1 = \text{diag}\{m_{11}, m_{22}\}$, and $\mathbf{P}_2 = \begin{bmatrix} m_{66} & \epsilon \\ \epsilon & m_{66}k_{p_\psi} \end{bmatrix}$.

9.2.1 Stability Proof

Theorem 9.1. *The origin of* $\mathbf{x} = [\mathbf{x}_1^T, \mathbf{x}_2^T, \mathbf{e}^T]^T$ *is UGS.*

Proof. Choose the Lyapunov function candidate:

$$V(\mathbf{x}) = W(\mathbf{x}_1,t) + \frac{1}{2}\mathbf{x}_2^T\boldsymbol{\Gamma}_1^{-1}\mathbf{x}_2 + \frac{1}{2}\widetilde{\mathbf{e}}^T\boldsymbol{\Gamma}_2^{-1}\widetilde{\mathbf{e}} > 0 \forall \mathbf{x} \neq \mathbf{0}, \boldsymbol{\Gamma}_1^T = \boldsymbol{\Gamma}_1 > 0, \boldsymbol{\Gamma}_2^T = \boldsymbol{\Gamma}_2 > 0$$

where the inequality holds if $\mathbf{P}_2$ is positive definite, which it is when $-m_{66}\sqrt{k_{p_\psi}} < \epsilon < m_{66}\sqrt{k_{p_\psi}}$. In addition, V is radially unbounded since $V \to \infty$ when $\|\mathbf{x}\| \to \infty$, which can be shown by lower bounding the problematic term $W(\mathbf{x}_1,t)$ with $k_1\|\mathbf{x}_1\|^2$. Then calculate the time derivative along the trajectories of the system

and check if it is negative semi-definite.

$$
\begin{aligned}
\dot{V}(\mathbf{x}) &= \frac{\partial W(\mathbf{x}_1,t)}{\partial \mathbf{x}_1}\left(\mathbf{h}(\mathbf{x}_1)+\mathbf{G}(\mathbf{x},t)\mathbf{x}_2+\boldsymbol{\sigma}(\mathbf{x}_1,\widetilde{\mathbf{e}})\right)\\
&\quad+\mathbf{x}_2^T\boldsymbol{\Gamma}_1^{-1}\dot{\mathbf{x}}_2+\widetilde{\mathbf{e}}^T\boldsymbol{\Gamma}_2^{-1}\dot{\widetilde{\mathbf{e}}}\\
&= \frac{\partial W(\mathbf{x}_1,t)}{\partial \mathbf{x}_1}\left(\mathbf{h}(\mathbf{x}_1)+\mathbf{G}(\mathbf{x},t)\mathbf{x}_2\right)-\frac{m_{22}^A-m_{11}^A}{m_{66}}(m_{66}\tilde{r}+\epsilon\tilde{\psi})\widetilde{\mathbf{e}}^T\boldsymbol{\alpha}_e\\
&\quad-\mathbf{x}_2^T\mathbf{G}(\mathbf{x},t)^T\left(\frac{\partial W(\mathbf{x}_1,t)}{\partial \mathbf{x}_1}\right)^T+\widetilde{\mathbf{e}}^T\boldsymbol{\Gamma}_2^{-1}\dot{\widetilde{\mathbf{e}}}\\
&= -\mathbf{x}_{11}^T\begin{bmatrix}d_{11}+m_{11}k_{p_u} & 0\\ 0 & d_{22}+m_{22}k_{p_v}\end{bmatrix}\mathbf{x}_{11}\\
&\quad-\mathbf{x}_{12}^T\begin{bmatrix}d_{66}+m_{66}k_{d_\psi}-\epsilon & \frac{1}{2}\epsilon(\frac{d_{66}}{m_{66}}+k_{d_\psi})\\ \frac{1}{2}\epsilon(\frac{d_{66}}{m_{66}}+k_{d_\psi}) & k_{p_\psi}\epsilon\end{bmatrix}\mathbf{x}_{12}\\
&\quad+\widetilde{\mathbf{e}}^T\boldsymbol{\Gamma}_2^{-1}\left(\dot{\widetilde{\mathbf{e}}}-\frac{m_{22}^A-m_{11}^A}{m_{66}}(m_{66}\tilde{r}+\epsilon\tilde{\psi})\boldsymbol{\Gamma}_2\boldsymbol{\alpha}_e\right)\\
&= -\mathbf{x}_{11}^T\begin{bmatrix}d_{11}+m_{11}k_{p_u} & 0\\ 0 & d_{22}+m_{22}k_{p_v}\end{bmatrix}\mathbf{x}_{11}\\
&\quad-\mathbf{x}_{12}^T\begin{bmatrix}d_{66}+m_{66}k_{d_\psi}-\epsilon & \frac{1}{2}\epsilon(\frac{d_{66}}{m_{66}}+k_{d_\psi})\\ \frac{1}{2}\epsilon(\frac{d_{66}}{m_{66}}+k_{d_\psi}) & k_{p_\psi}\epsilon\end{bmatrix}\mathbf{x}_{12}\\
&= -\mathbf{x}_1^T\boldsymbol{H}\mathbf{x}_1
\end{aligned}
$$

where it is defined that:

$$
\boldsymbol{H}=\begin{bmatrix}d_{11}+m_{11}k_{p_u} & 0 & 0 & 0\\ 0 & d_{22}+m_{22}k_{p_v} & 0 & 0\\ 0 & 0 & d_{66}+m_{66}k_{d_\psi}-\epsilon & \frac{1}{2}\epsilon(\frac{d_{66}}{m_{66}}+k_{d_\psi})\\ 0 & 0 & \frac{1}{2}\epsilon(\frac{d_{66}}{m_{66}}+k_{d_\psi}) & k_{p_\psi}\epsilon\end{bmatrix} \tag{9.20}
$$

in addition to choosing the term:

$$
\dot{\widetilde{\mathbf{e}}}\triangleq\boldsymbol{\Gamma}_2\boldsymbol{\alpha}_e\frac{m_{22}^A-m_{11}^A}{m_{66}}(m_{66}\tilde{r}+\epsilon\tilde{\psi}) \tag{9.21}
$$

Then with some additional boundings on ϵ, it can be proven that the matrix $\boldsymbol{H}$ is positive definite and $\dot{V}\leq 0\forall\mathbf{x}$, and origin of the closed-loop system in the beginning of Section 9.2 is uniformly globally stable per Theorem 4.1. Q.E.D.

The following conditions must hold for ϵ for $\dot{V}$ to be negative semidefinite:

$$\begin{aligned} &\begin{bmatrix} d_{66} + m_{66}k_{d_\psi} - \epsilon & \frac{1}{2}\epsilon(\frac{d_{66}}{m_{66}} + k_{d_\psi}) \\ \frac{1}{2}\epsilon(\frac{d_{66}}{m_{66}} + k_{d_\psi}) & k_{p_\psi}\epsilon \end{bmatrix} > 0 \\ \implies &-\epsilon\left(\left(k_{p_\psi} + \frac{1}{4}\left(\frac{d_{66}}{m_{66}} + k_{d_\psi}\right)^2\right)\epsilon - (d_{66}k_{p_\psi} + m_{66}k_{p_\psi}k_{d_\psi})\right) > 0 \\ &\vee \epsilon < d_{66} + m_{66}k_{d_\psi} \end{aligned} \tag{9.22}$$

where the first condition of the two in Eq.(9.22) holds only when:

$$0 < \epsilon < \frac{d_{66}k_{p_\psi} + m_{66}k_{p_\psi}k_{d_\psi}}{k_{p_\psi} + \frac{1}{4}\left(\frac{d_{66}}{m_{66}} + k_{d_\psi}\right)^2} \tag{9.23}$$

It is easily seen that when Eq.(9.23) is fulfilled, the second condition $\epsilon < d_{66} + m_{66}k_{d_\psi}$ also holds since the far right side of the inequality in Eq.(9.23) is always smaller. Note to assure that V is positive definite, ϵ still needs needs to be so small such that $\epsilon < m_{66}\sqrt{k_{p_\psi}}$ if the right hand of the inequality Eq.(9.23) is larger than $m_{66}\sqrt{k_{p_\psi}}$.

When ϵ is bounded this way, there exists constants $c_1, c_2 > 0$ such that:

$$-c_1\|\mathbf{x}_1\|^2 \leq \dot{V}(\mathbf{x}) \leq -c_2\|\mathbf{x}_1\|^2 \leq 0 \forall \mathbf{x} \tag{9.24}$$

Then since $\dot{V} \leq 0$ and $V \geq 0$, V is lower and upper bounded by constants $0 \leq V_\infty < \infty$ and $0 \leq V_0 < \infty$, there exists a constant $c > 0$ such that

$$0 \leq c\lim_{T\to\infty}\int_0^T \|\mathbf{x}_1\|^2 dt \leq -\lim_{T\to\infty}\int_0^T \dot{V}dt \leq V_0 - V_\infty < \infty \tag{9.25}$$

Theorem 9.2. *The system given by*

$$\dot{\mathbf{x}}_1 = \begin{bmatrix} \dot{\tilde{u}} & \dot{\tilde{v}} & \dot{\tilde{r}} & \dot{\tilde{\psi}} \end{bmatrix}^T \tag{9.26}$$

and

$$\dot{\mathbf{x}}_2 = \begin{bmatrix} \dot{\tilde{V}}_x & \dot{\tilde{V}}_y \end{bmatrix}^T \tag{9.27}$$

converges asymptotically to the origin.

Proof. A result of Eq.(9.25) is that $\dot{V}, \mathbf{x}_1 \in \mathcal{L}_2$. Furthermore, due to V being bounded means that $V \in \mathcal{L}_\infty \implies \mathbf{x}_1, \mathbf{x}_2 \in \mathcal{L}_\infty$. Looking at the equations for $\dot{\mathbf{x}}_1$ it is straightforward to show that it is also bounded which means that $\dot{\mathbf{x}}_1 \in \mathcal{L}_\infty$.

Using this Lyapunov function, $\dot{V}$ can be used to construct the integral bound to utilize Lemma 4.2. Continuing with the Lyapunov function found earlier:

$$\dot{V} = -\mathbf{x}_1^T \boldsymbol{H} \mathbf{x}_1 + \mathbf{x}_1^T \mathbf{x}_1 - \mathbf{x}_1^T \mathbf{x}_1 \tag{9.28}$$

where $\boldsymbol{H}$ is positive definite matrix with the bounds for ϵ that was calculated earlier.

$$\dot{V} \leq -\mathbf{x}_1^T \boldsymbol{H} \mathbf{x}_1 - \mathbf{x}_1^T \mathbf{x}_1 + |\mathbf{x}_1||\mathbf{x}_1| \tag{9.29}$$

define $\rho(|\mathbf{x}|)$ which is a κ_∞-function that bounds higher order terms of the system that comes from the fact that the origin of the full closed-loop system being stable and $\mathbf{x} \in \mathcal{L}_\infty$. This function $\rho(|\mathbf{x}|)$ can be written as a function of the number R that depends on the ball with radius $\boldsymbol{r}$ that is bounding the initial states of $\mathbf{x}$.

Using this it can be written to

$$\begin{aligned} \dot{V} &\leq -\phi_1(t,\mathbf{x})^2 + |\mathbf{x}_1|\rho(R(\boldsymbol{r})) \\ &\leq -\phi_1(t,\mathbf{x})^2 + \frac{1}{\epsilon_\rho}|\mathbf{x}_1|^2 + \epsilon_\rho \rho(R(\boldsymbol{r}))^2, \forall |\mathbf{x}_0| \leq \boldsymbol{r} \end{aligned} \tag{9.30}$$

Where ϵ_ρ is just an arbitrarily small number and $\phi_1(t,\mathbf{x})^2 = \mathbf{x}_1^T \boldsymbol{H} \mathbf{x}_1 + \mathbf{x}_1^T \mathbf{x}_1$. The last inequality step is just a result of Young's inequality. Defining:

$$\nu := \epsilon_\rho \rho(R(\boldsymbol{r}))^2 \tag{9.31}$$

then,

$$\begin{aligned} \dot{V} &\leq -[\phi_1(t,\mathbf{x})^2 - \nu] + \frac{1}{\epsilon_\rho}|\mathbf{x}_1|^2 \\ \int_{t_0}^{\infty} [\phi_1(t,\mathbf{x})^2 - \nu] dt &\leq \int_{t_0}^{\infty} \frac{1}{\epsilon_\rho}|\mathbf{x}_1|^2 dt - \int_{t_0}^{\infty} \dot{V} dt \\ \int_{t_0}^{\infty} [\phi_1(t,\mathbf{x})^2 - \nu] dt &\leq \beta_{\boldsymbol{r}\nu} \end{aligned} \tag{9.32}$$

where it can be seen that $\beta_{\boldsymbol{r}\nu} > 0$ by choosing ϵ_ρ small enough. It has also in addition been shown that $\mathbf{x}_1, \dot{V} \in \mathcal{L}_2$ so the integrals are bounded, such that $\beta_{\boldsymbol{r}\nu}$ is bounded but still strictly positive. Then, it is on the form of Eq.(4.7) and therefore by Lemma 4.2, the state $\mathbf{x}_1$ converges to the origin uniformly, globally and asymptotically. Q.E.D.

Remark 9.1. It is important that the operator tuning k_{p_ψ}, k_{d_ψ} and ϵ choose them carefully such that Eq.(9.23) holds, to assure the origin of the solutions of the system ODEs are UGS.

Part IV

Results

Chapter 10

ROV Simulation Setup

In this chapter, the matrices used for the model of Argus Mini ROV are presented, and the setup for the ROV is used in simulations and experiments. It will also present the tools that are used during simulations.

10.1 ROV Model

The dimension of the ROV are $[0.9\text{m}, 0.65\text{m}, 0.5\text{m}]^T$, with the assumptions that vehicle is symmetric in all directions along the NED-axes, in addition to the CO being placed in the CG. The matrices that are used for the 6-DOF process model of the ROV are:

$$\mathbf{M}_{RB} = \begin{bmatrix} 90 & 0 & 0 & 0 & 0 & 0 \\ 0 & 90 & 0 & 0 & 0 & 0 \\ 0 & 0 & 90 & 0 & 0 & 0 \\ 0 & 0 & 0 & 10 & 0 & 0 \\ 0 & 0 & 0 & 0 & 15 & 0 \\ 0 & 0 & 0 & 0 & 0 & 13 \end{bmatrix} \tag{10.1}$$

which is the rigid body mass of the model. In addition, the zero-frequency added mass matrix in 6-DOF is given as:

$$\mathbf{M}_A = \begin{bmatrix} 54 & 0 & 0 & 0 & 0 & 0 \\ 0 & 72 & 0 & 0 & 0 & 0 \\ 0 & 0 & 360 & 0 & 0 & 0 \\ 0 & 0 & 0 & 11 & 0 & 0 \\ 0 & 0 & 0 & 0 & 43.5 & 0 \\ 0 & 0 & 0 & 0 & 0 & 5.2 \end{bmatrix} \tag{10.2}$$

The total mass matrix is defined as $\mathbf{M} = \mathbf{M}_{RB} + \mathbf{M}_A$. The linear damping matrix in 6-DOF is given as:

$$\mathbf{D} = \begin{bmatrix} 250 & 0 & 0 & 0 & 0 & 0 \\ 0 & 200 & 0 & 0 & 0 & 0 \\ 0 & 0 & 175 & 0 & 0 & 0 \\ 0 & 0 & 0 & 20 & 0 & 0 \\ 0 & 0 & 0 & 0 & 20 & 0 \\ 0 & 0 & 0 & 0 & 0 & 15 \end{bmatrix} \tag{10.3}$$

and the nonlinear matrix

$$\mathbf{D}_n(\boldsymbol{\nu}_r) = \begin{bmatrix} 350|u_r| & 0 & 0 & 0 & 0 & 0 \\ 0 & 350|v_r| & 0 & 0 & 0 & 0 \\ 0 & 0 & 400|w_r| & 0 & 0 & 0 \\ 0 & 0 & 0 & 100|p| & 0 & 0 \\ 0 & 0 & 0 & 0 & 100|q| & 0 \\ 0 & 0 & 0 & 0 & 0 & 75|r| \end{bmatrix} \tag{10.4}$$

The total damping matrix is given by $\mathbf{D}(\boldsymbol{\nu}_r) = \mathbf{D} + \mathbf{D}_n(\boldsymbol{\nu}_r)$.

The CB is located at $\boldsymbol{o}_b^b = \begin{bmatrix} 0 & 0 & -0.18 \end{bmatrix}^T$. The ratio between the weight and the buoyancy forces are given as $W/B = 0.99$. All the values for these 6-DOF model are used to set up the process plant model in SINTEFs ROV simulator FhSim.

To insert these parameters into the controller only the 3-DOF models of these matrices are necessary. To find these matrices, the 6-DOF matrices are reduced to their 3-DOF counter-part:

$$\mathbf{M}_{RB} = \begin{bmatrix} 90 & 0 & 0 \\ 0 & 90 & 0 \\ 0 & 0 & 13 \end{bmatrix} \tag{10.5}$$

The zero-frequency added mass matrix in 3-DOF:

$$\mathbf{M}_A = \begin{bmatrix} 54 & 0 & 0 \\ 0 & 72 & 0 \\ 0 & 0 & 5.2 \end{bmatrix} \tag{10.6}$$

The total mass matrix is as with the 6-DOF given by $\mathbf{M} = \mathbf{M}_{RB} + \mathbf{M}_A$. The linear damping matrix in 3-DOF is reduced to:

$$\mathbf{D} = \begin{bmatrix} 250 & 0 & 0 \\ 0 & 200 & 0 \\ 0 & 0 & 15 \end{bmatrix} \tag{10.7}$$

and the nonlinear damping matrix:

$$\mathbf{D}_n(\boldsymbol{\nu}_r) = \begin{bmatrix} 350|u_r| & 0 & 0 \\ 0 & 350|v_r| & 0 \\ 0 & 0 & 75|r| \end{bmatrix} \tag{10.8}$$

The coriolis-centripetal matrices for 3-DOF are calculated to be:

$$\begin{aligned} \mathbf{C}_{RB}(\boldsymbol{\nu}) &= \begin{bmatrix} 0 & 0 & -90v \\ 0 & 0 & 90u \\ 90v & -90u & 0 \end{bmatrix} \\ \mathbf{C}_A(\boldsymbol{\nu}_r) &= \begin{bmatrix} 0 & 0 & -72v_r \\ 0 & 0 & 54u_r \\ 72v_r & -54u_r & 0 \end{bmatrix} \end{aligned} \tag{10.9}$$

Last but not least, the thruster allocation matrix for 3-DOF is given by:

$$\mathbf{B} = \begin{bmatrix} \cos(35°) & \sin(35°) & 0.202\sin(35°) + 0.216\cos(35°) \\ \cos(-35°) & \sin(-35°) & 0.202\sin(-35°) - 0.216\cos(-35°) \\ \cos(35°) & \sin(35°) & -0.265\sin(35°) - 0.195\cos(35°) \\ \cos(-35°) & \sin(-35°) & -0.265\sin(-35°) + 0.195\cos(-35°) \end{bmatrix}^T \tag{10.10}$$

with the thruster force vector $\boldsymbol{f} = [f_1, f_2, f_3, f_4]^T$ numerated as the thrusters in Figure 7.1. The saturation of the actuations are given in Table 7.2, and are more like an upper limit. In practice if the ROV for instance are moving for instance 45° relative to the x-axis and y-axis in BODY-frame, the maximum actuation it can give in surge and sway will be lower.

10.1.1 Sensors

According to [9], the Argus Mini is equipped with five sensors: an HD camera, a fluxgate compass, a depth sensor, a gyroscope, and a Nortek DVL 1000 model. The velocity of the ROV is measured with the DVL, which will measure the speed relative to the net of the fish pen. The fish pen is attached to the seafloor, and the net can therefore be seen as an earth-fixed reference point the ROV measures its speed relative to. However, it is necessary to be aware that the velocities of the net do change with changing ocean current velocity. But, the change of the ocean current locally will be so slow that the dynamics of the net are more or less nonexistent and negligible.

10.1.2 Net Following Algorithm

To be able to measure the velocity of the ROV, the ROV has to traverse along with the net. Therefore, a net following algorithm calculating the velocity references

and heading reference is used to test the velocity and heading controllers. In short, the net following algorithm generates waypoints for the ROV to follow and ensures that the ROV always points towards the net. The objective of this net following algorithm is to follow the net pen at a constant speed and can be formalized as:

$$\lim_{t\to\infty} y_e(t) = 0 \tag{10.11}$$

$$\lim_{t\to\infty} (\psi(t) - \psi_d(t)) = 0 \tag{10.12}$$

$$\lim_{t\to\infty} (U(t) - U_d) = 0 \tag{10.13}$$

where $U \triangleq \sqrt{u^2 + v^2}$ is the ROV speed, and $U_d > 0$ is the desired speed, y_e cross-track error calculated in the algorithm generating waypoints to assure that the ROV also maintains a constant distance from the net pen. An illustration of this net following algorithm in work from a simulation in [9] is shown in Figure 10.1 where the yellow points are the ROV and its orientation at different time steps in the simulation.

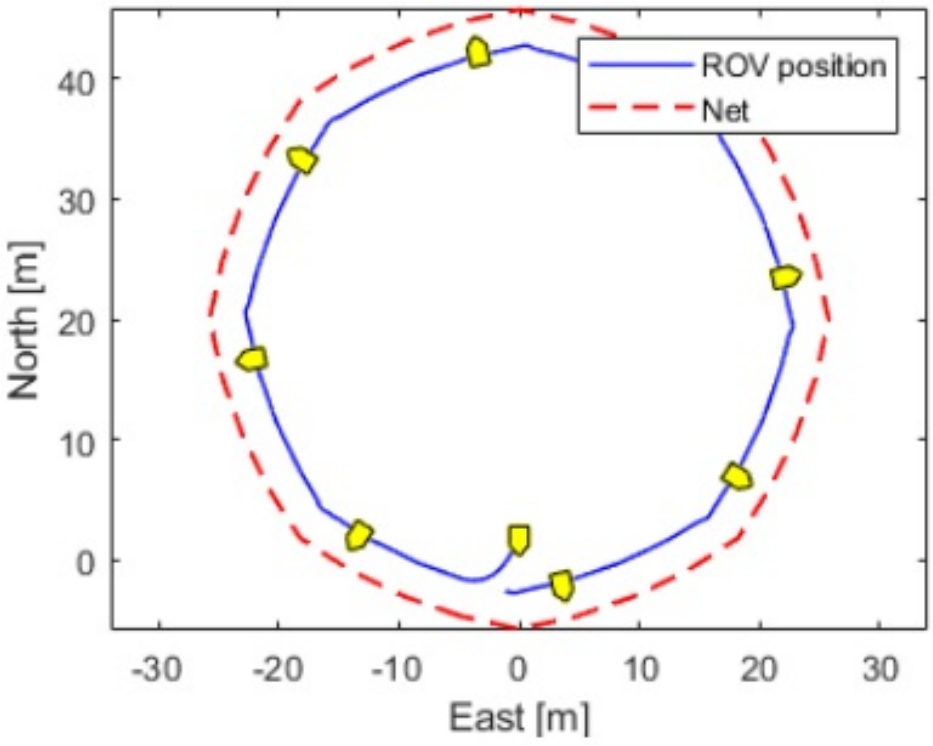

Figure 10.1: The simulation plot is taken from [9], and show how the ROV traverse the net pen with this algorithm

10.2 FhSim

The simulations conducted in this thesis are done in the SINTEF developed simulation platform for marine systems, FhSim. For a more detailed description of how FhSim is designed and works, the reader is referred to [30, 31].

FhSim is designed to solve ODEs and, more specifically, nonlinear ODEs. It is implemented in C++, and therefore makes it possible to develop and program object-oriented.

Each object in FhSim is implemented as what is called SimObjects, which are the fundament of FhSim. Each part of a physical system: Kalman filter, controllers, vehicle models, etc., is implemented as a SimObject. Each object is associated with a set of ODEs, which at each timestep transfers its state derivatives to an integrator. At the end of each timestep, the states are integrated based on a method that is chosen by the user [9].

To connect each SimObject to make up the whole ROV system, they have I/O

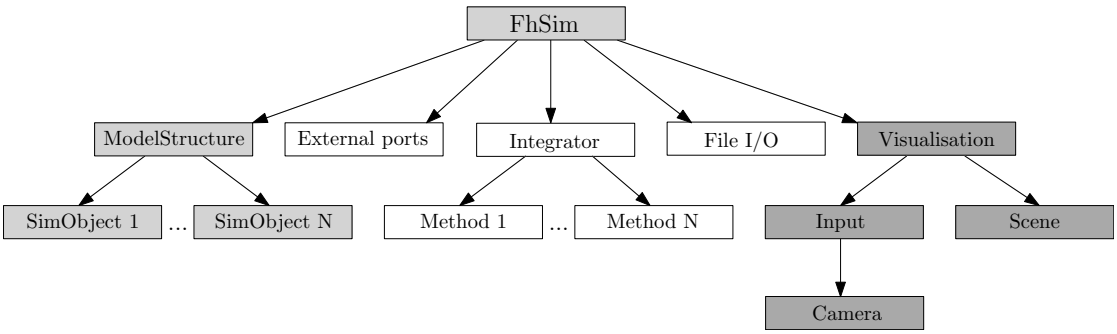

Figure 10.2: Overview of FhSim. Recreated from [30]

ports where the signal flows between the SimObjects as specified in an XML document the user sets up to connect the SimObjects. An overview of the architecture of FhSim is shown in Figure 10.2. The brilliant part of FhSim is that it can also communicate with external devices through a set of external ports. It is therefore not restricted to simulations but can be used in real-time hardware applications. The user can then easily go from simulation on the computer to a physical field test without changing the SimObject itself.

In the project for FhSim, several SimObjects have already been developed unrelated to this thesis, and through the structure of FhSim, many of these SimObjects were used during the simulations. Among these SimObjects that were used, like in

[9], was a 6-DOF ROV model, an environmental model, a static net cage structure, and heave and tilt controllers.

Chapter 11

Results for the First Controller (C1)

In this chapter, simulations and a brief discussion of the results for C1 are done. In addition, the results from the field experiments of the ROV at SINTEF ACE fish farm in Hitra are also presented and discussed. For this thesis, the most interesting states to look at will only be the states in the horizontal plane, that is, u, v, r, ψ. The testing of the velocity controllers are done using the net following algorithm that gives heading and surge and sway velocity references.

11.1 Simulation Results

The velocity controllers are tuned with the values given in Table 11.1 In addition

	Tuning	Description
k_{p_u}	4.0	Proportional gain for surge
k_{p_v}	4.0	Proportional gain for sway
γ_x	3.5	Integrator tuning for $\hat{V}_x$
γ_y	3.0	Integrator tuning for $\hat{V}_y$
ϵ_{V_i}	0.2	Projection tolerance
$V_{\max}$	0.5	Max Ocean velocity bound
T_u	0.5	Time constant reference model surge
T_v	0.5	Time constant reference model sway

Table 11.1: Controller simulation tuning parameters

to this tuning, the controller also had some parameters that were connected to the modelling of ROV, such as damping and mass coefficients. For testing of

robustness, the controller C1 is based on a control plant model with some modelling errors. It means, therefore, that the process plant model was set to have 10% higher damping coefficients than the damping coefficients the controller accounted for. The simulation was done going one round the fish pen once, and for the figures in this section only the timespan 200s − 400s of the simulation is shown.

11.1.1 Velocity Simulation Response

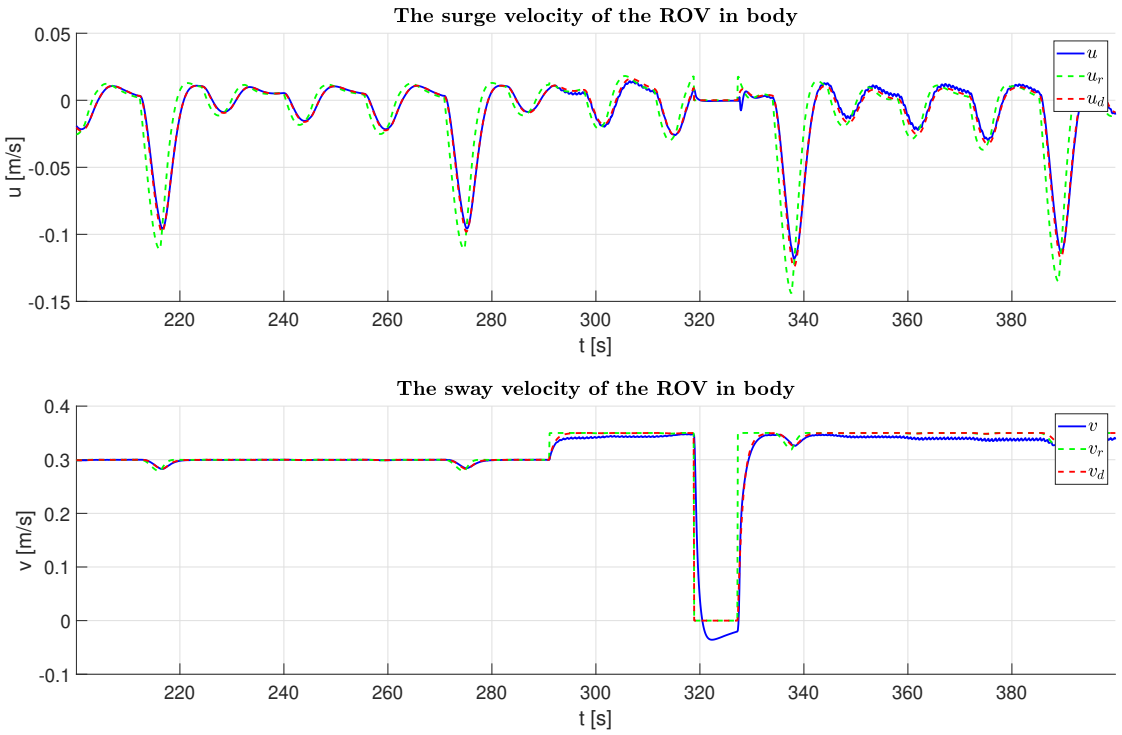

Figure 11.1: Surge and sway velocity responses where the process plant model had 10% higher damping than accounted for

In Figure 11.1, the green dotted lines are the reference values given by the net following algorithm, and the red dotted lines are the values given by the reference model. That is the green line smoothed out with the reference model. From this simulation, the control objective, which is to track the desired reference value, is to some extent fulfilled by the velocity controllers. At around 320s, the sway velocity overshoots when going from 0.35m/s to 0m/s; this might be due to the limitation of the thruster dynamics, which does not happen instantaneously. This will be closely looked at in the graphs for control inputs.

After 340s, especially sway velocity struggles to reach the desired reference value,

and frankly oscillates. This might suggest that the actuation has gone into saturation resulting in this response.

11.1.2 Velocity Actuation Response

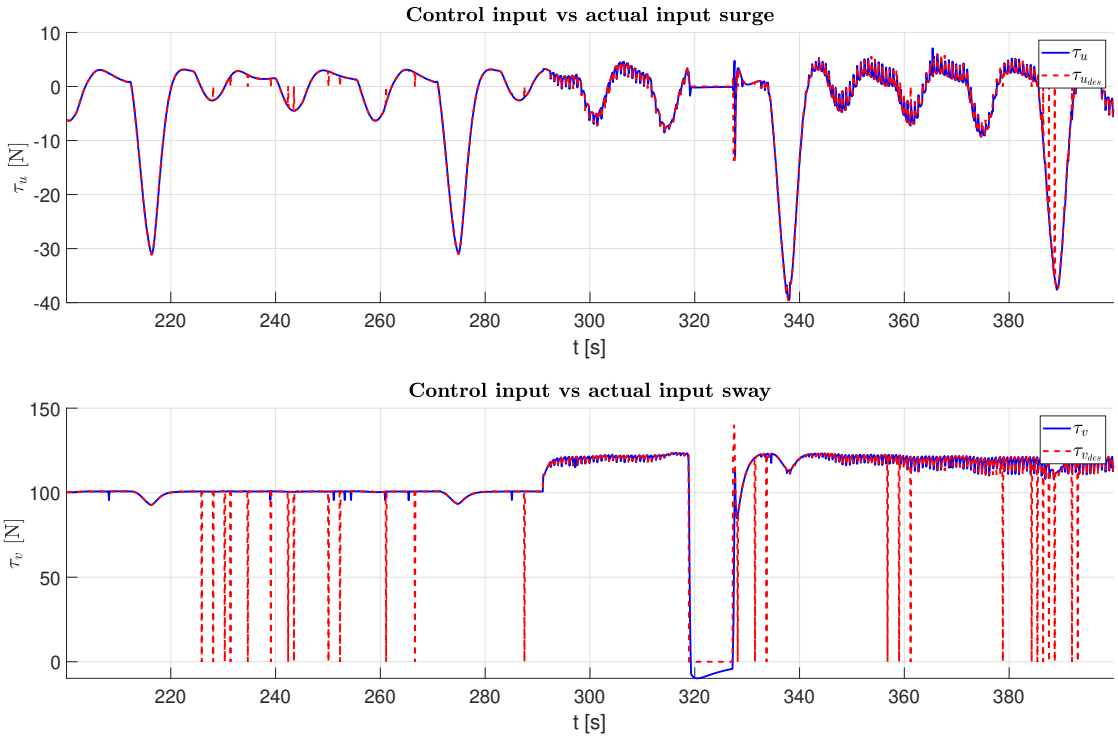

Figure 11.2: Actuation response for surge and sway

As suspected from the previous subsection, it is obvious in Figure 11.2 that the inputs to the ROV in surge and sway struggle at about 340s, but also in the area 290s − 320s. The red dotted lines here are the control law's desired control input, and the blue line is the actuation that the ROV gives. There are some spikes from the control input that go to 0 seemingly at random times, but this is the net following algorithm that is turning the velocity controller on and off so that the heading and speed controllers can, to some extent, work independently. The velocity controllers turning off is most likely why the ROV speed overshoots at 320s.

It might seem like the ROV manages to give the desired control input, but it oscillates, suggesting that the input goes into saturation, which should also be present in the integrator figures. It must be noted that in this simulation, the

operator attempts to push the control law to the limit. Under "normal" conditions, the controller had no problems achieving the control objective. However, the robustness of the controller can truly be tested when it is pushed to the cases where it is no longer "normal" conditions. The ROV is not actually intended to have a speed over 0.2m/s. Still, during these simulations, the speed was set to 0.35m/s, which might provoke some undesired behaviour that should be handled and taken into account in the software and simulations before testing it physically at the SINTEF Ace fish farm. Even though the speed might be set to a maximum of 0.2m/s, the ROV might even become saturated at a lower speed if there are much larger damping forces than accounted for in the ROV process model, as in this case. However, it is seen that even though the actuation goes into saturation, the closed-loop system is still stable, even though it does not reach the desired control references.

11.1.3 Ocean Current Estimations

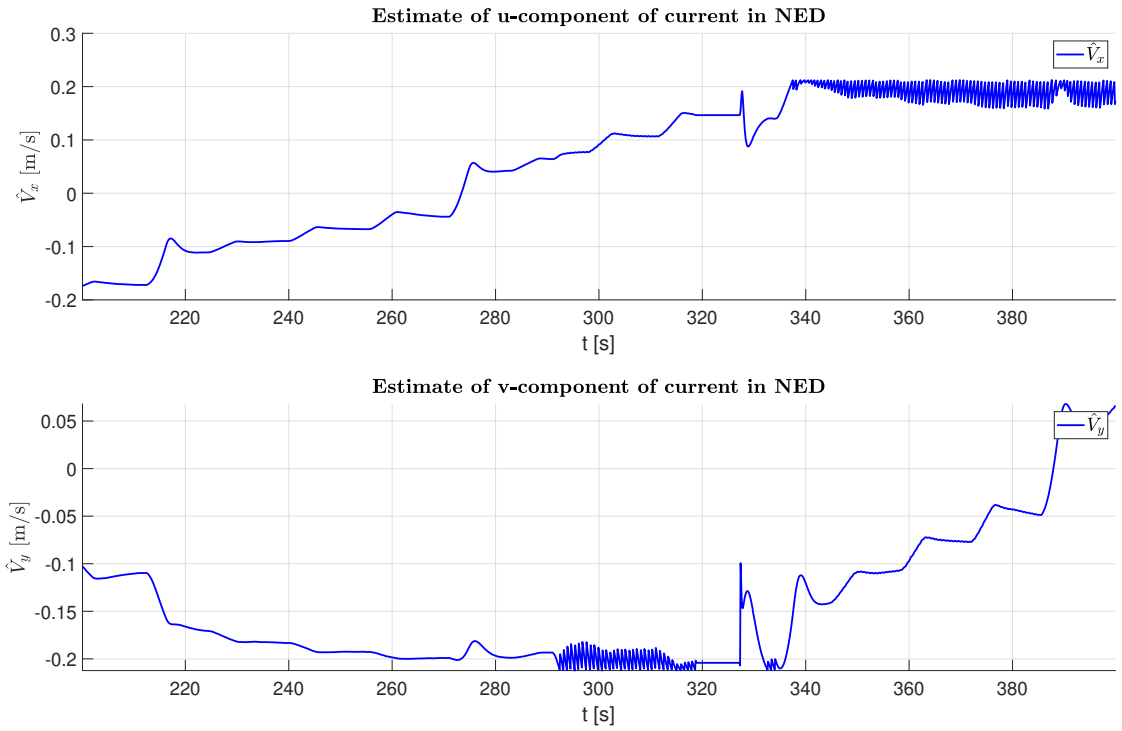

Figure 11.3: Integration terms behavior

From the estimates of the ocean current or the integration term, it can be seen that the projection operator is working to keep the estimates within a boundary. As expected, it starts to oscillate approximately simultaneously as the velocities

and the actuation begin to oscillate or go into saturation. For both components, it can be seen that they are to some extent kept within the bounds of ± 0.2m/s. How this connects to the tuning parameters of projection tolerance and max ocean velocity bound is not easy to say, but it seems like the projection operator tries to keep a leeway from the maximum bound with the tolerance value. Either way, this prevents integrator wind-up, which might have destabilized the closed-loop system if it became saturated over a longer period of time.

11.2 Field Testing Results

For the field testing, another tuning was used. Experiences show that some of the tuning parameters should be less aggressively tuned due to modelling errors. In this case, especially the gains connected to the current estimation or the integration terms were tuned less aggressively. Simulations showed that it was the integration term that was most prone to modelling errors, and it is therefore natural that it was tuned down from simulations. The tuning that was used for the experiments at the SINTEF ACE fish farm is given in Table 11.2. Since the recordings of the

	Tuning	Description
k_{p_u}	5.0	Proportional gain for surge
k_{p_v}	5.0	Proportional gain for sway
γ_x	2.0	Integrator tuning for $\hat{V}_x$
γ_y	2.0	Integrator tuning for $\hat{V}_y$
ϵ_{V_i}	1.0	Projection tolerance
$V_{\max}$	0.5	Upper bound for ocean velocity
T_u	1.0	Time constant reference model surge
T_v	1.0	Time constant reference model sway

Table 11.2: Tuning parameters for experiment number two

trials are not instantaneously starting the horizontal net following algorithm, only a timespan where it has started in the trial is shown. In this case the timespan $200\text{s} - 400\text{s}$ is shown for the figures from experimental field trial 2, which is one of the timespan where the horizontal net following is used.

11.2.1 Experimental Velocities Result

Like the simulations, in Figure 11.4, the blue lines are the velocities estimated with a Kalman Filter implemented in the ROV, the red line is the output of the reference model that smooths out the green dotted line, which is the output from

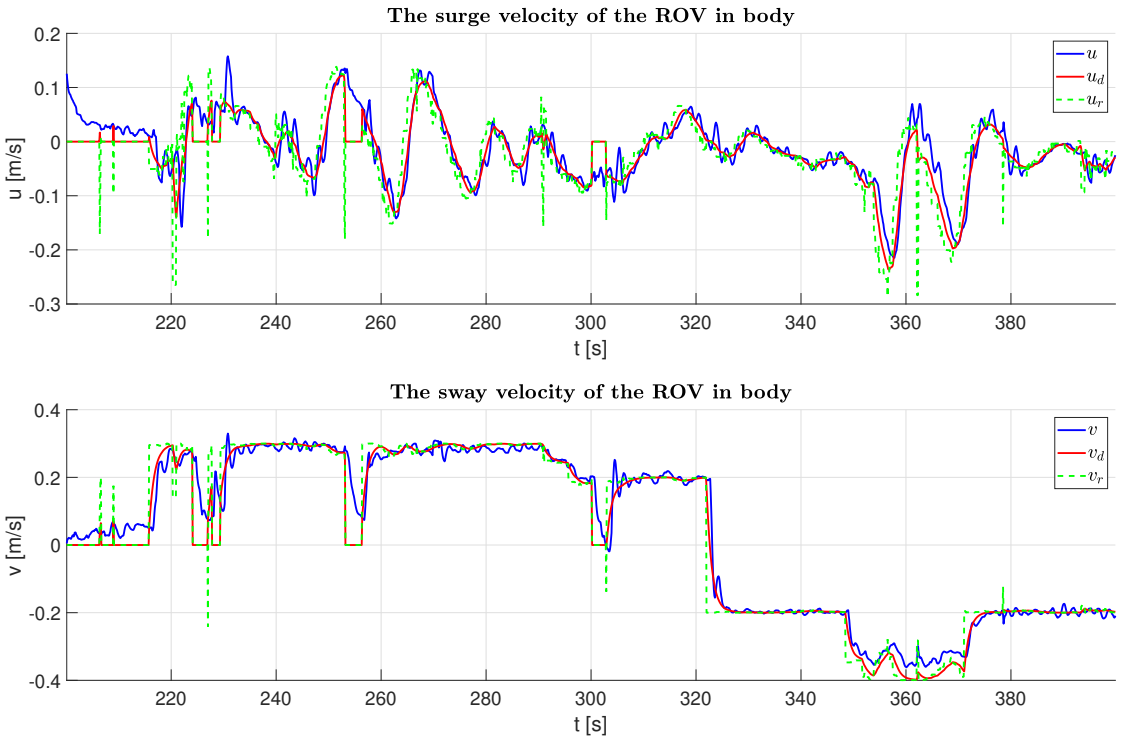

Figure 11.4: Velocity result from experiment trial 2 using C1

the net following algorithm. Note that at the beginning of this time series, the velocity references are close to 0, due to the net following algorithm not being active until somewhere about 220s. It can be seen that in the net following modus, the controllers follow the reference values pretty well. It oscillates around the reference value. However, this might be because other factors like the sensor measurements oscillate, and the Kalman Filter cannot sufficiently smooth the measurements. This is, however, still great results since it tracks the desired velocity with little to no deviation.

It is at the time 350s − 370s, the sway velocity, and to some extent, the surge velocity gets what seems like a constant deviation from the reference value. The figure shows that the reference model wants the ROV to go -0.4m/s in sway, which is at a higher speed than it has previously been assumed that the ROV can manage to go. This seems like in this timespan, the actuators of the ROV have gone into saturation which means it is actually not physically possible for the controller to reach the desired velocity. However, it does not oscillate like in the simulations, possibly caused by the real actuators having some dynamics, which works like a lowpass filter. Another possible explanation is that it is already oscillating, and it is just not as extreme as the simulations due to the dynamics of the thrusters. Yet,

another hypothesis for why it does not oscillate is that the velocity estimations was smoothed out by the output of the Kalman Filter.

In Figure 11.5 a standard PI controller runs in the same modus as with Figure 11.4.

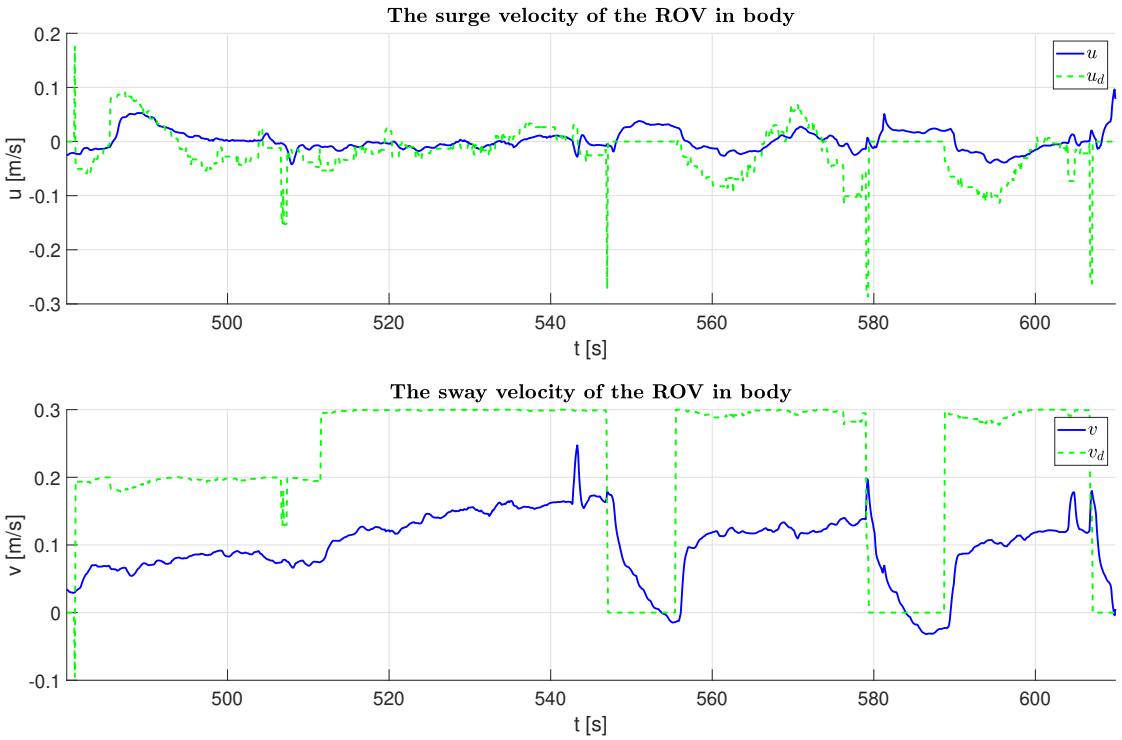

Figure 11.5: The velocity results from a standard PI controller at field testing

While the controller C1 manages to close the gap in sway with deviation of less than ±0.05m/s, the standard PI controller has a deviation larger than ±0.1m/s. The speed controller C1, designed for this master's thesis, arguably performs a lot better. Trying to put more concrete value for how much greater the performance of one controller has over the other, a metric used to calculate the error is the RMSE:

$$e_{RMS} = \sqrt{\frac{1}{N}\sum_{i=1}^{N}(x_{i_{ref}} - x_{i_{measurement}})^2} \tag{11.1}$$

where $x_{i_{ref}}$ is the reference value given from the net following algorithm, and $x_{i_{measurement}}$ is the value that the Kalman Filter estimates the velocities to be. This means that the reference model also counts towards the performance of the controller. This RMSE will be calculated for all data points where the ROV is in horizontal net following modus. This resulted in Table 11.3 which gives the

RMSE of the velocities for both trials done for C1 and one of the trials where the PI controller was run in net following modus. If we compare the error of C1 to the

	e_{RMS}
Adaptive controller trial 1 surge	0.0293
Adaptive controller trial 1 sway	0.0481
Adaptive controller trial 2 surge	0.0448
Adaptive controller trial 2 sway	0.0475
Standard PI controller surge	0.0607
Standard PI controller sway	0.1527

Table 11.3: The RMS-error for the velocities during the field experiments

PI controller in Table 11.3, it is safe to say that it is a massive improvement, at least in sway.

Another observation is that when the ROV uses the PI controllers for speed control, the measurements do not oscillate as much as the adaptive controller. The difference between these two trials might be debunking the hypothesis that Kalman Filter causes the oscillations. It seems more likely that the oscillation is caused by the actuator going into saturation when the speed is controlled with the adaptive controller.

11.2.2 Experimental Actuation Results

In Figure 11.6 the red dotted line is the desired control input from the designed control law, and the blue line is the estimated actuation that the ROV gives. The actuation of the ROV is calculated with measurements of the thrusters' rotation per minute related to the actuation force based on an interpolation of a thruster curve. The estimated actuation is originally designed for the Kalman Filter and is not a perfect estimate of the actual actuation. It is, however, precise enough for our purposes to say if it has gone into saturation or not.

It is apparent that the input for sway velocity is saturated. The input for sway has a constant deviation and frankly does not seem to give an actuation of more than $\pm$100N. It is, however, to some extent, able to reach the control objective as shown in Figure 11.4 when the speed goes up to 0.3m/s. It oscillates somewhat, and the cause may be that the integration term, which utilizes a projection operator, oscillates. The simulations have shown that the integrator oscillates when the estimates come close to the boundary.

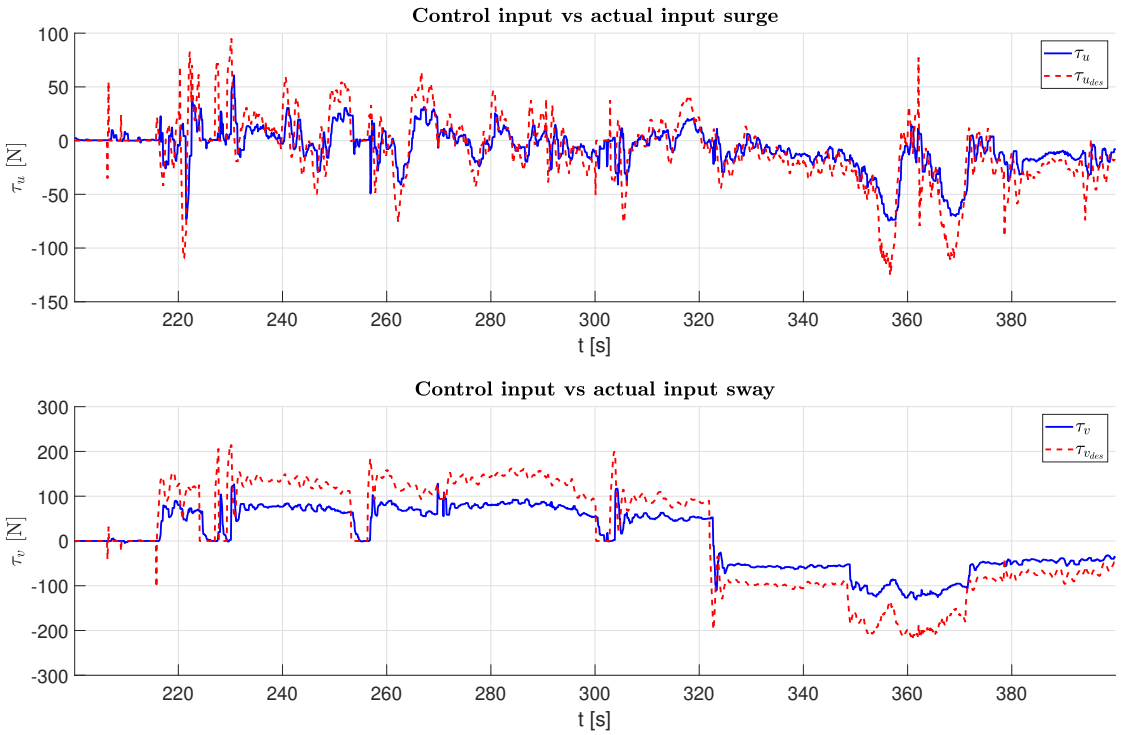

Figure 11.6: Actuation from the experiment trial 2

Other factors that might give this type of actuation response is the thruster allocation block. In the thruster allocation block, the desired force in each DOF is transformed to the force exerted from each thruster. The allocation block also saturates the control input with an upper and lower bound, in addition to using a slew rate limiter. This way, the thrusters will not be forced to their absolute limit and reduce wear and tear for an oscillating control input signal.

11.2.3 Experimental Ocean Current Estimations

In Figure 11.7, it can be seen that especially the estimate of the u-component of the current oscillates between $350\text{s} - 370\text{s}$, and slightly at the interval $240\text{s} - 290\text{s}$ as well. The oscillations are suspected to be the projection operator working to keep the integration term within the bounds. It shows that the anti-windup scheme ensures that even when the actuation is in saturation, the estimates do not grow unbounded and do not become larger than what can be physically accounted for by the actuator.

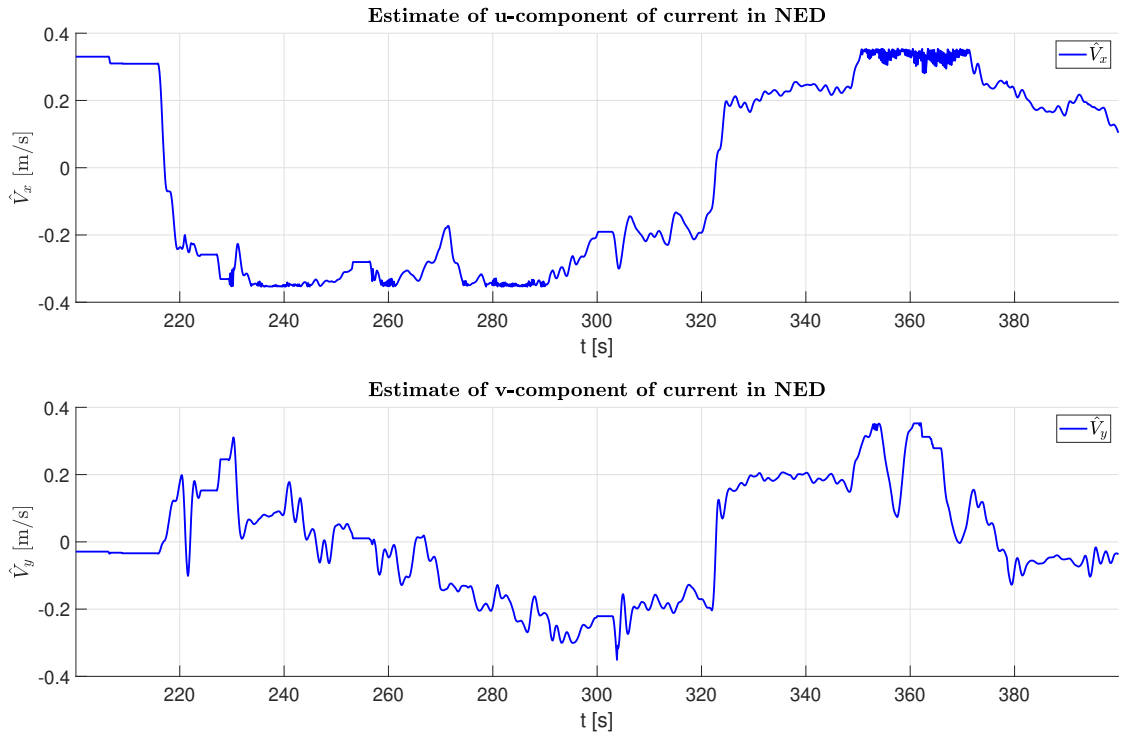

Figure 11.7: Ocean current estimates from the experiment trial 2

11.3 Heading Control

Recall from the derivation of the first controller for velocities that it was assumed that the heading was perfectly controlled, $\psi \to \psi_d$ UGES. The heading controller designed for the adaptive controller was a feed-forward PD-controller. Considering the control plant model was perfect, its error state converged exponentially to the origin of the closed-loop heading subsystem. By looking at the heading in the process plant model and the second control plant model from Chapter 7, the Coriolis-Centripetal force had a quadratic ocean current term that can be seen as a constant disturbance term resulting in constant deviation if not taken into account. It means, using the PD-controller that was designed will give a constant deviation from the desired reference value. Therefore, a PID controller is used for heading instead of a PD controller in the experimental field trials and simulations. In Figure 11.8, we can see that the heading controller manages to follow the desired reference with minor deviations in the simulations. Meanwhile, at the field trial, the heading had some more issues but still follows the contour of the desired heading, which for the trials that are done seems to be good enough. The main issue with $\psi \neq \psi_d$ is that it might affect the velocity controllers that have assumed that $\psi \to \psi_d$ when $t \to \infty$. However, as it has been shown with the plots for

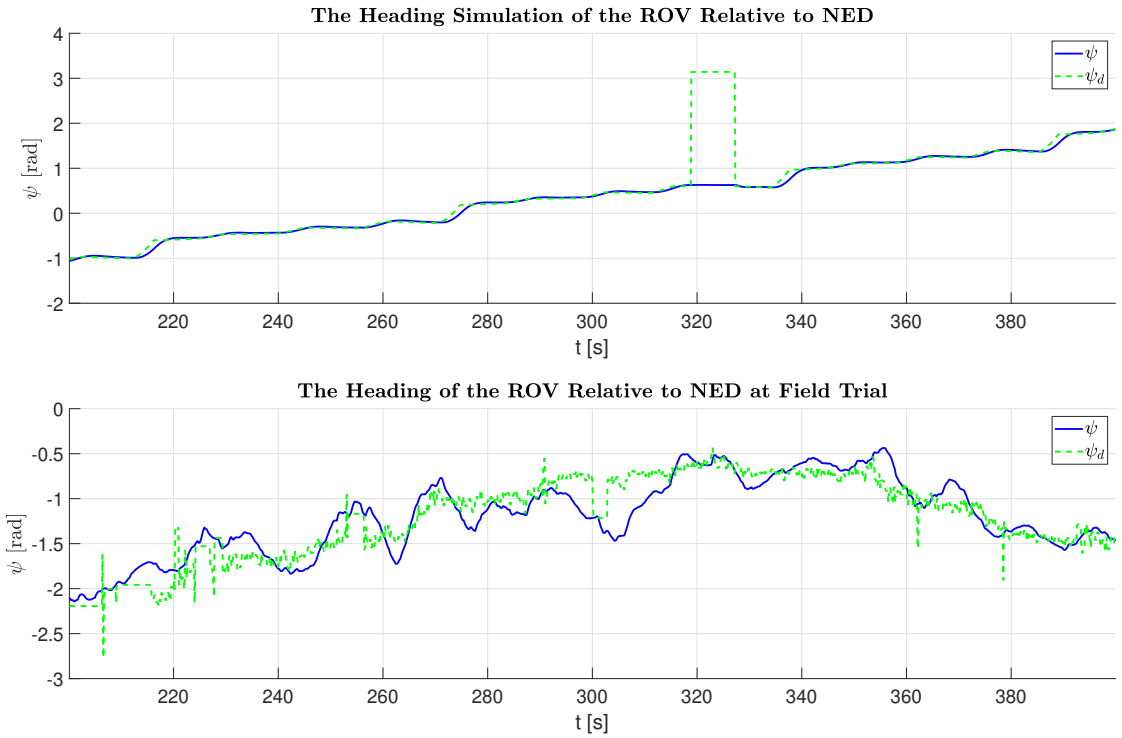

Figure 11.8: Heading response with PID controller

velocities, the velocities still manage to achieve the control objective.

The RMS-error for both heading is summarized in Table 11.4.

	e_{RMS}
PID controller simulation	0.0720
PID controller field trial	0.1930

Table 11.4: The RMS-error for the heading during the simulation and field trial

11.4 Summary

The field trials have validated that the speed controller is robust even when several factors are not the way it was assumed in theory. Modelling errors, non-perfect heading tracking and nonlinearities due to saturation in actuation was present as expected. Still, the experiments done at the fish farm showed that the speed controller worked great for our purposes. The designed controller, C1, was an improvement from the controller that was previously used. The theoretical part

proved that the controller was UGAS with the simplified control plant model. The simulations with a slightly more comprehensive process plant model still showed promising results, and the field trials validated that the controller worked well.

Chapter 12

Results of Augmented Controller (C2)

The augmented controller, C2, derived in Chapter 9 is implemented in FhSim running with the same process plant model as with Chapter 11. It must, however, be noted that the simulation with process plant model in this chapter uses the correct matrix values as given in Eq.(10.1)-(10.4). The controller is an extension of the adaptive controller, C1, derived in Chapter 8. Instead of assuming decoupled heading and velocity states, it is assumed coupled through the Coriolis-centripetal force. Thus, designing a horizontal controller that takes all the three horizontal states into account has been suggested in Chapter 9. The controller is tuned as given in Table 12.1.

12.1 Velocity Response

The dashed green line is the desired velocities from the net following algorithm, the dashed red line is the desired velocity smoothed out with a reference model, and the blue line is the velocity state of the ROV. Especially sway velocity is interesting to look at; it reaches a fairly high velocity with up to 0.5m/s without problems. It saturates when the desired speed is to 0.6m/s between $90\text{s} - 120\text{s}$, and 0.55m/s between $250\text{s} - 270\text{s}$. Compared to Chapter 11, this process plant model is modelled with the estimated real values and thus has lower damping than the simulations in Chapter 11. It manages to reach the desired value with minor problems and starts oscillating as expected when saturating. The RMSE of the velocities compared to the desired value from the net following algorithm is given in Table 12.2. In this table, the RMSE might become higher for C2 due to the saturation, and it might not perfectly represent how well the controller was.

	Tuning	Description
k_{p_u}	5.0	Proportional gain for surge
k_{p_v}	5.0	Proportional gain for sway
γ_x	0.01	Integrator tuning for $\hat{V}_x$
γ_y	0.01	Integrator tuning for $\hat{V}_y$
ϵ_{V_i}	0.2	Projection tolerance
$V_{\max}$	0.5	Max Ocean velocity bound
T_u	0.5	Time constant reference model surge
T_v	0.5	Time constant reference model sway
ϵ_ψ	0.1	Factor for cross-elements in matrix $\mathbf{P}_2$
k_{p_ψ}	46.6340	Proportional gain for yaw
k_{d_ψ}	14.0304	Derivative gain for yaw
γ_{e1}	0.0001	Integrator tuning for $\hat{V}_x^2$
γ_{e2}	0.0001	Integrator tuning for $\hat{V}_x\hat{V}_y$
γ_{e3}	0.0001	Integrator tuning for $\hat{V}_x^2$
ω_ψ	1.6	Bandwidth for reference model yaw (3rd order)
ζ_ψ	1.0	Damping ratio for reference model yaw (3rd order)

Table 12.1: Tuning parameters for the augmented controller

12.2 Velocity Controller Input Response

From Figure 12.2, the maximum output it can give before it starts to oscillate is at 200N for the input in sway, which is significantly higher than Figure 11.6, which oscillated at 125N. This is mainly caused that the process plant model has lower damping than the simulation done for the first designed controller. It can, however, exert a significantly higher thruster force, which might not be explained by the difference in damping from the previous simulations. A possible reason for this might be the clamping and projection operator implemented in the controller. It seems like the saturation limits are lower. The projection operator might have been effective at a lower level causing the controller to demand less force due to the underestimation of the damping terms used in the integrator for the controller C1. That is, the control law calculates less thruster force in the case of C1 since the control law is implemented with the assumption of less damping than the process plant model has. Meanwhile, C2, in this case, manages to give more thrust until it clamps and saturates itself since it utilizes the same coefficients in its control plant model and the process plant model.

Another possibility explaining the saturation is that the PID controller in yaw demands higher inputs than the heading controller used here. Since the four

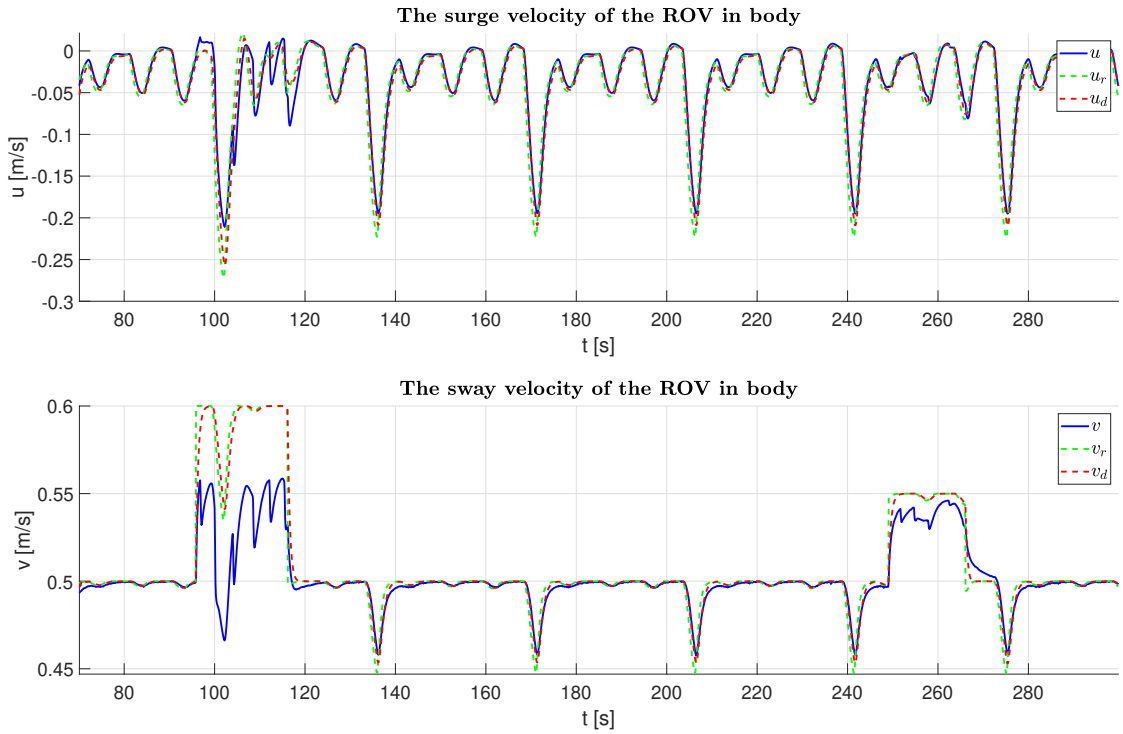

Figure 12.1: Velocity response of augmented controller

thrusters actuate surge, sway and yaw simultaneously, a higher control activity from the heading controller gives less thrust for the velocity controllers to use. However, the ROV in FhSim has an implemented a switch that makes sure that the surge and sway are decoupled from yaw to some extent by switching between the heading controller and speed controller.

12.3 Heading Simulation Response

From Figure 12.3, the heading follows the desired input to a great extent. The desired heading in green is given from the net following algorithm and is smoothed out with a third-order reference model resulting in the red line. The blue line seems to follow the heading reference closely, and it has more or less no deviations from the reference model. The more considerable change from the net following algorithm are smoothed out by the reference model, giving a smaller deviation. The RMSE of the heading and the desired heading from the net following algorithm, in this case, is also calculated to compare this heading controller to the PID controller. For calculation of the RMSE in this case, it is important to note that when looking at error in angles, the smallest signed angle is necessary to consider

	e_{RMS}
Surge velocity using C1	0.0175
Sway velocity using C1	0.0194
Surge velocity using C2	0.0259
Sway velocity using c2	0.0200

Table 12.2: The RMS-error for the velocities during the simulations of both controllers from this thesis

to obtain the correct deviation. The RMSE between the heading and the reference model is compared since the controller follows the reference model, which is significantly slower than a step response. The RMSE of these two cases are given in Table 12.3. It is important to note that since a reference model is used, the

	e_{RMS}
Horizontal controller compared to desired value	0.0910
Horizontal controller compared to smoothed value	0.0204
PID controller simulation	0.0720

Table 12.3: The RMSE for the heading during the simulation of the horizontal controller and the PID controller regiven again here

reference model's dynamics is important as well, and if it works with the reference model does not necessarily mean it will perform great without in this case. The simulations in this chapter are mainly used to validate the mathematics done for this controller and show that it works. It still needs some extensive testing to be concluded that it works well in practice.

The thruster input seems to manage well and only goes to saturation at the spikes connected to the significant change in heading. In addition to the more considerable change, it also seems like the heading input goes into saturation simultaneously as the speed controller does. All in all, this seems like a good response and could be a possible substitute for the PID controller used in the ROV, but a controller validation in a field test is necessary to be sure that it performs better than the PID controller.

It is also essential to notice that since the PID controller is simulated with a process plant model with higher damping, it achieves a slower response than the simulation using the augmented adaptive controller. This also needs to be taken into account since, in this case, a high RMSE for the PID controller does not entirely reflect how well it works in practice.

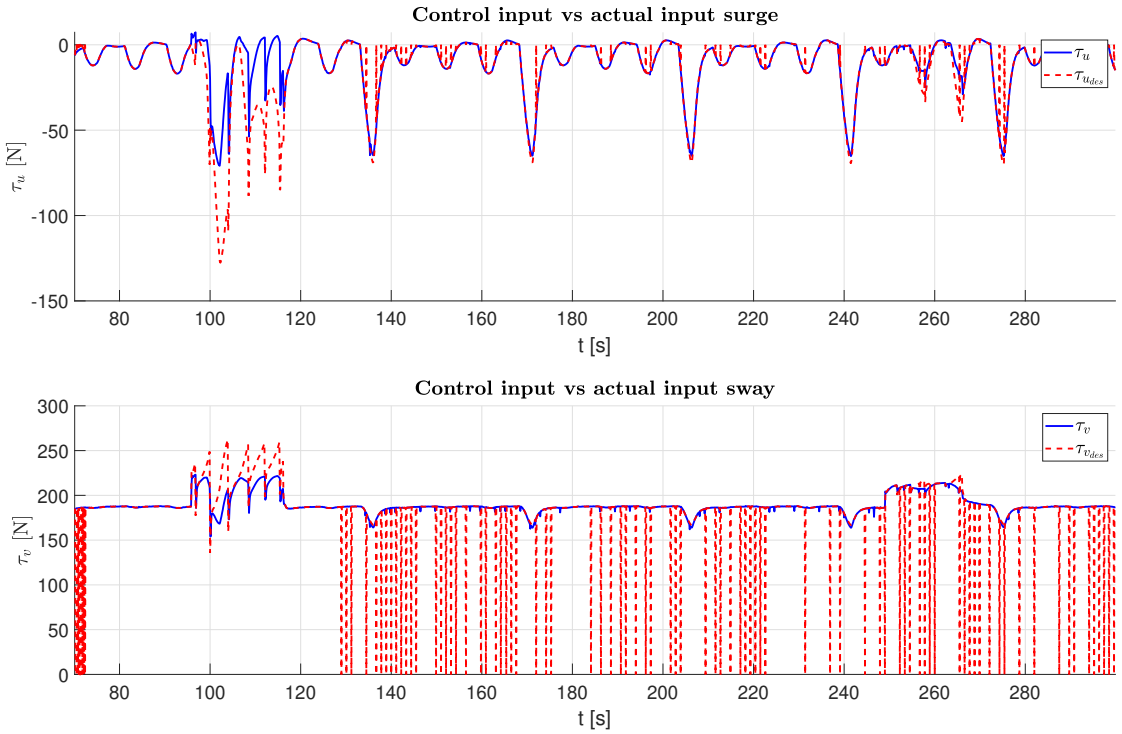

Figure 12.2: Control input of augmented speed controller

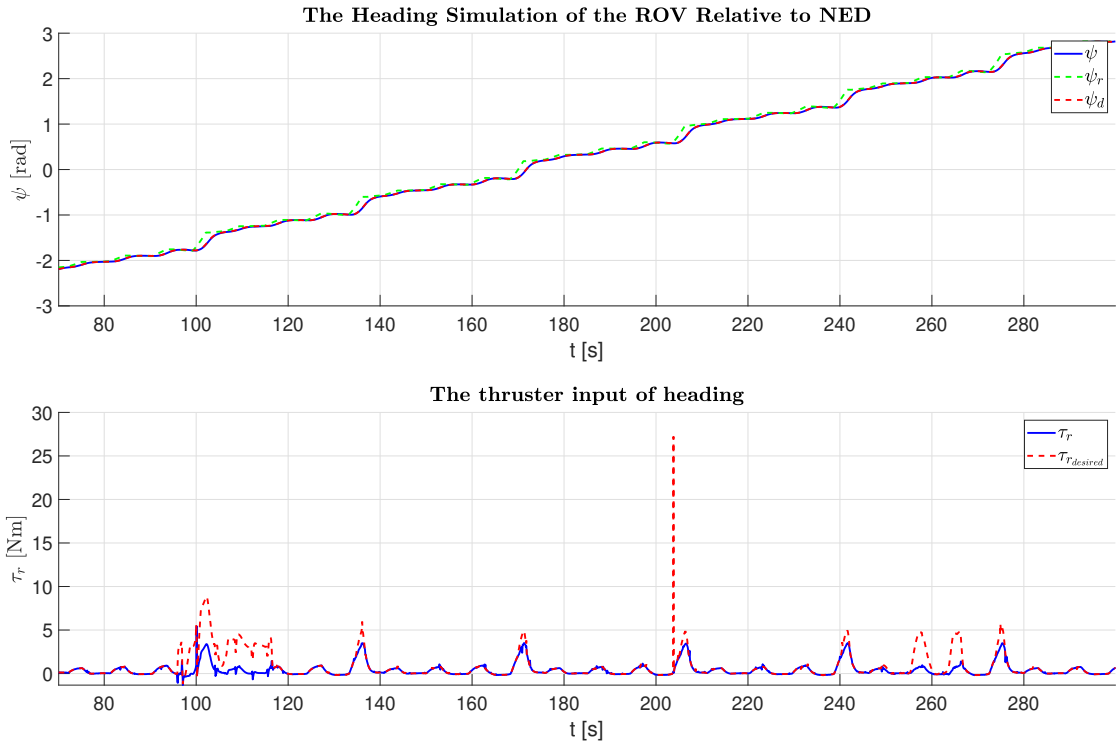

Figure 12.3: The heading response with its control input

Part V

Discussion

Chapter 13

Discussion

This chapter discusses the results that were found in the last part. A discussion around the experiments themselves, the speed controllers and comparison of the speed controllers are also done. The adaptive controller, C1, based on the simplifiedDP control plant model, will be compared to the PI speed controllers on achieving the control objective. Then, the augmented controller, C2, based on the more complex control plant model, will be compared to C1 on achieving the control objective. The PID controller in the heading will also be compared to the heading part of the augmented controller.

13.1 Discussion of the Experimental Results

In this section, C1 is compared to the PI controller. This comparison will be based on how well the controllers achieve the control objective using the RMSE as a metric. In some cases, the metric chosen might be flawed due to some factors that need to taken into account when discussing the RMSE. This will be discussed more in detail in this section.

In Section 11.2.1 it was shown that C1 performed better than a regular PI controller. The adaptive controller in field experiments achieved a significantly lower RMSE than the PI controller. It makes sense, due to the RMSE from the field experiments, to prefer C1 over the PI controller. However, the RMSE metric squares the error between the desired reference value and the estimated ROV velocity before they are averaged. It means that large deviations are weighted more heavily than small deviations with this metric. This means that a large RMSE does not necessarily reflect what actually happened. For instance, if the step responses in one of the tests are larger in amplitude than the other, this would have affected the RMSE to become much larger even if the system generally follows the refer-

ence signals well. Meanwhile, a small constant deviation and small step responses would not have affected the RMSE as much. The RMSE for the PI controller was still significantly higher than the adaptive controller, especially in sway; it can, therefore, be argued that C1 objectively performed better.

In addition, in this case, looking at Figure 11.4 and Figure 11.5 the PI controllers objectively achieve worse results due to the large constant deviation, possibly making a metric for error measurement obsolete. But, if a metric needs to be used, the mean absolute error (MAE) might have been a better alternative to measure the amount of constant deviation, which weighs all error equally. This metric weigh small constant deviations and large constant deviations equally. MAE was not used in this thesis for consistency of what was chosen first. In this experimental field testing, however, between the two controllers, the PI speed controllers have bad performance overall due to a large constant deviation compared to the adaptive controller, C1, in addition to a significantly high RMSE.

A source of error for comparing these two controllers that also needs to be discussed is that the PI controller was not tested as extensively as the adaptive controller. Out of six trials that were done this day, only one of them used the PI speed controller long enough to get some comparable results. That brings up the question if the PI controller was optimally tuned for the desired response, mainly to compensate for the constant deviation in this trial. The PI controller has been tuned in earlier field trials, and the tuning was therefore not prioritized to consider the constant deviations during this trial. The adaptive controller was tested with two trials the day before the PI controller, where the idea was to tune the controller differently. Still, since the trials for the adaptive controller gave satisfying results, only the adaptive gains were modified after the first trial run to reduce oscillations. It has been experienced from previous experiments that to compensate for the constant deviation, the PI controller has to increase its integral gain. However, by increasing the integral gain, the system becomes more oscillatory, and due to saturation and integral windup, the system might become destabilized with increased integral gain. It is therefore not desired to increase the integral gain more than necessary. It is believed that even if the constant deviation would have been handled, the system would, in practice, be oscillatory and unstable or close to unstable, yielding worse results. A possible solution for the oscillations from the integral term is to add a derivative term, which can be interpreted as a damping term. This would, however, have resulted in a slower settling time, as described in Chapter 3.

13.2 Discussion of the Nonlinear Controllers

It was clear that C1 outperformed the PI controller, but how did it perform compared to the augmented adaptive controller, C2? Comparing Figure 11.1 and Figure 12.1 the first observation is that C2 obtains a higher velocity than C1. Meanwhile, it seems like C1 has a maximum velocity at 0.35m/s, C2 manages 0.5m/s without issues. This seems mainly caused by that C1 was simulated on a process plant model with 10% higher damping coefficients. Another possibility is that the anti-windup schemes in C1 saturate the control input before the ROV thrusters themselves do it.

It is not easy to conclude the best performance or compare two control laws that were simulated on, in practice, two different process plant models. Meanwhile, the first adaptive controller was simulated on a process plant model with 10% higher damping; the augmented controller was simulated on a process plant model with damping as given in Eq. (10.3). Therefore, the differences between the two control laws might have several external factors and more sources of errors for these results. One big source of error is that the difference in RMSE between these two control laws might become significantly more different than if it was simulated on the same process plant model. The biggest effect the different damping has on the comparison is that the RMSE might become higher for C2 since the step response is larger when trying to achieve a higher speed than C1. However, based on the simulations, the biggest difference between the two process plant models when simulating the controllers was that the saturation limit was higher for C2. Still, the general performance of trajectory tracking was more or less the same. Therefore, the simulations with the correct process plant model were not included for the first adaptive controller since the response was generally similar to the simulations that have been presented here.

The hypothesis for saturation from the anti-windup-scheme might be inspected closer by looking at the control input plots Figure 11.2 and Figure 12.2, but also Figure 11.6. The control input in sway for the augmented controller seems to manage a control input of 180N before oscillating. Meanwhile, the first adaptive controller manages 125N in simulations and in practice 80N in field trials. Especially the field trials show that the maximum actuation is lower than the simulations, so having an anti-windup scheme clamping the integrator at a lower input might be advantageous in this case. The first adaptive controller's simulations show that it oscillates but still manages to reach an actuation of the desired value, suggesting the anti-windup scheme also affects the ROV from reaching a higher velocity.

Nonetheless, simulations are just simulations and only gives an indicator of what

to expect in practice. Ultimately, the field trials are the results that validate the properties and robustness of a controller. The augmented controller showed excellent results in the simulations and seemed promising for an eventual experimental field trial.

Comparing the velocities from the simulations using the RMSE in Table 12.2, both speed controllers have small differences in RMSE. As argued earlier, a large step response might give a higher RMSE than small deviations over time. In this case, maybe the RMSE is not preferable to use as a basis for comparison, especially since the velocity part of the augmented controller is controlled to a higher speed reference and set to well over what it is assumed the ROV can actuate at several times. Even if the RMSE shows that C1 performed better, achieving a lower RMSE, the difference is not large enough to conclude that one controller outperforms the other based on this metric.

One difference between the two controllers is that the augmented controller uses measurements to a larger extent than the first adaptive controller. First of all, the augmented controller removes known nonlinearities with feedback linearization, which is only removed perfectly if the modelling of the ROV is correct. In addition, it requires the measurements for the feedback to be close to perfect. Which, due to measurement uncertainties, is not always the case. The DP model-based adaptive controller does not need to do this because the control plant model is more or less linear in all the fully known terms. This error from measurement uncertainties is therefore not as present.

Another, more significant difference between the two controllers is the implementation of the integration term. The simplified DP model-based controller constructs the $\mathbf{G}$ matrix with only reference values of the heading and therefore relying on the heading controller managing to reach this reference value. The augmented controller has a $\mathbf{G}$ matrix that uses measurement to construct the matrix, making it prone to measurement uncertainties and oscillations. The measurement uncertainties might in simulations give excellent results if assuming perfect measurements but unsatisfying in practice. The augmented controller is, however, not as equally dependent on the ROV reaches the desired reference values, but it loses the properties that the heading state is decoupled from the velocities..

Another factor to be considered is the number of tuning parameters. Let us assume that both controllers do not need a reference model, which means that only ψ_d, u_d, v_d is fed to the controllers; the higher-order terms are set to zero. This still means that the simplified DP model-based adaptive controller has six tuning

parameters in addition to three tuning parameters for the heading PID controller, nine in total. The augmented controller has 12 tuning parameters, which is more tuning parameters. Some of the tuning parameters are bounded, which requires knowledge of it, and it might be hard to interpret their impact on the response. This means that going from simulations to a field trial might give some undesired response, meaning figuring out which tuning parameter for the augmented controller can be changed to counteract the response might become complicated. With the reference models for both controllers, the number of tuning parameters increases again. However, these are often chosen beforehand and are not affected equally by a different environment.

13.3 Comparison of Yaw Controllers

The cardinal reason for using the more complicated augmented controller over the simplified DP model-based adaptive controller is that it considers some of the couplings in the ROV model, especially in the heading. The augmented controller controls surge, sway and yaw; meanwhile, the DP model-based adaptive controller only controls surge and sway and utilizing the well tested PID controller for yaw. In this section, a discussion of the heading control results will be done to argue if the augmented nonlinear controller is a viable candidate for some further developing and testing.

In the result section comparing Figure 11.8 and Figure 12.3 the response looks similar in the sense that both the augmented controller and the PID controller seems to track the reference pretty well. Comparing the RMSE of the two using Table 12.3 it looks like the controllers have only small differences when following the desired reference ψ_d. Frankly, it seems like the reference model is the limiting factor for the augmented controller C2. It was not simulated without a reference model, so it is difficult to suggest that one controller performed better than the other using this error metric. In addition, higher damping might have affected the PID controller so that it achieved a slower response than it would in practice.

However, it has been proven that the PID controller works satisfyingly in field experiments. Due to similarities in the simulation results, one should expect that the augmented controller would perform somewhat the same if tested in field experiments. It is, however, not accurate to use the simulations to conclude that it will achieve the same without actually trying it in a field experiment. One can draw parallels between the PID controller and the augmented controller by reading it term for term. The augmented controller is a sum of feedback linearizing terms, feedforward terms and a PID control law term. The integrator part in the PID

term, like with the DP model-based control law, integrates a more sophisticated error term by multiplying it with the **G** matrix. However, as mentioned before, the **G** matrix uses measurements instead of reference values which might yield an inadequate result due to measurement uncertainties.

Looking at the result from the field trials in Figure 11.8, unlike the velocity plots, the heading does not have a constant deviation. This might mean that improving the integrator term, which the augmented controller essentially does, might not result in a better response. The problem seems to lie in the heading controller being too slow relative to the changes occurring for yaw, which means that the problem does not necessarily lie in the control law but rather the physical properties of the actuators in the ROV. Doing calculations for the mean absolute error for the PID controller during the field experiments resulted in a mean absolute error of 0.1483 rad, an average error of about 8°, which is minor. However, it is possible that it might have achieved less mean absolute error if it was simulated on the correct process plant model instead of the process plant model with higher damping. Nonetheless, the error in the heading is not that large in practice.

Chapter 14

Conclusion

In this thesis, two control laws have been proposed and analyzed. The main task was to design and implement robust control laws capable of trajectory tracking, which improves the level of autonomy for underwater vehicles. Autonomous operations in aquaculture increase safety and lower operational costs, and having control laws capable of trajectory tracking is a step towards realizing this goal.

An adaptive control law was designed with a control plant model from a simplified dynamic positioning model. The control law resulted in uniformly globally asymptotically and uniformly locally exponentially stable origin of the closed-loop system. UGAS and ULES of the control law were proven by utilizing that the closed-loop system matrices had some bounded properties and then applying the result from [3]. The result and proof from [3] was then used as a basis to design the next control law.

The control plant model was expanded to consider the coupled states, mainly from Coriolis-centripetal forces. Therefore, the first adaptive controller was modified to take this into account, mainly by modifying the integrator term and adding an adaptive regressor to remove an unknown quadratic term in the control plant model. The closed-loop system utilizing this augmented adaptive controller was proven that the ROV error states converged uniformly, globally and asymptotically to the origin. Meanwhile, the rest of the states was only shown to be bounded around the origin.

The first adaptive controller for the velocities that was developed yielded great results through simulations and field experiments. The tracking errors for surge and sway velocity converged to the origin and followed time-varying references, meaning it achieved great trajectory tracking. The adaptive law, which was interpreted as an integrator, had a problem with integrator windup that was handled

applying two anti-windup schemes: projection operator and clamping, which could be used due to some knowledge of the bounds of different adaptive variables. As expected, the field experiments showed different responses than the simulations but still managed to perform better and had only minor tracking errors compared to the previously used PI control law.

The second augmented adaptive controller for the velocities and yaw also showed great results through simulations. The tracking errors for surge and sway velocity and the heading converged to the origin and were also able to follow time-varying references. This means that with a guidance law, in this instance, a net following algorithm, the ROV managed great path following. The advantage with this controller is that it also takes into account heading, possibly replacing the PID controller in yaw. However, to take this controller to the next step, field experiments need to be done to test that it also yields good results in practice. Unlike the first adaptive controller, robustness analysis was not done with this controller and may need to be done more extensively before doing field experiments.

In conclusion, two proposed controller was designed that achieved the control objective set for this thesis. The adaptive controller for a simplified DP control plant model is simple to utilize and has been field validated, giving excellent results for the velocities. The control plant model was expanded, and a control law was designed to control heading with this expanded control plant model as well. This second controller achieved software validation based on its great performance during the simulations. The main advantage of using a more simple control plant model is that it simplifies a lot of the design and essentially decouples all the states on the horizontal plane. However, unmodelled terms might cause constant deviation, especially in heading, which in the first controller is handled by adding a pure integrator term, resulting in a PID controller for heading. The augmented controller considers and addresses the deviation in heading the same way as the deviation is handled in the velocities. Either way, it seems like both controllers that were designed improved the existing controller used before and did well to achieve the control objective set for the thesis.

14.1 Future Work

The controllers designed in the thesis still have potential for improvement. As it was discussed in Chapter 13, feedback linearizing terms and $\mathbf{G}$ matrix in the integrator term for the augmented controller are prone to measurement uncertainties and sensor readings with error. One unattempted idea that might resolve the issue is to split the terms containing $\cos(\cdot)$ and $\sin(\cdot)$ in $\mathbf{G}$ in error state terms and

reference value terms. This is like it was done in the DP control plant model for $\widetilde{\psi}$ utilizing trigonometric identities. Then an analysis of the part of the $\mathbf{G}$ with reference values and treating the other part of $\mathbf{G}$ containing the error states as a perturbation term can be done. The part of $\mathbf{G}$ with reference value can be used as part of the nominal system that is handled with the control law and attempt to prove that it is at least locally exponentially stable. Then if this nominal system is ULES, the perturbation theory might be used to prove that the whole system still maintains exponential stability. The math might prove difficult, but if it works, the integrator term in the control law might not be as prone to measurement error as it is now.

Before attempting to improve the augmented controller, it is believed that it can also be proven that $\mathbf{x}_2$ in the closed-loop system in Chapter 9 uniformly and globally converges asymptotically to the origin. The preliminary simulation results using the control plant model showed convergence of those states as well. However, the mathematics needed to do this was out of what the author in this thesis was capable of handling. It has already been proven that the origin for $\mathbf{x}_2$ is UGS, and it is believed that the proof of [20, Lemma 2] might be utilized to prove uniform attractivity of the origin for $\mathbf{x}_2$. With this proof, $\mathbf{x}_2$ will have been proven to asymptotically converge to the origin uniformly.

A paper publishing the results achieved in this thesis, are from the time this thesis is delivered in writing. A draft paper of the paper to be published is given in Appendix B.

Appendices

Appendix A

Trigonometric identity

$$\begin{aligned}\cos(\tilde{\psi}+\psi_d) &= \cos(\psi_d)\cos(\tilde{\psi}) - \sin(\psi_d)\sin(\tilde{\psi}) - \cos(\psi_d) + \cos(\psi_d) \\ &= \tilde{\psi}\left[\cos(\psi_d)\frac{\cos(\tilde{\psi})-1}{\tilde{\psi}} - \sin(\psi_d)\frac{\sin(\tilde{\psi})}{\tilde{\psi}}\right] + \cos(\psi_d) \qquad \text{(A.1)} \\ \sin(\tilde{\psi}+\psi_d) &= \cos(\psi_d)\sin(\tilde{\psi}) + \sin(\psi_d)\cos(\tilde{\psi}) - \sin(\psi_d) + \sin(\psi_d) \\ &= \tilde{\psi}\left[\sin(\psi_d)\frac{\cos(\tilde{\psi})-1}{\tilde{\psi}} + \cos(\psi_d)\frac{\sin(\tilde{\psi})}{\tilde{\psi}}\right] + \sin(\psi_d) \qquad \text{(A.2)}\end{aligned}$$

Appendix B

Paper to be Submitted

The paper titled "Robust Control of Autonomous ROV at Exposed Aquaculture Sites" is appended here.

Robust Control of Autonomous ROV at Exposed Aquaculture Sites

Kenny Hoang Nguyen
Norwegian University of Science and Technology
Trondheim, Norway

Walter Caharija
SINTEF Ocean
Trondheim, Norway

Sveinung Johan Ohrem
SINTEF Ocean
Trondheim, Norway

Jan Tommy Gravdahl
Department of Engineering Cybernetics
Norwegian University of Science and Technology
Trondheim, Norway

***Abstract*—This paper presents two control laws for error-free trajectory tracking of velocity and the heading for a remotely operated vehicle (ROV), making it possible to autonomously traverse an aquaculture net pen in combination with a net-following algorithm. Stability proofs for the closed-loop system using these proposed control laws were provided. For the first control law, the closed-loop system with an adaptive law was proven to be uniformly globally asymptotically stable (UGAS) at the origin for all error states. For the second control law, the closed-loop system with the derived adaptive laws was proven to be uniformly globally stable (UGS) at the origin. For this second control law, proof that the error states for the velocities and heading globally converged asymptotically and uniformly to the origin was provided. Simulations for both controllers were done, yielding excellent results achieving the control objective. The first controller was also validated through sea trials, completing the control objective in practice as well.**

***Index Terms*—adaptive control, nonlinear control, modelling, remotely operated vehicle (ROV), aquaculture, path following**

I. Introduction

Norway is a leading producer of farmed salmon worldwide and produced 1.36 million tonnes with a value of 68 BNOK in 2019 [1]. In order to increase production and deal with some of the issues related to today's production methods, e.g. sea lice infestations, many fish farmers believe moving their facilities to more exposed locations forestall these issues. However, many of today's aquaculture industry operations depend on manual labour and close human interaction. One such operation is the control of ROVs. The workload on ROV operators is often quite intense, as they are required to both navigate the ROV in a dynamically changing environment while monitoring and avoiding the structures. Therefore, increasing the level of autonomy of an ROV could be beneficial to the ROV operators, but also the fish farmers, as it could lower the costs and improve the effectiveness of the operations [2].

Autonomous ROVs operating in dynamically changing environments require robust control laws to achieve the desired objectives, e.g. maintain a specific heading angle or follow a path. At SINTEF Ocean, an Argus Mini ROV is currently used as a research vehicle for testing different control strategies and autonomous functions. This ROV is presently equipped with PI speed controllers in the surge and sway velocity DOF and a PID controller in the heading DOF. The speed controllers are suboptimal, as the ROV is not able to reach the desired speed when influenced by ocean currents. This leads to sub-optimal performance during path following. As a step towards more robust autonomous operations for ROVs in general, it is, therefore, of interest to develop a more robust control algorithm for the surge, sway and heading DOFs.

The developed controller must ensure that the ROV is capable of following a time-varying speed and heading references while under the influence of ocean currents. The controller should also be robust towards variations and uncertainties in the system parameters, such as mass and damping coefficients, as these are not perfectly known. Therefore, this paper aims to primarily develop a control law for surge, sway and heading DOFs. For these control laws, it will be attempted to prove that the closed-loop systems of their respective control plant models have desired stability properties.

In [3] an adaptive feedback linearizing controller was proposed for control of the horizontal DOFs for the Argus Mini ROV. The simulations in [3] showed that the controller more or less tracked the desired velocities perfectly. However, field tests from the same article showed that it had significantly deteriorating results than the simulations. Basin wall following using DVL showed great results where the controller managed to a large extent track the velocity references, with some deviations. When the ROV reached a corner, it struggled to follow the reference from what seems like a too fast and large change so that it was not physically possible for it to reach the reference. However, the biggest problem for this controller was that during the net-pen following trial, where the velocity reference was constant, the closed-loop system got a constant deviation and, at the same time, became more oscillatory. However, based on the data from these two field tests in [3] it seems as the controller used was somewhat satisfactory but still has potential for improvement since the controllers had deviations with velocity tracking.

The contributions of this paper are two model-based control laws for marine vehicles in 3-DOF: surge, sway and yaw, are proposed. The first controller is derived using a simplified linearized 3-DOF control plant model, while the second

controller considers a more complex, nonlinear 3-DOF control plant model. The first controller, referred to as C1 for the remainder of the paper, is based upon [4], utilizes an adaption law to ensure that the origin of the full error system is uniformly globally asymptotically stable (UGAS) and uniformly locally exponentially stable (ULES), even without persistent excited input signals. The second controller, referred to as C2 for the remainder of this paper, is a modified version of C1. In C2, the adaptive law is expanded and overparameterized to consider some unknown quadratic ocean current terms. Furthermore, C2 utilizes a more complex control plant model, and as such, this controller is assumed to be more robust than C1. Due to the complexity of the control plant model, the origin for only some of the states of the closed-loop system with C2 was only proven to be UGAS through Lyapunov stability theory, with the origin of the remaining states being proven to be uniformly globally stable (UGS).
Both controllers were validated in simulations, and C1 was tested in a field experiment.
In Section II the control plant models used for the control designs are derived. Section III presents the subsystem that generates the time-varying reference values the ROV are tracking.Section IV proposes two control laws and also provides the stability proofs for the closed-loop systems. Section V presents the limitations of C1 and suggests implementations to C1 that handle the limitations. Section VI presents the results from simulations and the full-scale sea trials.

II. Control Plant Model

The two control plant models used for the design of the controllers are proposed in this section. The assumptions needed for them to hold are also given here, with assumptions that yield both models and the specific assumptions for each of the models.
The control plant model of the ROV is described in 3 degrees of freedom (DOF): surge, sway and yaw. The kinematics of the vehicle are given in North-East-Down (NED) frame, denoted $\{n\}$, meanwhile the kinetic dynamics are described in the body-fixed coordinate frame, denoted $\{b\}$.

Assumption 1. The roll and pitch motion of the ROV can be neglected due to the nature of the passive stabilization properties from gravity.

Assumption 2. The ROV is neutrally buoyant, and the motion in the heave can be neglected. In addition, the vehicle centre of gravity (CG) and the centre of buoyancy (CB) are located in the same vertical axis in $\{b\}$

Remark 1. Most ROVs are designed to be slightly positive buoyant. Therefore, in the case of a system shut down, the ROV will slowly rise to the surface. The ROV can, however, for all practical purposes be assumed neutrally buoyant.

Assumption 3. The ROV is symmetric in port-starboard, fore-aft and bottom-top.

Assumption 4. The body-fixed frame center of origin (CO) is located in the CG.

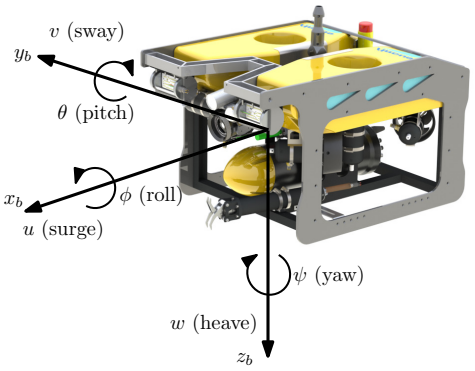

Fig. 1: Body frame axis on the Argus Mini ROV

Remark 2. Assumption 1-4 are common assumptions in ROV modelling, which can be seen in other literatures such as [5, 3]

Assumption 5. The hydrodynamic damping is linear.

Remark 3. Nonlinear damping is not considered to reduce the complexity of the controllers. For low-speed manoeuvring, Assumption 5 is considered as a mild assumption since the passive nature of any nonlinear hydrodynamic damping should enhance the directional stability of the vehicle. [6, 3].

The state of the ROV is given by the vector $[\boldsymbol{\eta}^T, \boldsymbol{\nu}^T]^T$. In this case $\boldsymbol{\eta}^n = [x, y, \psi]^T$ is the generalized vector describing position and orientation of the ROV in $\{n\}$. $\boldsymbol{\nu}^b = [u, v, r]^T$ describes the linear and angular velocity of the ROV in $\{b\}$.

Assumption 6. The ROV is not able to reach speed over $2\mathrm{m/s}$.

Remark 4. The ROV has four thrusters actuating the DOF considered in this paper, and the thrusters cannot generate enough force for the ROV to achieve a speed over $2\mathrm{m/s}$.

Assumption 7. The ocean current is constant, irrotational and bounded with a velocity vector $\mathbf{V}_c^n = [V_x, V_y, 0]^T$ in $\{n\}$. Therefore there exists a constant $V_{\max} > 0$ such that $V_{\max} > \sqrt{V_x^2 + V_y^2}$. Furthermore, due to the current being constant in $\{n\}$, the time-derivative is $\dot{\mathbf{V}}_c^n = \mathbf{0}$ in the inertial frame $\{n\}$.

Remark 5. Assumption 7 on the ocean current is made in the $\{n\}$ reference frame. In many earlier works on control the current is assumed to be constant in the BODY frame, which is easily violated during turning [7].

A. First Control Plant Model

With the Assumption 6, the low-frequency control plant model of [8], similar to the linearized DP model from [9] can be considered. In the low-frequency model the ocean current disturbance is modelled in a bias vector, in this paper the disturbance is instead modelled using the relative velocity

vector. The maneuvering model of the 3-DOF ROV considered is:

$$\dot{\boldsymbol{\eta}}^n = \boldsymbol{R}(\psi)\boldsymbol{\nu}^b \tag{1}$$

$$\boldsymbol{M}_{RB}\dot{\boldsymbol{\nu}}^b + \boldsymbol{M}_A\dot{\boldsymbol{\nu}}_r^b + \boldsymbol{D}\boldsymbol{\nu}_r^b = \boldsymbol{B}\boldsymbol{f} \tag{2}$$

The matrix $\boldsymbol{R}(\psi)$ is the principal rotation matrix around the z-axis. In addition, $\boldsymbol{\nu}_r^b \triangleq \boldsymbol{\nu}^b - \boldsymbol{\nu}_c^b$ is the relative velocity vector between the vehicle and the ocean current. In $\{b\}$, the current velocity is $\boldsymbol{\nu}_c = \boldsymbol{R}^T(\psi)\mathbf{V}_c = [u_c, v_c, 0]^T$. The rigid-body inertia matrix is $\boldsymbol{M}_{RB} = \boldsymbol{M}_{RB}^T > 0$, the hydrodynamic added mass inertia matrix is $\boldsymbol{M}_A = \boldsymbol{M}_A^T > 0$ and $\boldsymbol{D} > 0$ is the damping matrix. The matrices $\boldsymbol{R}(\psi), \boldsymbol{M}_{RB}, \boldsymbol{M}_A$ and $\boldsymbol{D}$ with the assumptions have the following structure:

$$\boldsymbol{R}(\psi) \triangleq \begin{bmatrix} \cos(\psi) & -\sin(\psi) & 0 \\ \sin(\psi) & \cos(\psi) & 0 \\ 0 & 0 & 1 \end{bmatrix} \tag{3}$$

$$\boldsymbol{M}_i \triangleq \begin{bmatrix} m_{11}^i & 0 & 0 \\ 0 & m_{22}^i & 0 \\ 0 & 0 & m_{33}^i \end{bmatrix}, \boldsymbol{D} \triangleq \begin{bmatrix} d_{11} & 0 & 0 \\ 0 & d_{22} & 0 \\ 0 & 0 & d_{33} \end{bmatrix} \tag{4}$$

where $i \in \{RB, A\}$.
The matrix $\boldsymbol{B} \in \mathbb{R}^{3\times n}$ is a constant thrust allocation matrix, mapping the thruster control input vector $\boldsymbol{f} \in \mathbb{R}^n$ to the forces and moments acting on the vehicle, where $n \geq 3$ is the number of thrusters working on the horizontal plane. The control forces and moments acting on the vehicle are described by the vector $[\tau_u, \tau_v, \tau_r]^T \triangleq \boldsymbol{B}\boldsymbol{f}$.

Assumption 8. The thrust allocation matrix $\boldsymbol{B}$ has full rank, that is rank$(\boldsymbol{B}) = 3$, so the ROV is fully actuated in surge, sway and yaw.

Remark 6. The size and elements of $\boldsymbol{B}$ depend on the thruster configuration, and for generality, it will not be specified any further here beyond the requirement in Assumption 8.

B. Component Form for First Model

To solve the control design problem it can be useful to expand the kinematic and kinetic equations, (1) and (2), into component form. The time-derivative of the current velocity vector in $\{b\}$ is

$$\dot{\boldsymbol{\nu}}_c = \frac{\mathrm{d}}{\mathrm{d}t}\left(\boldsymbol{R}^T(\psi, r)\mathbf{V}_c\right) = [rv_c, -ru_c, 0]^T \tag{5}$$

the 3-DOF control plant model can then be written as

$$\dot{x} = u\cos(\psi) - v\sin(\psi) \tag{6a}$$

$$\dot{y} = u\sin(\psi) + v\cos(\psi) \tag{6b}$$

$$\dot{\psi} = r \tag{6c}$$

$$\dot{u} = -\frac{d_{11}}{m_{11}}u + \boldsymbol{\phi}_u^T\boldsymbol{V}_c + \frac{1}{m_{11}}\tau_u \tag{6d}$$

$$\dot{u} = -\frac{d_{22}}{m_{22}}v + \boldsymbol{\phi}_v^T\boldsymbol{V}_c + \frac{1}{m_{22}}\tau_v \tag{6e}$$

$$\dot{r} = -\frac{d_{33}}{m_{33}}r + \frac{1}{m_{33}}\tau_r \tag{6f}$$

where it is defined that $m_{ij} \triangleq m_{ij}^{RB} + m_{ij}^A$, $\boldsymbol{V}_c = [V_x, V_y]^T$. The expressions $\boldsymbol{\phi}_u$, $\boldsymbol{\phi}_v$ is defined as

$$\boldsymbol{\phi}_u = \begin{bmatrix} -d_{11}\cos(\psi) + m_{11}^A r\sin(\psi) \\ -d_{11}\sin(\psi) - m_{11}^A r\cos(\psi) \end{bmatrix} \tag{7a}$$

$$\boldsymbol{\phi}_v = \begin{bmatrix} d_{22}\sin(\psi) + m_{22}^A r\cos(\psi) \\ -d_{22}\cos(\psi) + m_{22}^A r\sin(\psi) \end{bmatrix} \tag{7b}$$

C. Second Control Plant Model

The first control plant model proposed, essentially neglects the Coriolis-Centripetal forces comparing it to the general maneuvering model given in [9]. This control plant model expands the first control plant model to also consider the non-linear term form Coriolis-Centripetal forces. The maneuvering model of the 3-DOF ROV considered is:

$$\dot{\boldsymbol{\eta}} = \boldsymbol{R}(\psi)\boldsymbol{\nu} \tag{8}$$

$$\boldsymbol{M}_{RB}\dot{\boldsymbol{\nu}} + \boldsymbol{M}_A\dot{\boldsymbol{\nu}}_r + \boldsymbol{D}\boldsymbol{\nu}_r + \boldsymbol{C}_{RB}(\boldsymbol{\nu})\boldsymbol{\nu} + \boldsymbol{C}_A(\boldsymbol{\nu}_r)\boldsymbol{\nu}_r = \boldsymbol{\tau} \tag{9}$$

where the matrices and vectors are defined as with the first control plant model (3) and (4), but in addition $\boldsymbol{\tau} = \boldsymbol{B}\boldsymbol{f}$ and the Coriolis-Centripetal force matrix is defined as:

$$\boldsymbol{C}_i(\boldsymbol{\nu}) = \begin{bmatrix} 0 & 0 & -m_{22}^i v \\ 0 & 0 & m_{11}^i u \\ m_{22}^i v & -m_{11}^i u & 0 \end{bmatrix} \tag{10}$$

where $i \in \{RB, A\}$. In component form it can be written as

$$\dot{x} = u\cos(\psi) - v\sin(\psi) \tag{11a}$$

$$\dot{y} = u\sin(\psi) + v\cos(\psi) \tag{11b}$$

$$\dot{\psi} = r \tag{11c}$$

$$\begin{aligned} m_{11}\dot{u} + (m_{11}^A - m_{22}^A)r(V_x\sin(\psi) - V_y\cos(\psi)) \\ + d_{11}(u - V_x\cos(\psi) - V_y\sin(\psi)) - m_{22}vr = \tau_u \end{aligned} \tag{11d}$$

$$\begin{aligned} m_{22}\dot{v} - (m_{11}^A - m_{22}^A)r(V_x\cos(\psi) + V_y\sin(\psi)) \\ + d_{22}(v + V_x\sin(\psi) - V_y\cos(\psi)) + m_{11}ur = \tau_v \end{aligned} \tag{11e}$$

$$\begin{aligned} m_{33}\dot{r} + d_{33}r + (m_{22} - m_{11})uv - (m_{11}^A - m_{22}^A)\boldsymbol{v}^T\boldsymbol{\phi}(\psi)\boldsymbol{V}_c \\ + \frac{1}{2}(m_{11}^A - m_{22}^A)\boldsymbol{V}_c^T(\boldsymbol{\phi})(2\psi)\boldsymbol{V}_c = \tau_r \end{aligned} \tag{11f}$$

where it is defined that $\boldsymbol{V}_c = [V_x, V_y]^T$, $\boldsymbol{v} = [u, v]^T$ and the matrix:

$$\boldsymbol{\phi}(x) = \begin{bmatrix} \sin(x) & -\cos(x) \\ -\cos(x) & -\sin(x) \end{bmatrix} \tag{12}$$

III. Guidance systems

The guidance systems used for generation of time-varying references are presented. Two guidance systems in cascade is used, whereas the first ensures path following for traversing the net pen, and the second smooths out the reference value to avoid step responses in reference values given to the control systems.

A. Path Following Algorithm

Traversing the net pen utilizes the guidance law that was derived in [3]. It is a path following algorithm for following the net pen at a constant speed with a constant distance from the net structure. Formalized the algorithm solves

$$\lim_{t\to\infty} y_e(t) = 0 \tag{13a}$$

$$\lim_{t\to\infty} (\psi(t) - \psi_d(t)) = 0 \tag{13b}$$

$$\lim_{t\to\infty} (U(t) - U_d) = 0 \tag{13c}$$

where $U \triangleq \sqrt{u^2 + v^2}$ is the ROV speed, and $U_d > 0$ is the desired speed for traversing the net pen. y_e is the crosstrack-error calculated in the algorithm to generate waypoints to assure the ROV maintains a constant distance from the net pen.

B. Reference model

The reference model smooths out step responses to avoid bandwidth problems in the control system. In addition to smoothing out the step responses, the reference model provides reference values for higher-order reference terms. Mainly, a first-order lowpass filter is proposed for the velocity references smoothing out the desired velocity value. It is given as

$$T\dot{u}_r + u_r = u_d \tag{14}$$

Equation (14) smooths out the reference value u_d from the path following algorithm and provides the time-varying reference values $\dot{u}_r$ and u_r that the velocity control laws make the ROV track. The reference value u_r is essentially u_d smoothed out with a time constant T.

For the second controller, a third-order reference model for the heading was designed. This reference model provides reference values for yaw, yaw rate and its derivative as well. It is given by the equation

$$\dddot{\psi}_r + 2\omega_n\zeta\ddot{\psi}_r + \omega_n^2\dot{\psi}_r = \omega_n^2\psi_d \tag{15}$$

where ψ_d from the path following algorithm is smoothed out by this model obtaining the reference values $\ddot{\psi}_r, \dot{\psi}_r$ and ψ_r.

IV. Control System

This section presents the control objective to be achieved, in addition to proposes the control law achieving this control objective. The control objective to be achieved in this paper is: The control law designed for the control plant model should result in robust error-free trajectory tracking of time-varying references. More formalized, especially achieve:

$$\lim_{t\to\infty} (u(t) - u_d(t)) = 0 \tag{16a}$$

$$\lim_{t\to\infty} (v(t) - v_d(t)) = 0 \tag{16b}$$

$$\lim_{t\to\infty} (\psi(t) - \psi_d(t)) = 0 \tag{16c}$$

Moreover, the closed-loop system with the control law should result in an UGAS equilibrium point at the origin. The control law should be robust enough such that perfect knowledge of the modelling parameters is not necessary. It should also address limitations such as saturation of actuators does not become a problem, for instance with integrator windup.

A. Surge, Sway and Yaw Control for First Model

This part proposes a control law for the first control plant model given by (1) and (2).

To track the heading $\psi_d(t)$, the following control law is proposed:

$$\tau_r = m_{33}\dot{r}_d + d_{33}r_d - k_{p_\psi}(\psi - \psi_d) - k_{d_\psi}(r - r_d) \tag{17}$$

Where $k_{p_\psi}, k_{d_\psi} > 0$ is constant controller gains. This is a PD-controller with feedforward. To track the velocities $u_d(t)$ and $v_d(t)$ the following control law is proposed:

$$\boldsymbol{\tau}_2 = \boldsymbol{D}_2\boldsymbol{v}_d + \boldsymbol{M}_2\dot{\boldsymbol{v}}_d - \boldsymbol{M}_2\boldsymbol{K}_p(\boldsymbol{v} - \boldsymbol{v}_d) - \boldsymbol{M}_2\boldsymbol{G}(t)\hat{\boldsymbol{V}}_c \tag{18}$$

$$\dot{\hat{\boldsymbol{V}}}_c = \boldsymbol{\Gamma}\boldsymbol{G}^T(t)(\boldsymbol{v} - \boldsymbol{v}_d) \tag{19}$$

where the vectors are defined as: $\boldsymbol{\tau}_2 = [\tau_u, \tau_r]^T$, $\dot{\boldsymbol{v}}_d = [\dot{u}_d, \dot{v}_d]^T$, $\boldsymbol{v}_d = [u_d, v_d]^T$ and $\boldsymbol{v} = [u, v]^T$ and the matrices are defined as:

$$\boldsymbol{M}_2 = \begin{bmatrix} m_{11} & 0 \\ 0 & m_{22} \end{bmatrix}, \boldsymbol{D}_2 = \begin{bmatrix} d_{11} & 0 \\ 0 & d_{22} \end{bmatrix} \tag{20}$$

$$\boldsymbol{K}_p = \begin{bmatrix} k_{p_u} & 0 \\ 0 & k_{p_v} \end{bmatrix} \tag{21}$$

$$\boldsymbol{G(t)} = \begin{bmatrix} \frac{d_{11}}{m_{11}}\cos(\psi_d) & \frac{d_{11}}{m_{11}}\sin(\psi_d) \\ -\frac{d_{22}}{m_{22}}\sin(\psi_d) & \frac{d_{22}}{m_{22}}\cos(\psi_d) \end{bmatrix} \tag{22}$$

where $k_{p_u}, k_{p_v} > 0$ are the constant controller gains and the matrix $\boldsymbol{\Gamma} = \boldsymbol{\Gamma}^T > 0$ is a diagonal matrix containing the constant adaption gains for $\hat{\boldsymbol{V}}_c = [\hat{V}_x, \hat{V}_y]^T$. $\hat{\boldsymbol{V}}_c$ are the estimates for the ocean current V_x and V_y. This controller is an adaptive P-controller with feedforward.

It will now be shown that the proposed controllers will make the surge velocity, sway velocity and yaw angle converge to their reference values.

Define the following tracking errors:

$$\begin{aligned} \widetilde{\boldsymbol{v}} &\triangleq \boldsymbol{v} - \boldsymbol{v}_d \\ \widetilde{r} &\triangleq r - r_d \\ \widetilde{\psi} &\triangleq \psi - \psi_d \end{aligned} \tag{23}$$

and the estimation error:

$$\widetilde{\boldsymbol{V}}_c = \boldsymbol{V}_c - \hat{\boldsymbol{V}}_c \tag{24}$$

Inserting the control laws for surge velocity, sway velocity and yaw, the following closed-loop error dynamics are achieved:

$$\dot{\widetilde{r}} = -\left(\frac{d_{33} + k_{d_\psi}}{m_{33}}\right)\widetilde{r} - \frac{k_{p_\psi}}{m_{33}}\widetilde{\psi} \tag{25a}$$

$$\dot{\widetilde{\psi}} = \widetilde{r} \tag{25b}$$

$$\dot{\widetilde{\boldsymbol{v}}} = -(\boldsymbol{M}_2^{-1}\boldsymbol{D}_2 + \boldsymbol{K}_p)\widetilde{\boldsymbol{v}} + \boldsymbol{G}(t)\widetilde{\boldsymbol{V}}_c + \boldsymbol{g}(t)\boldsymbol{\theta} \tag{25c}$$

$$\dot{\widetilde{\boldsymbol{V}}}_c = -\boldsymbol{\Gamma}\boldsymbol{G}^T(t)\widetilde{\boldsymbol{v}} \tag{25d}$$

where it is defined that $\boldsymbol{\theta} \triangleq [r, \widetilde{\psi}]^T$ and it can be shown that $\boldsymbol{g}(t)$ is a bounded matrix giving the dynamics for $\boldsymbol{\theta}$ in the

velocity states. The structure of $\boldsymbol{g}(t)$ is given in the appendix. It will be shown that since the origin of the error system for the heading dynamics is UGES, then that term can be omitted for the control design.

Lemma 1. The origin of the closed-loop subsystem for yaw described by (25a) and (25b) is uniformly globally exponentially stable (UGES).

Proof. Calculating the eigenvalues of the subsystem, which is linear in $\widetilde{r}, \widetilde{\psi}$ by finding the zeros of the characteristic equation:

$$\lambda^2 + \frac{d_{33} + k_{d_\psi}}{m_{33}}\lambda + \frac{k_{p_\psi}}{m_{33}} = 0 \tag{26}$$

it is then straightforward to see that the eigenvalues are strictly negative, and thus will the solution converge uniformly and exponentially to the origin for any initial values $(\widetilde{r}_0, \widetilde{\psi}_0)$. □

Lemma 2. The origin of the closed-loop subsystem for the velocities and adaptive law given by (25c) and (25d) is UGAS and ULES.

Proof. First assume that $\boldsymbol{\theta} \equiv \mathbf{0}$, thus omitting the last term in (25c). It needs to be shown that the nominal system:

$$\dot{\widetilde{\boldsymbol{v}}} = -(\boldsymbol{M}_2^{-1}\boldsymbol{D}_2 + \boldsymbol{K}_p)\widetilde{\boldsymbol{v}} \tag{27}$$

is UGES. Consider the positive definite radially unbounded Lyapunov function:

$$k_1\|\widetilde{\boldsymbol{v}}\|^2 \leq V(\widetilde{\boldsymbol{v}}) = \frac{1}{2}\widetilde{\boldsymbol{v}}^T\widetilde{\boldsymbol{v}} \leq k_2\|\widetilde{\boldsymbol{v}}\|^2 \tag{28}$$

it can then be shown that there exists a $k_3 > 0$ such that:

$$\dot{V(\widetilde{\boldsymbol{v}})} = -\widetilde{\boldsymbol{v}}^T(\boldsymbol{M}_2^{-1}\boldsymbol{D}_2 + \boldsymbol{K}_p)\widetilde{\boldsymbol{v}} \leq k_3\|\widetilde{\boldsymbol{v}}\|^2 \tag{29}$$

Then, using [10] the origin of the nominal system is UGES. Furthermore, it can be shown that

$$\boldsymbol{G}^T(t)\boldsymbol{G}(t) > 0 \tag{30}$$

by utilizing Sylvester's criterion and show that the principle minors of the matrix is strictly positive.
Then by the theorem given in [4], all the assumptions holds resulting in that the origin of (25c) and (25d) is UGAS. Moreover, the origin is also ULES using the same theorem in [4]. □

Theorem 1. The origin of the closed-loop system with the adaptive laws is UGAS.

Proof. Define the closed-loop system for the heading (25a) and (25b) as subsystem Σ_1, and defined the closed-loop system for the velocities with the adaptive laws (25c) and (25d) as the subsystem Σ_2. It can then be seen that the system Σ_1 provides the input $\boldsymbol{\theta}$ to system Σ_2. Illustration of the cascaded system is given in Figure 2. It has been shown with Lemma 1 and Lemma 2 that the origin of both subsystem in the cascade is UGAS. Moreover, the heading dynamics are UGES and the velocities dynamics with the adaptive laws are ULES.
Furthermore, with $\boldsymbol{g}(t)$ defined as in the appendix. Using

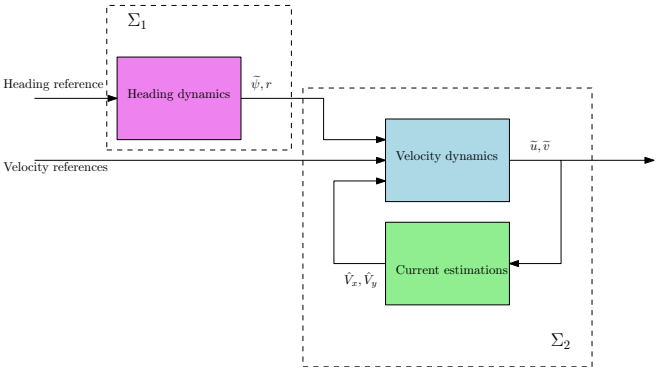

Fig. 2: The cascaded system

L'Hôpital's rule for the terms with possible singularities, it can be shown that the matrix element-wise is bounded. In other words, the interconnection between subsystem Σ_1 and Σ_2 is bounded. Then by utilizing the result and theorems from [11, 12] the origin of the fully cascaded system is UGAS. □

To conclude, this means that the closed-loop system of the first control plant model using the proposed controller obtains UGAS equilibrium point at the origin. Moreover, the heading dynamics have equilibrium point at the origin that is UGES and the velocities dynamics have equilibrium point at the origin that is ULES.

B. Surge, Sway and Yaw Control for Second Model

In this part a control law for the 3-DOF control plant model given by (8) and (9) is proposed.

$$\boldsymbol{\tau} = \boldsymbol{M}\dot{\boldsymbol{\nu}}_d + \boldsymbol{D}\boldsymbol{\nu}_d + \boldsymbol{s} + \hat{\boldsymbol{a}} - \boldsymbol{M}\boldsymbol{K}\widetilde{\boldsymbol{\nu}}_{\text{aug}} - \boldsymbol{M}_{\text{aug}}\boldsymbol{G}(\boldsymbol{\nu}_{\text{aug}}, t)\hat{\boldsymbol{V}}_c \tag{31}$$

where it is defined that $\boldsymbol{M} \triangleq \boldsymbol{M}_{RB} + \boldsymbol{M}_A$, $\boldsymbol{\nu}_d = [u_d, v_d, r_d]^T$, $\dot{\boldsymbol{\nu}}_d = [\dot{u}_d, \dot{v}_d, \dot{r}_d]^T$ and $\widetilde{\boldsymbol{\nu}}_{\text{aug}} = [\widetilde{u}, \widetilde{v}, \widetilde{r}, \widetilde{\psi}]^T$. The feedback linearizing vector and the vector for handling unknown quadratic terms are defined as:

$$\boldsymbol{s} = \begin{bmatrix} -m_{22}vr \\ m_{11}ur \\ (m_{22} - m_{11})uv \end{bmatrix} \tag{32}$$

$$\hat{\boldsymbol{a}} = \begin{bmatrix} 0 \\ 0 \\ (m_{22}^A - m_{11}^A)\boldsymbol{\alpha}_e^T\hat{\boldsymbol{e}} \end{bmatrix} \tag{33}$$

where the vectors are defined as:

$$\boldsymbol{\alpha}_e = \begin{bmatrix} -\frac{1}{2}\sin(2\psi) \\ \cos(2\psi) \\ \frac{1}{2}\sin(2\psi) \end{bmatrix}, \hat{\boldsymbol{e}} = \begin{bmatrix} \widehat{V_x^2} \\ \widehat{V_x V_y} \\ \widehat{V_y^2} \end{bmatrix} \tag{34}$$

The matrices are defined as in (4), in addition to:

$$\boldsymbol{M}_{\text{aug}} \triangleq \begin{bmatrix} m_{11} & 0 & 0 & 0 \\ 0 & m_{22} & 0 & 0 \\ 0 & 0 & m_{33} & 0 \end{bmatrix} \tag{35}$$

$$\boldsymbol{K} \triangleq \begin{bmatrix} k_{p_u} & 0 & 0 & 0 \\ 0 & k_{p_v} & 0 & 0 \\ 0 & 0 & k_{d_\psi} & k_{p_\psi} \end{bmatrix} \tag{36}$$

$$\boldsymbol{G}(\boldsymbol{\nu}_{\text{aug}}, t) \triangleq \begin{bmatrix} G_{11} & G_{12} \\ G_{21} & G_{22} \\ G_{31} & G_{32} \\ 0 & 0 \end{bmatrix} \tag{37}$$

where the values in the matrix $\boldsymbol{G}$ are defined as

$$G_{11} = \frac{m_{22}^A - m_{11}^A}{m_{11}} r \sin(\psi) + \frac{d_{11}}{m_{11}} \cos(\psi) \tag{38a}$$

$$G_{12} = -\frac{m_{22}^A - m_{11}^A}{m_{11}} r \cos(\psi) + \frac{d_{11}}{m_{11}} \sin(\psi) \tag{38b}$$

$$G_{21} = -\frac{m_{22}^A - m_{11}^A}{m_{22}} r \cos(\psi) - \frac{d_{22}}{m_{22}} \sin(\psi) \tag{38c}$$

$$G_{22} = -\frac{m_{22}^A - m_{11}^A}{m_{22}} r \sin(\psi) + \frac{d_{22}}{m_{22}} \cos(\psi) \tag{38d}$$

$$G_{31} = -\frac{m_{22}^A - m_{11}^A}{m_{33}} (u \sin(\psi) - v \cos(\psi)) \tag{38e}$$

$$G_{32} = \frac{m_{22}^A - m_{11}^A}{m_{33}} (u \cos(\psi) + v \sin(\psi)) \tag{38f}$$

In addition the estimates for $\hat{\boldsymbol{V}}_c$ and $\hat{\boldsymbol{e}}$ have the dynamics:

$$\dot{\hat{\boldsymbol{V}}}_c = \boldsymbol{\Gamma}_1 \boldsymbol{G}^T(\boldsymbol{\nu}_{\text{aug}}, t) \left(\frac{\partial W(\widetilde{\boldsymbol{\nu}}_{\text{aug}})}{\partial \boldsymbol{\nu}_{\text{aug}}} \right)^T \tag{39}$$

and the error for the adaptive quadratic term:

$$\dot{\hat{\boldsymbol{e}}} = -\frac{m_{22}^A - m_{11}^A}{m_{33}} \boldsymbol{\Gamma}_2 \boldsymbol{\alpha}_e (m_{66} \widetilde{r} + \epsilon \widetilde{\psi}) \tag{40}$$

Due to assumption of constant ocean current, then it means that $\dot{\widetilde{\boldsymbol{e}}} = -\dot{\hat{\boldsymbol{e}}}$. For the adaptive laws it is defined that $\boldsymbol{\Gamma}_1 \in \mathbb{R}^{2\times 2}$ and $\boldsymbol{\Gamma}_2 \in \mathbb{R}^{3\times 3}$ are positive definite diagonal tuning matrices. That is, the tuning parameters are on the diagonals of the matrices with positive values, and off-diagonal elements are set to 0. In addition the tuning parameter ϵ is defined such as:

$$0 < \epsilon < \frac{d_{33} k_{p_\psi} + m_{66} k_{p_\psi} k_{d_\psi}}{k_{p_\psi} + \frac{1}{4} \left(\frac{d_{66}}{m_{66}} + k_{d_\psi} \right)} \wedge \epsilon < m_{66} \sqrt{k_{p_\psi}} \tag{41}$$

Last but not least define:

$$W(\widetilde{\boldsymbol{\nu}}_{\text{aug}}) = \frac{1}{2} \widetilde{\boldsymbol{\nu}}_{\text{aug}}^T \boldsymbol{P} \widetilde{\boldsymbol{\nu}}_{\text{aug}} \tag{42a}$$

$$\left(\frac{\partial W(\widetilde{\boldsymbol{\nu}}_{\text{aug}})}{\partial \boldsymbol{\nu}_{\text{aug}}} \right)^T = \begin{bmatrix} m_{11} \widetilde{u} \\ m_{22} \widetilde{v} \\ m_{33} \widetilde{r} + \epsilon \widetilde{\psi} \\ m_{33} k_{p_\psi} \widetilde{\psi} + \epsilon \widetilde{r} \end{bmatrix} \tag{42b}$$

where

$$\boldsymbol{P} = \begin{bmatrix} m_{11} & 0 & 0 & 0 \\ 0 & m_{22} & 0 & 0 \\ 0 & 0 & m_{33} & \epsilon \\ 0 & 0 & \epsilon & m_{33} k_{p_\psi} \end{bmatrix} \tag{43}$$

Inserting the control law (31) into (9), and define the error variables:

$$\begin{aligned} \widetilde{u} &= u - u_d \\ \widetilde{v} &= v - v_d \\ \widetilde{r} &= r - r_d \\ \widetilde{\psi} &= \psi - \psi_d \end{aligned} \tag{44}$$

and the estimation errors as:

$$\begin{aligned} \widetilde{\boldsymbol{V}}_c &= \boldsymbol{V}_c - \hat{\boldsymbol{V}}_c \\ \widetilde{\boldsymbol{e}} &= \begin{bmatrix} V_x V_x - \widehat{V_x V_x} \\ V_x V_y - \widehat{V_x V_y} \\ V_y V_y - \widehat{V_y V_y} \end{bmatrix} \end{aligned} \tag{45}$$

then the closed-loop system of the ROV can be written as:

$$\dot{\widetilde{\boldsymbol{\nu}}}_{\text{aug}} = -\boldsymbol{A} \widetilde{\boldsymbol{\nu}}_{\text{aug}} + \boldsymbol{\sigma}(\boldsymbol{v}, \widetilde{\boldsymbol{e}}) + \boldsymbol{G}(\boldsymbol{\nu}_{\mathbf{aug}}, t) \widetilde{\boldsymbol{V}}_c \tag{46}$$

where it is defined that

$$\boldsymbol{A} = \begin{bmatrix} \frac{d_{11}}{m_{11}} + k_{p_u} & 0 & 0 & 0 \\ 0 & \frac{d_{22}}{m_{22}} + k_{p_v} & 0 & 0 \\ 0 & 0 & \frac{d_{33}}{m_{33}} + k_{d_\psi} & k_{p_\psi} \\ 0 & 0 & 1 & 0 \end{bmatrix} \tag{47}$$

and

$$\boldsymbol{\sigma}(\boldsymbol{v}, \widetilde{\boldsymbol{e}}) = \begin{bmatrix} 0 \\ 0 \\ \frac{m_{11}^A - m_{22}^A}{m_{33}} \widetilde{\boldsymbol{e}}^T \boldsymbol{\alpha}_e \\ 0 \end{bmatrix} \tag{48}$$

Lemma 3. The origin of the full closed-loop system with the adaptive laws are UGS.

Proof. Choose the positive definite and radially unbounded Lyapunov function candidate:

$$V(\boldsymbol{x}) = W(\widetilde{\boldsymbol{\nu}}_{\text{aug}}) + \frac{1}{2} \widetilde{\boldsymbol{V}}_c \boldsymbol{\Gamma}_1^{-1} \widetilde{\boldsymbol{V}}_c + \frac{1}{2} \widetilde{\boldsymbol{e}} \boldsymbol{\Gamma}_2^{-1} \widetilde{\boldsymbol{e}} \tag{49}$$

then the derivative along the trajectories of $\boldsymbol{x}$, with the chosen adaptive laws results in:

$$\dot{V} = -\widetilde{\boldsymbol{\nu}}_{\text{aug}}^T \boldsymbol{H} \widetilde{\boldsymbol{\nu}}_{\text{aug}} \tag{50}$$

where

$$\boldsymbol{H} = \begin{bmatrix} \boldsymbol{H}_1 & 0_{2\times 2} \\ \mathbf{0}_{2\times 2} & \boldsymbol{H}_2 \end{bmatrix} \tag{51}$$

where $\boldsymbol{H}_1 = \text{diag}\{d_{11} + m_{11} k_{p_u}, d_{22} + m_{22} k_{p_v}\}$ and

$$\boldsymbol{H}_2 = \begin{bmatrix} d_{66} + m_{66} k_{d_\psi} - \epsilon & \frac{1}{2}\epsilon(\frac{d_{66}}{m_{66}} + k_{d_\psi}) \\ \frac{1}{2}\epsilon(\frac{d_{66}}{m_{66}} + k_{d_\psi}) & k_{p_\psi} \epsilon \end{bmatrix} \tag{52}$$

where $\boldsymbol{H}$ is positive definite, proven with Sylvester's criterion, when ϵ is chosen such that the bounds that has been set on it in (41) holds. Thus, the origin of the closed-loop system is UGS according to [10]. □

Furthermore,

Corollary 1. $\widetilde{\boldsymbol{\nu}}_{\text{aug}}$ uniformly and globally asymptotically converges to the equilibrium point at the origin.

Proof. Using the Lyapunov function it can be written to:

$$\begin{aligned}\dot{V} &= -\widetilde{\boldsymbol{\nu}}_{\text{aug}}^T \boldsymbol{H} \widetilde{\boldsymbol{\nu}}_{\text{aug}} - \widetilde{\boldsymbol{\nu}}_{\text{aug}}^T \widetilde{\boldsymbol{\nu}}_{\text{aug}} + \widetilde{\boldsymbol{\nu}}_{\text{aug}}^T \widetilde{\boldsymbol{\nu}}_{\text{aug}} \\ &\leq -\widetilde{\boldsymbol{\nu}}_{\text{aug}}^T \boldsymbol{H} \widetilde{\boldsymbol{\nu}}_{\text{aug}} - \widetilde{\boldsymbol{\nu}}_{\text{aug}}^T \widetilde{\boldsymbol{\nu}}_{\text{aug}} + |\widetilde{\boldsymbol{\nu}}_{\text{aug}}^T||\widetilde{\boldsymbol{\nu}}_{\text{aug}}|\end{aligned} \tag{53}$$

since it was proven that $\widetilde{\boldsymbol{\nu}}_{\text{aug}}$ is UGS then there exists a κ_∞-function $\rho(R(\boldsymbol{r}))$ which is a function of the number R that depends on the ball with radius $\boldsymbol{r}$ that is bounding all the initial states for the full system with adaptive laws. In addition it can be shown that $\phi_1(t, \widetilde{\boldsymbol{\nu}}_{\text{aug}})^2 = \widetilde{\boldsymbol{\nu}}_{\text{aug}}^T \boldsymbol{H} \widetilde{\boldsymbol{\nu}}_{\text{aug}} + \widetilde{\boldsymbol{\nu}}_{\text{aug}}^T \widetilde{\boldsymbol{\nu}}_{\text{aug}}$. Thus,

$$\begin{aligned}\dot{V} &\leq -\phi_1(t, \widetilde{\boldsymbol{\nu}}_{\text{aug}})^2 + |\widetilde{\boldsymbol{\nu}}_{\text{aug}}^T| \rho(R(\boldsymbol{r})), \forall |\boldsymbol{x}_0| \leq \boldsymbol{r} \\ &\leq -\phi_1(t, \widetilde{\boldsymbol{\nu}}_{\text{aug}})^2 + \frac{1}{\epsilon_\rho} |\widetilde{\boldsymbol{\nu}}_{\text{aug}}|^2 + \epsilon_\rho \rho(R(\boldsymbol{r}))^2\end{aligned} \tag{54}$$

where $\epsilon_\rho > 0$ and the last inequality is a result of Young's inequality. Then, by choosing $\nu := \epsilon_\rho \rho(R(\boldsymbol{r}))^2$ then:

$$\begin{aligned}\dot{V} &\leq -[\phi_1(t, \widetilde{\boldsymbol{\nu}}_{\text{aug}})^2 - \nu] + \frac{1}{\epsilon_\rho} |\widetilde{\boldsymbol{\nu}}_{\text{aug}}|^2 \\ \int_{t_0}^{\infty} [\phi_1(t, \widetilde{\boldsymbol{\nu}}_{\text{aug}})^2 - \nu] dt &\leq \int_{t_0}^{\infty} \frac{1}{\epsilon_\rho} |\widetilde{\boldsymbol{\nu}}_{\text{aug}}|^2 dt - \int_{t_0}^{\infty} \dot{V} dt \\ \int_{t_0}^{\infty} [\phi_1(t, \widetilde{\boldsymbol{\nu}}_{\text{aug}})^2 - \nu] dt &\leq \beta_{\boldsymbol{r}\nu}\end{aligned} \tag{55}$$

Furthermore, from the properties that $\dot{V} \leq 0$ then it can be shown that $\dot{V}, \widetilde{\boldsymbol{\nu}}_{\text{aug}} \in \mathcal{L}_2, \mathcal{L}_\infty$. This is used to show that $\beta_{\boldsymbol{r}\nu} > 0$ since $\epsilon_\rho > 0$ can be chosen arbitrarily small dominating the negative term from the integration of $\dot{V}$ which is bounded. Then by [13, Lemma 2] the equilibrium point at the origin of $\widetilde{\boldsymbol{\nu}}_{\text{aug}}$ is UGAS. □

V. Amelioriating The First Control Law

The adaptive law for the first control law can in many ways be interpreted as an integrator term in a PI-controller. A limitation of this adaptive law that needs to be addressed is integrator windup occurring when actuation becomes saturated. The controller, therefore, required anti-windup schemes to be implemented in the control laws integral terms to handle the effects of thruster saturation. The first control law implemented two anti-windup schemes to address this limitation.

A. Clamping

The first anti-windup scheme implemented was clamping. It is a reasonably simple anti-windup scheme and stops the integral states from growing when the thrusters are saturated. The implementation for this control law was to calculate the max actuation force the ROV can exert. The control input was then compared to the limit and checked if the adaptive law was growing or descending towards the origin. If the control input was above the limit and the adaptive law was increasing, the clamping algorithm set $\dot{\hat{\boldsymbol{V}}}_c = \boldsymbol{0}$, otherwise, the adaptive law ran according to the equation given in (25c).

B. Projection

The second anti-windup scheme implemented was projection. It works as an operator, and are designed to keep the integral states within a pre-defined bound. Since the adaptive laws essentially are estimates of the ocean current in $\{n\}$, they must therefore be upper bounded by a value $\hat{V}_{\max} \geq V_{\max}$. This can be utilized by implementing the projection operator given in [14]. If $\dot{\hat{\boldsymbol{V}}}_c$ makes $\hat{\boldsymbol{V}}_c$ out of bounds, the operator project the change such that it is pushed back in. More formalized the projection operator are implemented for each $\hat{V}_x$ and $\hat{V}_y$ as:

$$\dot{\hat{V}}_i = \gamma_i \text{Proj}(\hat{V}_i, \boldsymbol{G}^T \widetilde{\boldsymbol{v}}) \tag{56}$$

where

$$\text{Proj}(\hat{V}_i, y) \triangleq \begin{cases} y, \text{if } g(\hat{V}_i) < 0 \vee g(\hat{V}_i) \geq 0 \wedge \nabla g^T y \leq 0 \\ y - \frac{\nabla g \nabla g^T y g}{\|\nabla g\|^2}, \text{if } g(\hat{V}_i) \geq 0 \wedge \nabla g^T y \geq 0 \end{cases} \tag{57}$$

and

$$g(\hat{V}_i) = \frac{(\epsilon_{V_i} + 1)\hat{V}_i^T \hat{V}_i - V_{\max}^2}{\epsilon_{V_i} V_{\max}^2} \tag{58}$$

VI. Simulations and Experiments

This section presents the simulation results and results from experiments for verification of the proposed control laws. The first proposed control law was simulated, then tested at SINTEF ACE live fish farm for aquaculture experiments. While the second control law was only simulated. All the results will be presented.

A. Vehicle Model

The vehicle used was a 90 kg Argus Mini ROV with dimensions $[0.9\text{m}, 0.65\text{m}, 0.6\text{m}]^T$. In order to have simulations directly compared to the experiments, a process plant model as close to the vehicle while still satisfying all the Assumptions 1-7 is used.

The ROV has four horizontal thrusters and two vertical thrusters. The horizontal thrusters have azimuth angles of $\pm 35°$, actuating surge, sway and yaw DOFs. In the simulations, the thrusters have been saturated, and their rate of change limited with a slew rate limiter to achieve as realistic response as possible.

B. Simulation Setup

The simulation results were obtained for net pen following utilizing either one of the two control laws that have been proposed.

All simulations are run using FhSim software, which can be read more about in [15] and [16]. FhSim is a framework hosted by SINTEF Ocean, which is developed for time-domain simulations of surface vessels, underwater vehicles and marine structure operating in fisheries and aquaculture.

The net pen is simulated with a simulation model of a static circular net cage and is constructed from a large number of vertices. For the guidance law, the desired distance to the net is set to 3 m, while the desired speed U_d is set to 0.3m/s for the first control law and 0.5m/s for the simulation of the

second control law. At the field trial, the desired speed was varying, but at the highest, it was set to $0.3\mathrm{m/s}$.

C. Control Law 1

The first control law was essentially a PD-controller for the heading in parallel with adaptive P-controllers for the velocities. However, due to unmodelled dynamics in the heading, preliminary simulations showed that with a PD-controller, a constant deviation was present. The heading controller was, therefore, in the simulations modified also to include an integral error term, becoming a PID-controller; this modification took care of the constant deviation.

For the simulations the reference models for the velocity controllers were tuned with a time constant of $T = 0.5\mathrm{s}$ for both surge and sway. The anti-windup scheme, the projection operator, was tuned with a maximum ocean velocity bound $V_{\max} = 0.5$ and projection tolerance $\epsilon_{V_i} = 0.2$. The adaptive laws was tuned with $\gamma_x = 3.5$ for estimation of $\hat{V}_x$ and $\gamma_y = 3.0$ for estimation of $\hat{V}_y$. The P-controller was tuned with the gains $k_{p_u} = k_{p_v} = 4.0$ for both surge and sway velocity. The PID controller was tuned with $k_{p_\psi} = 15$, $k_{i_\psi} = 0.5$ and $k_{d_\psi} = 0.1$.

For the field trial, from experience, the controller often needs to be tuned less aggressively. For the results presented, the tuning that was used was therefore $T = 1.0\mathrm{s}$ for the reference models in surge and sway. The anti-windup scheme was tuned with $V_{\max} = 0.5$ and projection tolerance $\epsilon_{V_i} = 1.0$. The adaptive laws was tuned with $\gamma_x = \gamma_y = 2.0$ and the proportional gain $k_{p_u} = k_{p_v} = 5.0$. The PID controller for the heading was tuned with $k_{p_\psi} = 15$, $k_{i_\psi} = 0.5$ and $k_{d_\psi} = 1.0$.

D. Control Law 2

The second control law was implemented and simulated with first-order reference models for the velocities and a third-order reference model for the heading in FhSim. The first-order reference model was tuned with time constant $T = 0.5\mathrm{s}$ for both surge and sway, meanwhile the third-order reference model was tuned with bandwidth and damping ratio $\omega_n = 1.6$ and $\zeta = 1.0$ respectively. The projection operator was tuned with $\epsilon_{V_i} = 0.2$ and $V_{\max} = 0.5$. The factor for the cross-elements had to be tuned with a value bounded by (41) and was chosen to be $\epsilon_\psi = 0.1$. The adaptive law for the unknown quadratic term was tuned with $\gamma_{ei} = 0.0001$ for all three diagonal elements in $\mathbf{\Gamma}_2$, and $\gamma_x = \gamma_y = 0.01$ for the diagonal elements in $\mathbf{\Gamma}_1$. The P-controller for the velocities was tuned with $k_{p_u} = k_{p_v} = 5.0$. The last tuning parameter, the PD-part of the heading controller, was tuned $k_{p_\psi} = 46.6340$ and $k_{d_\psi} = 14.0304$.

E. Simulation results

Figure 3 is the simulation of C1, and shows that the controller tracks the velocity references with less to none error. The velocities of the ROV in Figure 3a-3b is given in blue, the green dashed line is the desired velocity from the net following algorithm and the red dashed line is the reference values from the reference models. It is only due to the dynamics of the reference model that gives an error in the tracking of the desired value u_r and v_r given by the net following algorithm by looking at the spikes. The controller itself manages to follow the reference values more or less perfectly.

The thruster dynamics in simulation of C1 is given in Figure 3c-3d and shows the desired control input calculated by the control law in red and the actual actuation of the ROV given in blue. The ROV rarely goes into saturation, and could have been simulated to do so to demonstrate the anti-windup schemes working. The spikes in the thruster figures is going quickly to 0 due to the simulation set up having a switch so that the velocity controllers are turned off, or set to 0 when controlling the heading. It is only in short bursts it is turnt off and due to this should not affect the velocities significantly.

The ocean current dynamics, or rather the integrator terms, are given in Figure 3e-3f. It is not much to say for these plots, except that it seems to work as intended achieving varying estimations based on the position of the ROV in the net pen.

Figure 4 is the simulation of C2. The figure shows that this controller tracks the velocity references with minor deviations. It also seems to be limited by the reference models tracking it more or less perfectly but having some minor deviation relative to the desired values from the net following algorithm at the step responses. It only seems to oscillate and struggle when the desired speed is set at a value the ROV is not physically able to reach due to thruster limitations. However, it oscillates mostly when the thrusters are in saturation, which is confirmed with the thruster plots, Figure 4c-4d, showing that it cannot reach the desired control input.

F. Sea trials

Figure 5 shows the simulation of C1 at SINTEF ACE live fish farm for aquaculture experiments. The velocity figures show that it is tracking the velocities satisfyingly with little deviations. At $350\mathrm{s} - 370\mathrm{s}$, the thrusters goes into saturation, where the deviation becomes significant. The velocity references are, otherwise, tracked, showing excellent results compared to the formerly used PI controller in Figure 6.

Looking at Figure 5e-5f, it is seen that at the moment the thrusters go into saturation, the estimates oscillate violently. This shows that the projection operator works as intended and prevents a higher integral value than the ROV can account for. It also makes sure that the velocities do not oscillate as much when it is in saturation, which is promising with robustness in mind.

G. Heading

The yaw dynamics in Figure 7b only struggle when the yaw changes significantly, much like the PID controller in Figure 7a. However, it still manages to follow the reference values from the reference model, suggesting that it is limited by the reference model itself and not the ROV limitations.

The heading plots in Figure 7c, shows that the PID controller

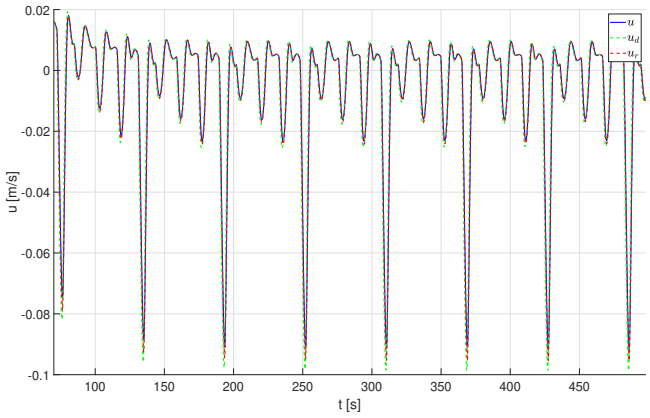

(a) Surge velocity

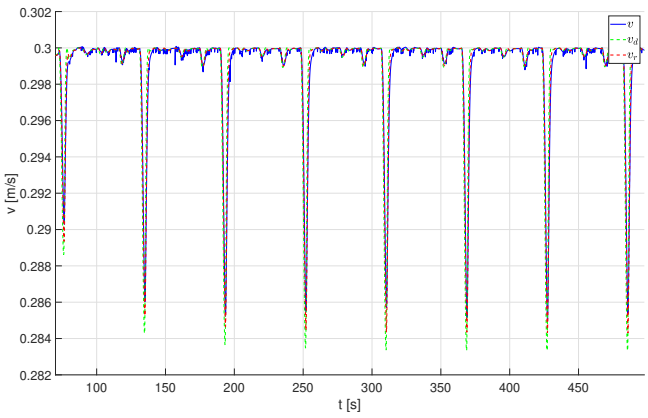

(b) Sway velocity

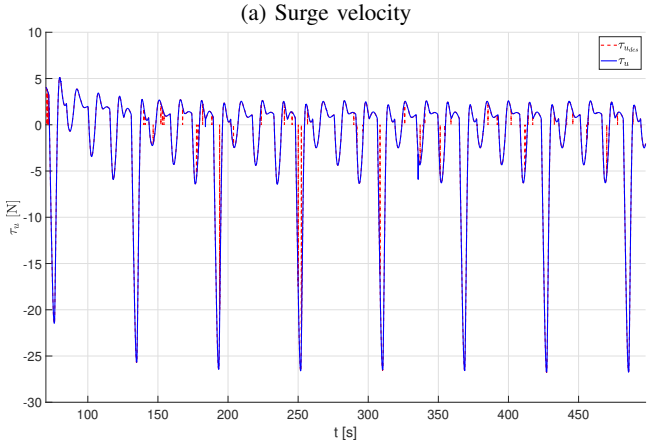

(c) Surge actuation

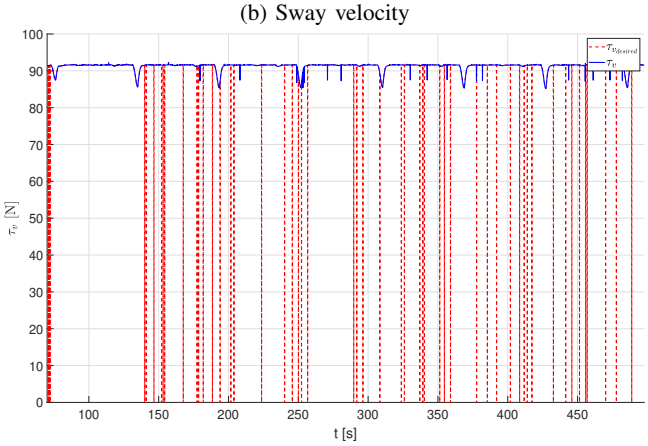

(d) Sway actuation

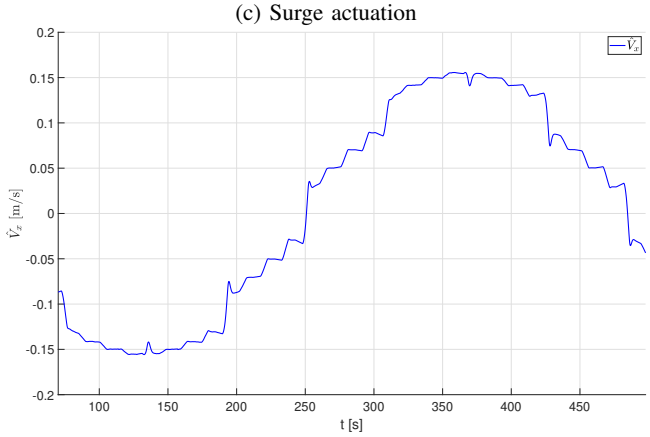

(e) Ocean current estimate u in NED

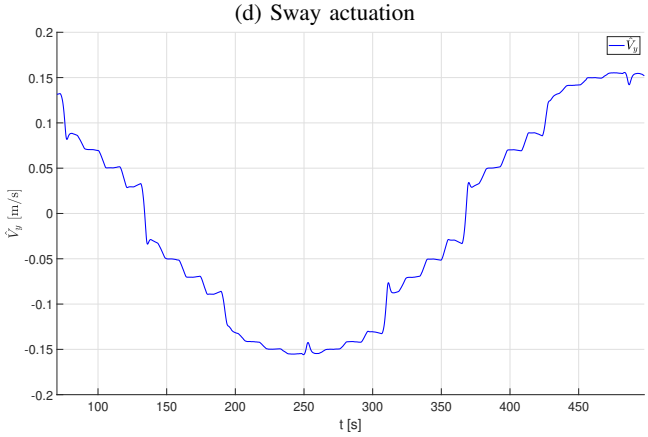

(f) Ocean current estimate v in NED

Fig. 3: Results from simulation of controller 1 with process plant model

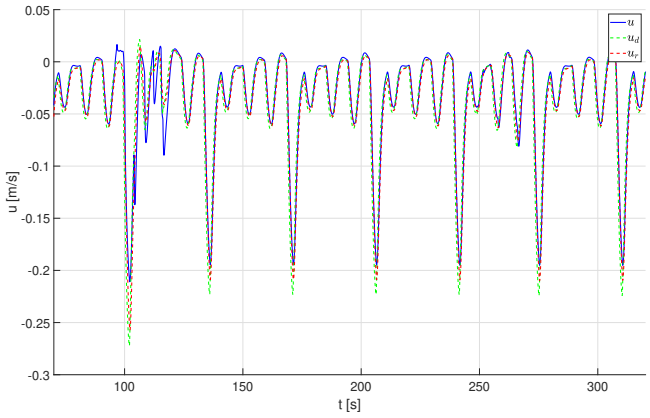

(a) Surge velocity

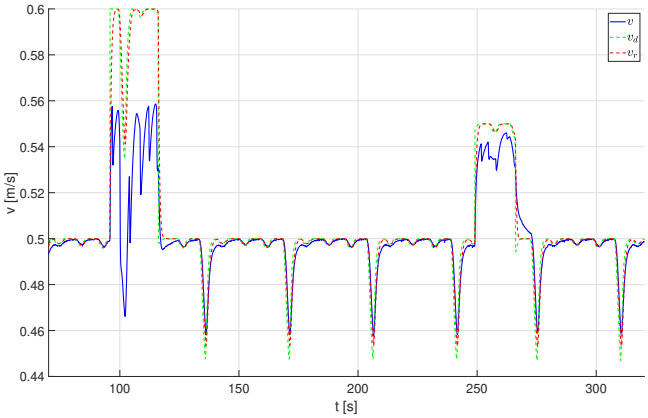

(b) Sway velocity

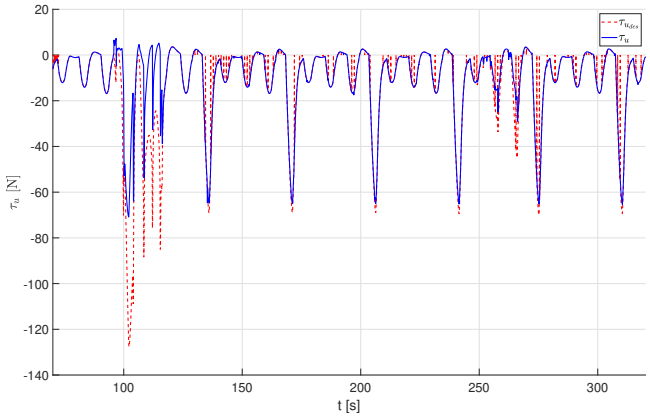

(c) Surge actuation

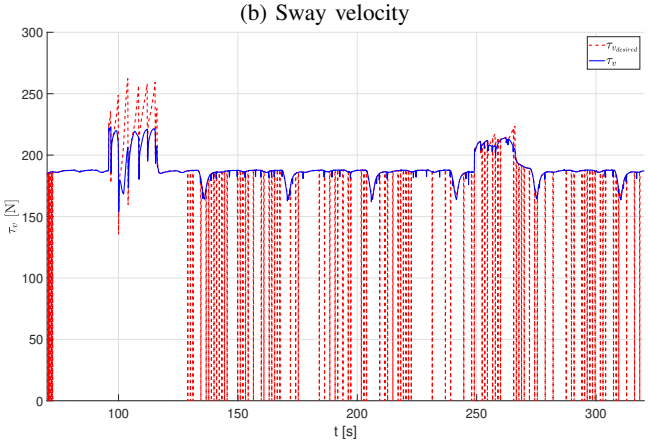

(d) Sway actuation

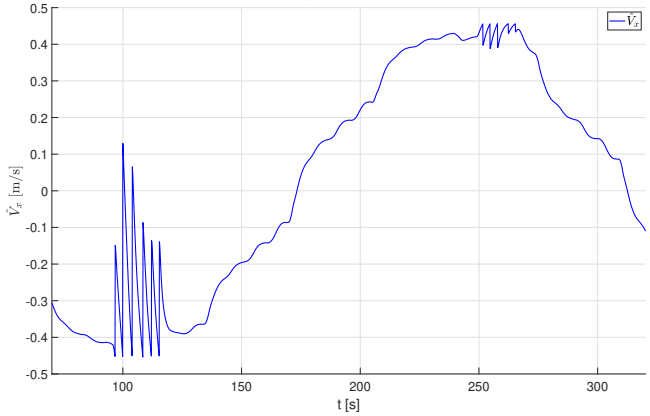

(e) Ocean current estimate u in NED

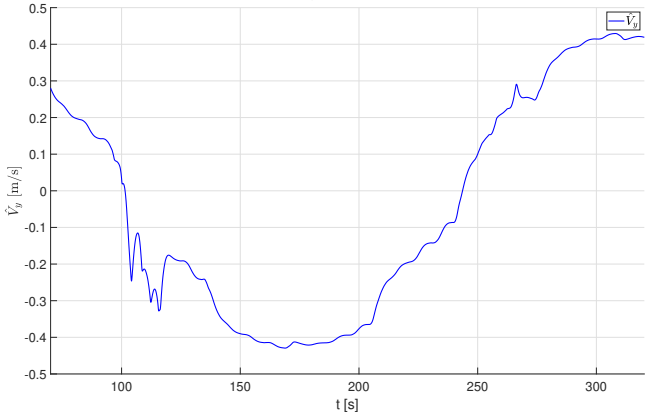

(f) Ocean current estimate v in NED

Fig. 4: Results from simulation of controller 2 with process plant model

follows the contour of the desired reference values at field trial. As suggested earlier, it might be that the thrusters of the ROV cannot exert enough torque so that the heading of the ROV follows a quick varying reference value.
Overall, the simulations shows that C2 performs more or less as good as C1 or the PID controller does. However, at field trial the PID controller obtained worse response by not tracking the reference perfectly. The PID controller does, however, follow the contour of the heading which is arguably good enough for the path following. Overall, C2 has promising heading results and is a candidate for further testing before doing it with field experiments.

VII. Conclusion and Future Work

This paper has presented two control laws for tracking time-varying reference values in the surge, sway, and yaw DOF to optimally autonomously traverse an aquaculture net pen. The main contribution of this paper is proposed control laws with properties that asymptotically converges to the time-varying reference values.
For C1, the closed-loop system using this controller with the adaptive law was proven to be UGAS in the equilibrium point at the origin. Furthermore, to consider saturation and integrator windup that might have caused oscillations for the closed-loop system, or in worse case destabilized it, anti-windup schemes were implemented. The anti-windup methods, clamping and projection, assured that the limitation of the ROV was properly handled. The controller was then validated through simulations and sea trials, yielding great results. C1 managed to achieve the control objective.
For C2, the closed-loop system with the adaptive laws was proven to be UGS in the equilibrium point at the origin. This controller was an augmented version of C1, which also considered the deviation in heading and attempted to suppress the deviation. It was proven that the error states for the velocities and yaw globally converged asymptotically and uniformly to the equilibrium point at the origin. This controller was validated through simulations and also showed excellent results. It managed to track the reference values for the velocities, as well as track the reference value for heading. C2 was not tested extensively as C1 for robustness properties. The robustness properties of the second controller still have to be validated in the simulations. If the results are satisfactory, this controller can also be validated in field trials and compared to the first controller. This remains future work.

Appendix

$$\boldsymbol{g}(t) = \begin{bmatrix} g_{11} & g_{12} \\ g_{21} & g_{22} \end{bmatrix} \tag{59}$$

where

$$\begin{aligned} g_{11} &= m_{11}^{A}(V_x \sin(\psi) + V_y \cos(\psi)) \\ g_{12} &= -d_{11}(V_x \beta_1 + V_y \beta_2) \\ g_{21} &= m_{22}^{A}(-V_x \cos(\psi) + V_y \sin(\psi)) \\ g_{22} &= d_{22}(V_x \beta_2 - V_y \beta_1) \end{aligned} \tag{60}$$

and it is defined that

$$\beta_1 = \cos(\psi_d)\frac{\cos(\widetilde{\psi}) - 1}{\widetilde{\psi}} - \sin(\psi_d)\frac{\sin(\widetilde{\psi})}{\widetilde{\psi}} \tag{61a}$$

$$\beta_2 = \sin(\psi_d)\frac{\cos(\widetilde{\psi}) - 1}{\widetilde{\psi}} + \cos(\psi_d)\frac{\sin(\widetilde{\psi})}{\widetilde{\psi}} \tag{61b}$$

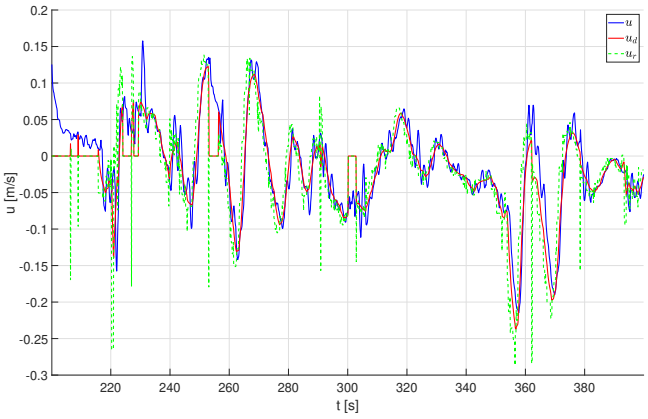

(a) Surge velocity

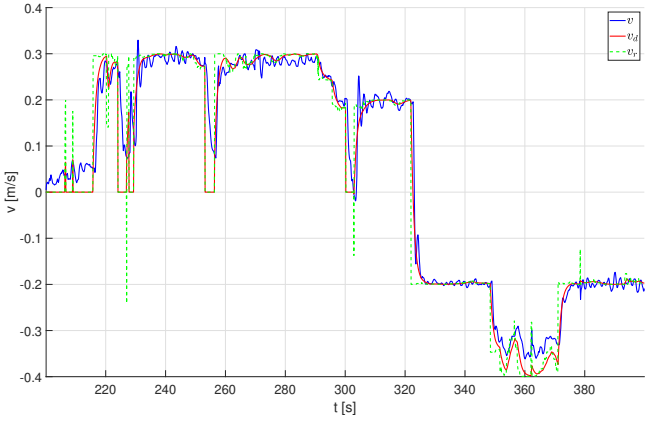

(b) Sway velocity

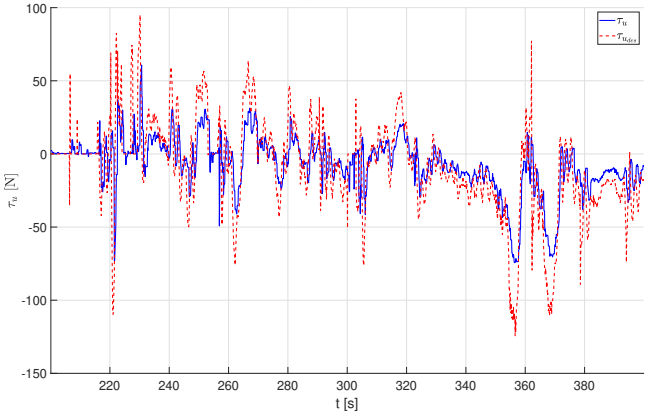

(c) Surge actuation

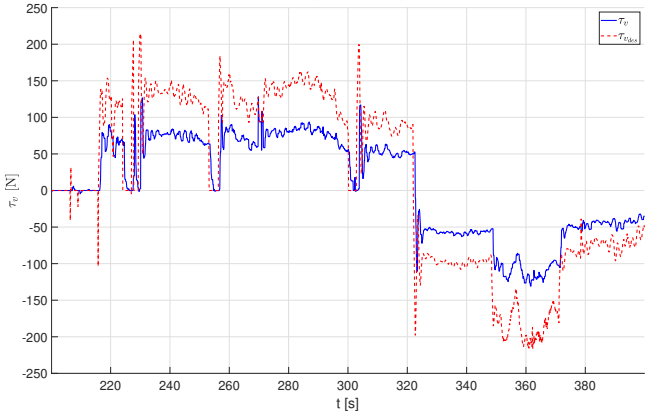

(d) Sway actuation

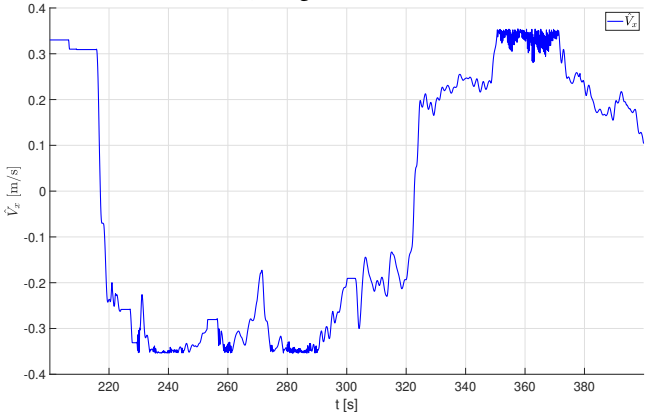

(e) Ocean current estimate u in NED

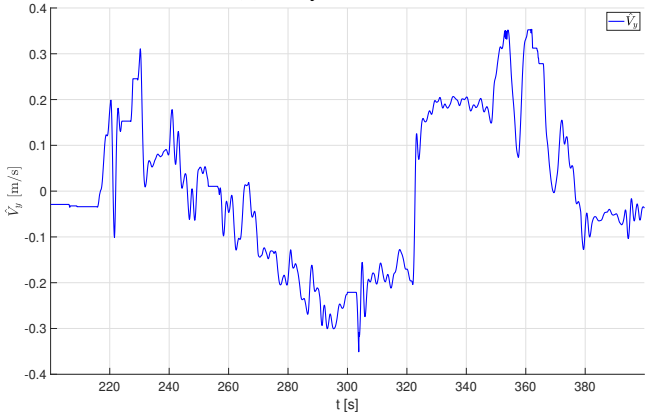

(f) Ocean current estimate v in NED

Fig. 5: Results from field trial at SINTEF ACE for controller 1

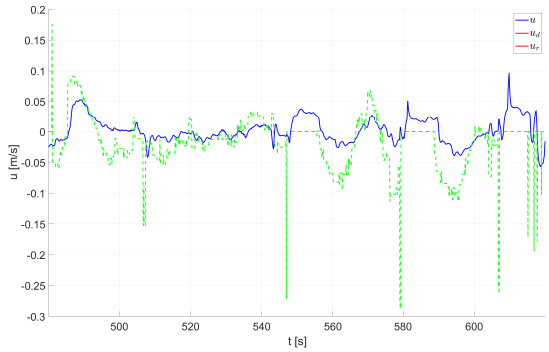

(a) Surge velocity at field trial on SINTEF ACE with PI controller

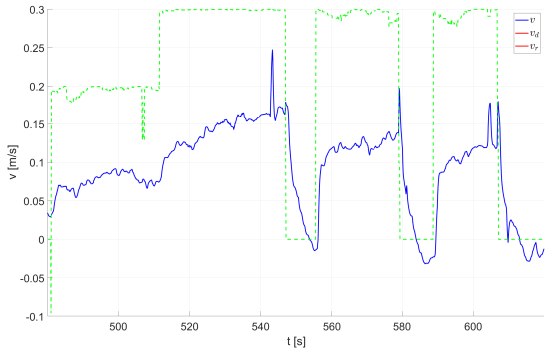

(b) Sway velocity at field trial on SINTEF ACE with PI controller

Fig. 6: The velocities with PI controller at field trial

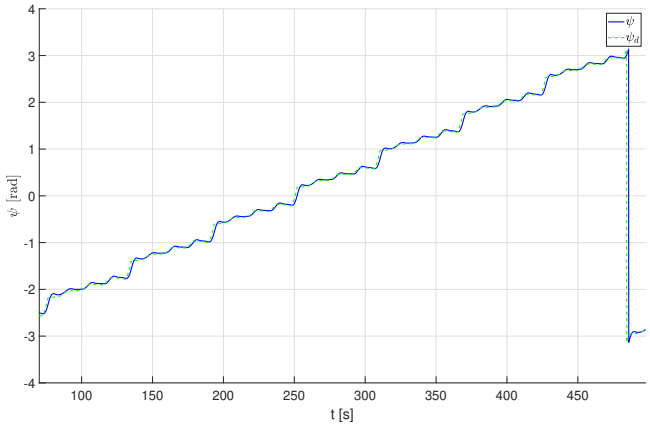

(a) Simulation of heading with PID controller

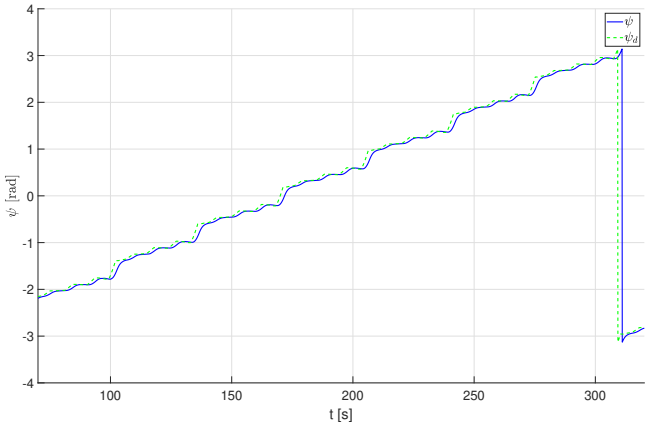

(b) Simulation of heading with C2

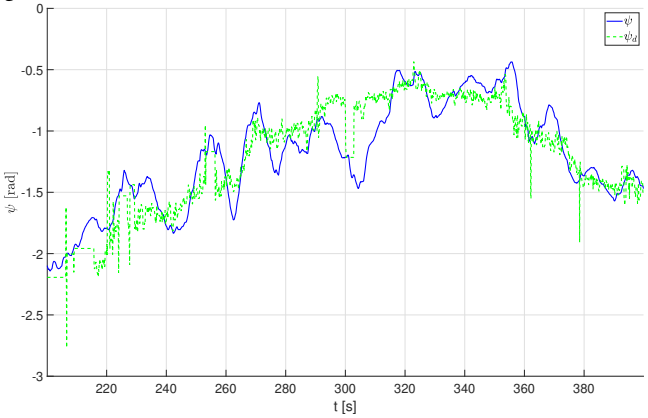

(c) Field trial at SINTEF ACE using PID for heading control

Fig. 7: The heading of the different controllers in simulation and field trial

References

[1] *Akvakultur*. https://www.ssb.no/fiskeoppdrett. Accessed: 2021-06-05.

[2] M. Føre, K. Frank, T. Norton, E. Svendsen, J. A. Alfredsen, T. Dempster, H. Eguiraun, W. Watson, A. Stahl, L. M. Sunde, C. Schellewald, K. R. Skøien, M. O. Alver, and D. Berckmans. "Precision fish farming: A new framework to improve production in aquaculture". In: *Biosystems Engineering* 173 (2018), pp. 176–193.

[3] H. B. Amundsen, W. Caharija, and K. Y. Pettersen. "Autonomous ROV inspections of aquaculture net pens using DVL". In: (2021). [Submitted].

[4] T. I. Fossen, A. Loria, and A. Teel. "A Theorem for UGAS and ULES of (Passive) Nonautonomous Systems: Robust Control of Mechanical Systems and Ships". In: *International Journal of Robust and Nonlinear Control* 11 (2001), pp. 95–108.

[5] G. Antonelli. *Underwater Robots: Motion and Force Control of Vehicle-Manipulator Systems*. Springer, 2006.

[6] S. Moe, W. Caharija, K. Y. Pettersen, and I. Schjølberg. "Path Following of Underactuated Marine Surface Vessels in the Presence of Unknown Ocean Currents". In: *Proc. of American Control Conference (ACC)* (2014).

[7] E. Børhaug, A. Pavlov, and K. Y. Pettersen. "Integral LOS Control for Path Following of Underactuated Marine Surface Vessels in the Presence of Constant Ocean Currents". In: *Proceedings of the 47th IEEE Conference on Decision and Control* (2008).

[8] A. J. Sørensen. "Structural issues in the design and operation of marine control systems". In: *Annual Reviews in Control* 29 (2005), pp. 125–149.

[9] T. I. Fossen. *Handbook of Marine Craft Hydrodynamics and Motion Control*. John Wiley & Sons Ltd, 2011.

[10] H. Khalil. *Nonlinear systems*. 3rd ed. Prentice Hall, 2002.

[11] E. Panteley, E. Lefeber, and A. Loría. "Exponential Tracking Control of a Mobile Car Using a Cascaded Approach". In: *IFAC Proceedings Volumes* 31 (27 1998), pp. 201–206.

[12] E. Panteley and A. Loría. "On Global Uniform Asymptotic Stability of Nonlinear Time-varying Systems in Cascade". In: *Systems & Control Letters* 33 (2 1998), pp. 131–138.

[13] E. Panteley, A. Loría, and A. Teel. "Relaxed Persistency of Excitation for Uniform Asymptotic Stability". In: *IEEE Transactions on Automatic Control* 46 (12 2001), pp. 1874–1886.

[14] S. J. Ohrem, T. T. Kristoffersen, and C. Holden. "Adaptive Feedback Linearizing Control of a Gas Liquid Cylindrical Cyclone". In: *IEEE Conference on Control Technology and Applications (CCTA)* (2017).

[15] K.-J. Reite, M. Føre, K. G. Aarsæther, J. Jensen, P. Rundtop, L. T. Kyllingstad, P. C. Endresen, D. Kristiansen, V. Johansen, and A. Fredheim. "FHSIM - Time Domain Simulation of Marine Systems". In: *Proceedings of the ASME 2014 33rd International Conference on Ocean, Offshore and Arctic Engineering* (2014).

[16] B. Su, K.-J. Reite, M. Føre, K. G. Aarsæther, M. O. Alver, P. C. Endresen, D. Kristiansen, J. Haugen, W. Caharija, and A. Tsarau. "A Multipurpose Framework For Modelling and Simulation of Marine Aquaculture Systems". In: *Proceedings of the ASME 2019 38th International Conference on Oceanm Offshore and Arctic Engineering* (2019).

Bibliography

[1] *Akvakultur*. `https://www.ssb.no/fiskeoppdrett`. Accessed: 2021-06-05.

[2] M. Føre, K. Frank, T. Norton, E. Svendsen, J. A. Alfredsen, T. Dempster, H. Eguiraun, W. Watson, A. Stahl, L. M. Sunde, C. Schellewald, K. R. Skøien, M. O. Alver and D. Berckmans. 'Precision fish farming: A new framework to improve production in aquaculture'. In: *Biosystems Engineering* 173 (2018), pp. 176–193.

[3] T. I. Fossen, A. Loria and A. Teel. 'A Theorem for UGAS and ULES of (Passive) Nonautonomous Systems: Robust Control of Mechanical Systems and Ships'. In: *International Journal of Robust and Nonlinear Control* 11 (2001), pp. 95–108.

[4] K. H. Nguyen. 'Control of unmanned surface and subsea vehicles operating at exposed fish farms in presence of time varying environmental disturbances'. Project thesis. MSc. Norwegian University of Science and Technology, 2020.

[5] A. J. Sørensen. 'Structural issues in the design and operation of marine control systems'. In: *Annual Reviews in Control* 29 (2005), pp. 125–149.

[6] T. I. Fossen. *Handbook of Marine Craft Hydrodynamics and Motion Control*. John Wiley & Sons Ltd, 2011.

[7] S. of Naval Architects, M. E. U. Technical and R. C. H. Subcommittee. *Nomenclature for Treating the Motion of a Submerged Body Through a Fluid: Report of the American Towing Tank Conference*. Technical and research bulletin. Society of Naval Architects and Marine Engineers, 1950.

[8] S. J. Ohrem. 'Development of a Dynamic Positioning System for Merlin WR 200 ROV'. MSc. Norwegian University of Science and Technology, 2015.

[9] H. B. Amundsen. 'Robust Nonlinear ROV Motion Control for Autonomous Inspections of Aquaculture Net Pens'. MSc. Norwegian University of Science and Technology, 2020.

[10] G. Antonelli. *Underwater Robots: Motion and Force Control of Vehicle-Manipulator Systems*. Springer, 2006.

[11] F. Dukan. 'ROV Motion Control Systems'. PhD thesis. Norwegian University of Science and Technology, 2014.

[12] *Argus Mini*. https://argus-rs.no/argus-rovs/11/argus-mini. Accessed: 2020-11-19.

[13] H. B. Amundsen, W. Caharija and K. Y. Pettersen. 'Autonomous ROV inspections of aquaculture net pens using DVL'. In: (2021). [Submitted].

[14] E. Børhaug, A. Pavlov and K. Y. Pettersen. 'Integral LOS Control for Path Following of Underactuated Marine Surface Vessels in the Presence of Constant Ocean Currents'. In: *Proceedings of the 47th IEEE Conference on Decision and Control* (2008).

[15] K. H. Ang, G. Chong and Y. Li. 'PID Control System Analysis, Design, and Technology'. In: *IEEE Transactions on Control Systems Technology* 13 (2005).

[16] J. G. Balchen, T. Andresen and B. A. Foss. *Reguleringsteknikk*. Norwegian University of Science and Technology, Department of Engineering Cybernetics, 2000. URL: https://www.nb.no/items/d651336c82c4eb6e1c3d709f702f1bfa?page=259&searchText=reguleringsteknikk.

[17] H. Khalil. *Nonlinear systems*. 3rd ed. Prentice Hall, 2002.

[18] N. Shneydor. 'Chapter 1 - Terminology and Definitions'. In: *Missile Guidance and Pursuit*. Ed. by N. Shneydor. Woodhead Publishing, 1998, pp. 1–9. URL: https://www.sciencedirect.com/science/article/pii/B978190427537450006X.

[19] P. Ioannou and J. Sun. *Robust Adaptive Control*. Dover Books on Electrical Engineering Series. Dover Publications, Incorporated, 2012.

[20] E. Panteley, A. Loría and A. Teel. 'Relaxed Persistency of Excitation for Uniform Asymptotic Stability'. In: *IEEE Transactions on Automatic Control* 46 (12 2001), pp. 1874–1886.

[21] W. Caharija, K. Y. Pettersen, M. Bibuli, P. Calado, E. Zereik, J. Braga, J. T. Gravdahl, A. J. Sørensen, M. Milovanović and B. Gabriele. 'Integral Line-of-Sight Guidance and Control of Underactuated Marine Vehicles: Theory, Simulations and Experiments'. In: *IEEE Transactions on Control Systems Technology* 24 (2016).

[22] S. Moe, W. Caharija, K. Y. Pettersen and I. Schjølberg. 'Path Following of Underactuated Marine Surface Vessels in the Presence of Unknown Ocean Currents'. In: *Proc. of American Control Conference (ACC)* (2014).

[23] I.-L. G. Borlaug, K. Y. Pettersen and J. T. Gravdahl. 'Tracking control of an articulated intervention AUV in 6DOF using the generalized super-twisting algorithm'. In: *American Control Conference (ACC)* (2019).

[24] E. Panteley, E. Lefeber and A. Loría. 'Exponential Tracking Control of a Mobile Car Using a Cascaded Approach'. In: *IFAC Proceedings Volumes* 31 (27 1998), pp. 201–206.

[25] E. Panteley and A. Loría. 'On Global Uniform Asymptotic Stability of Nonlinear Time-varying Systems in Cascade'. In: *Systems & Control Letters* 33 (2 1998), pp. 131–138.

[26] A. E. Taylor. 'L'Hospital's Rule'. In: *The American Mathematical Monthly* 59.1 (1952), pp. 20–24. URL: `http://www.jstor.org/stable/2307183`.

[27] K. J. Åström and L. Rundqwist. 'Integrator Windup and How to Avoid it'. In: *Proceedings of the 1989 American Control Conference* (1989), pp. 1693–1698.

[28] R. W. Beard and T. W. McLain. *Small unmanned aircraft: Theory and practice.* Princeton University press, 2012.

[29] S. J. Ohrem, T. T. Kristoffersen and C. Holden. 'Adaptive Feedback Linearizing Control of a Gas Liquid Cylindrical Cyclone'. In: *IEEE Conference on Control Technology and Applications (CCTA)* (2017).

[30] K.-J. Reite, M. Føre, K. G. Aarsæther, J. Jensen, P. Rundtop, L. T. Kyllingstad, P. C. Endresen, D. Kristiansen, V. Johansen and A. Fredheim. 'FHSIM - Time Domain Simulation of Marine Systems'. In: *Proceedings of the ASME 2014 33rd International Conference on Ocean, Offshore and Arctic Engineering* (2014).

[31] B. Su, K.-J. Reite, M. Føre, K. G. Aarsæther, M. O. Alver, P. C. Endresen, D. Kristiansen, J. Haugen, W. Caharija and A. Tsarau. 'A Multipurpose Framework For Modelling and Simulation of Marine Aquaculture Systems'. In: *Proceedings of the ASME 2019 38th International Conference on Oceanm Offshore and Arctic Engineering* (2019).

Kenny Hoang Nguyen

Master's thesis

NTNU
Norwegian University of
Science and Technology